

STRUCTURE OF ATMOSPHERIC TURBULENCE  
IN THE SURFACE LAYER

by

ROBERT ARMSTRONG DERRICKSON, Jr.

B.S., United States Military Academy  
(1949)

M.S., New York University  
(1954)

SUBMITTED IN PARTIAL FULFILLMENT OF THE REQUIREMENTS

FOR THE DEGREE OF DOCTOR OF PHILOSOPHY

at the

MASSACHUSETTS INSTITUTE OF TECHNOLOGY

June, 1964

WITHDRAWN  
FROM  
LIBRARY  
MIT LIBRARIES  
LINDGREN

Signature of Author .....

Department of Meteorology, May 15, 1964

Certified by .....

Thesis Supervisor

Accepted by .....

Chairman, Departmental Committee on  
Graduate Students.

**STRUCTURE OF ATMOSPHERIC TURBULENCE IN THE SURFACE LAYER**

by

**Robert A. Derrickson, Jr.**

Submitted to the Department of Meteorology on May 15, 1964  
in partial fulfillment of the requirement for the degree  
of Doctor of Philosophy

**ABSTRACT**

Power spectra and cospectra of the orthogonal velocity components and temperature for twenty one-hour runs at 16 and 40 meters height (data taken by Dr. H.E. Gramer's group at Round Hill Field Station [M.I.T.], South Dartmouth, Mass.) are analyzed, using a variety of normalizations and coordinate systems. The dependability of the data, particularly in the low frequency range under convective conditions, is considered.

Algebraic functions for power spectral data in Monin-Obukhov similarity coordinates are obtained empirically; graphical functions for the same data, using  $\bar{U}^2$  and  $(\Delta T)^2$ -normalizations, are obtained by regression analysis. Both these sets of functions have stability as a parameter. The standard deviation of the azimuth angle,  $\sigma_A$ , was selected from a number of possibilities, as the most practical parameter for expressing stratification. Site roughness is described by the standard deviation of the azimuth angle under neutral conditions,  $\sigma_N$ .

Using three separate criteria, the isotropic range in the atmospheric surface layer is defined.

The observed energy spectral density functions are compared to several theoretical functions with the following results: Kolmogoroff or Heisenberg spectra ( $E(\pi) \propto \pi^{-5/3}$ ) agree with the data within limits of observational error, in the isotropic range. Below the lower limit of isotropy but at higher frequencies than where there is mechanical energy input, the Kraichnan spectra ( $E(\pi) \propto \pi^{-3/2}$ ) is the closest to the observed data. In the low frequency range, none of these spectra are valid since this region is dominated by stability dependence and lower boundary effects, exhibiting very little energy under stable conditions and a large peak of very low frequency energy under unstable conditions.

A model is suggested viewing the  $U^{-2}$ -normalized energy spectral density functions as the consequence of mechanical site dependent roughness energy input and convective stability dependent energy input and the subsequent inertial transfer of energy to higher frequencies. Both mechanical roughness and the convective excitation are expressed in terms of the frequencies they involve.

Thesis Supervisor: Edward N. Lorenz, Sc.D.  
Title: Professor of Meteorology

Table of Contents		Page
I.	Introduction	9
II.	Objectives of the research.	14
III.	A review of pertinent literature	16
	A. Brief historical review of research in atmospheric turbulence.	16
	B. Outline of various approaches to the problem.	18
	C. Resumes of selected papers.	24
IV.	Data collection and processing techniques.	38
	A. Detailed description of the measurements.	38
	B. Explanation of the data processing	39
	C. Data reliability.	41
V.	Description of the research.	46
	A. Method of approach.	46
	B. Definition of derived turbulence statistics.	46
	C. Choice of parameters describing effects of stratification and the lower boundary.	55
	D. Presentation of power spectra in similarity coordinates.	63
	E. Results	64
	1) Algebraic expressions for energy spectral density functions in similarity coordinates.	64
	2) Various methods of estimating stress and heat flux.	74
	3) Regression analysis of power spectra.	77
	4) Discussion of normalizing techniques.	93
	5) Lower bound of isotropy in the surface layer.	105
	6) Form of spectra at intermediate frequencies.	116
	7) Form of spectra at low frequencies.	117
	8) Comparison of results with those of other investigators.	118
	F. Comparison of results with theoretical predictions.	122
	G. A composite model of energy spectra density functions in the surface layer.	134
VI.	Summary and conclusions.	136
VII.	Suggested further research.	140
VIII.	Acknowledgments.	142
IX.	Appendix	143
	A. Resumes of papers (continuation of part III c.)	143
	B. List of algebraic expressions for the orthogonal components and temperature power spectra in similarity coordinates.	145
	C. Various methods of estimating stress and heat flux.	149
X.	Bibliography.	152

List of Tables.		Page
Table 1.	Sample computation sheet for the Monin-Obukhov similarity normalization (Run 67 A, 16 meters)	47
Table 2.	Sample computation sheet for the Monin-Obukhov similarity normalization (Run 67 A, 40 meters)	48
Table 3.	General statistics for the twenty runs, Part A.	49
Table 4.	General statistics for the twenty runs, Part B.	50
Table 5.	General statistics for the twenty runs, Auxiliary data.	51
Table 6.	Vertical profile data for mean temperature and mean horizontal wind.	52
Table 7.	Total variance of u, v, w and T fluctuations before and after filtering (high-pass).	53
Table 8.	$\bar{U}^2$ -normalized energy spectral density values for selected frequencies ( $nz/\bar{U}$ ).	88
Table 9.	Derived data for power spectral density versus frequency ( $nz/\bar{U}$ ). a. from regression b. from algebraic functions	89
Table 10.	Isotropic ratios as a function of $nz/\bar{U}$ for five runs.	109
Table 11.	Values for average slope and values for $nz/\bar{U}$ , defining the extent of the various regions; isotropic data and uniform slope data summary.	110
	A composite of four small tables (tables 12, 16, 17 and 18).	112
Table 12.	Per cent probability of observing a coherence as high as $\beta$ , when the true value is zero.	112
Table 16.	Average values for $nz/\bar{U}$ at the low frequency limit of the uniform slope region.	112
Table 17.	Average values for the uniform slope, just below the lower limit of isotropy.	112
Table 18.	Period associated with maximum of the $\mathcal{N}S(\nu)$ function.	112
Table 13.	Coherence values for u, w fluctuations as a function of period.	113
Table 14.	wT coherence as a function of period.	114
Table 15.	uT coherence as a function of period.	115

List of Figures.		Page
Figure 1.	Qualitative graph of kinetic energy of surface winds as a function of the time scale.	10
Figure 2.	Schematic of energy spectral density versus frequency in non-dimensional coordinates.	23
Figure 3.	Theoretical heat flux as a function of $z/bz$ .	32
Figure 4.	Response of statistical filter versus frequency, $n$ .	44
Figure 5.	General functional form of non-dimensional energy spectral density on non-dimensional frequency and stability.	54
Figure 6.	Standard deviation of azimuth angle versus $z/bz$ between 4 and 32 meters.	58
Figure 7.	Schematic of $n \cdot \sigma_n / \bar{U}^2$ versus $\log n z / \bar{U}$ of two sites of different roughness.	61
Figure 8.	Longitudinal energy spectral density at 16 meters in similarity coordinates, for the individual runs.	65
Figure 9.	Transverse energy spectral density at 16 meters in similarity coordinates for the individual runs.	66
Figure 10.	Energy spectral density of vertical component at 16 meters in similarity coordinates for the individual runs.	67
Figure 11.	Energy spectral density of temperature fluctuations at 16 meters in similarity coordinates for individual runs.	68
Figure 12.	Longitudinal energy spectral density at 40 meters in similarity coordinates for individual runs.	69
Figure 13.	Transverse energy spectral density at 40 meters in similarity coordinates for individual runs.	70
Figure 14.	Energy spectral density of vertical component at 40 meters in similarity coordinates for individual runs.	71
Figure 15.	Energy spectral density of temperature fluctuations at 40 meters in similarity coordinates for individual runs.	72
Figure 16.	Energy spectral density from algebraic expressions for the longitudinal and transverse components.	75
Figure 17.	Energy spectral density from algebraic expressions for the vertical component and temperature fluctuations.	76

Figure 18.	Heat and momentum flux as a function of the mean wind speed and modified stability parameters.	78
Figure 19.	a) Stress as a function of the mean wind speed and temperature difference between the surface and 8 meters. b) Stress as a function of wind shear and the temperature difference between the surface and 8 meters.	79
Figure 20.	Heat flux as a function of $\partial\theta/\partial z$ , at 16 and 40 meters.	80
Figure 21.	Heat flux and flux divergence as a function of the mean wind and temperature difference between the surface and 8 meters.	81
Figure 22.	Sample of regression graphs for individual frequencies.	82
Figure 23.	Continuation of Figure 22.	83
Figure 24.	Energy spectral density as a function of stability for the u and v-components, obtained by regression.	84
Figure 25.	Energy spectral density as a function of stability for w and temperature fluctuations, obtained by regression.	85
Figure 26.	Same data as Figure 24 in semi-log coordinates.	86
Figure 27.	Same data as Figure 25 in semi-log coordinates.	87
Figure 28.	Comparison of energy spectral density functions at 16 and 40 meters.	91
Figure 29.	Comparison of energy spectral density functions of the u- and v-components.	92
Figure 30.	Energy spectral density for selected runs as a function of period for u- and v-components, using $\bar{U}^2$ (2 meters)-normalization.	95
Figure 31.	Same data as Figure 30 using coordinates $\frac{S_{i,z}}{\bar{U}_{(z)}^2}$ versus $\frac{\eta z}{U_z}$ where $i = u, v$ $z = 16, 40$ meters	96
Figure 32.	Power spectra for nine runs in coordinates $\eta S_{u,16}$ versus log(period).	97
Figure 33.	Power spectra for nine runs in coordinates $\eta S_{v,16}$ versus log(period).	98
Figure 34.	Power spectra for nine runs in coordinates $\eta S_{w,16}$ versus log(period).	99

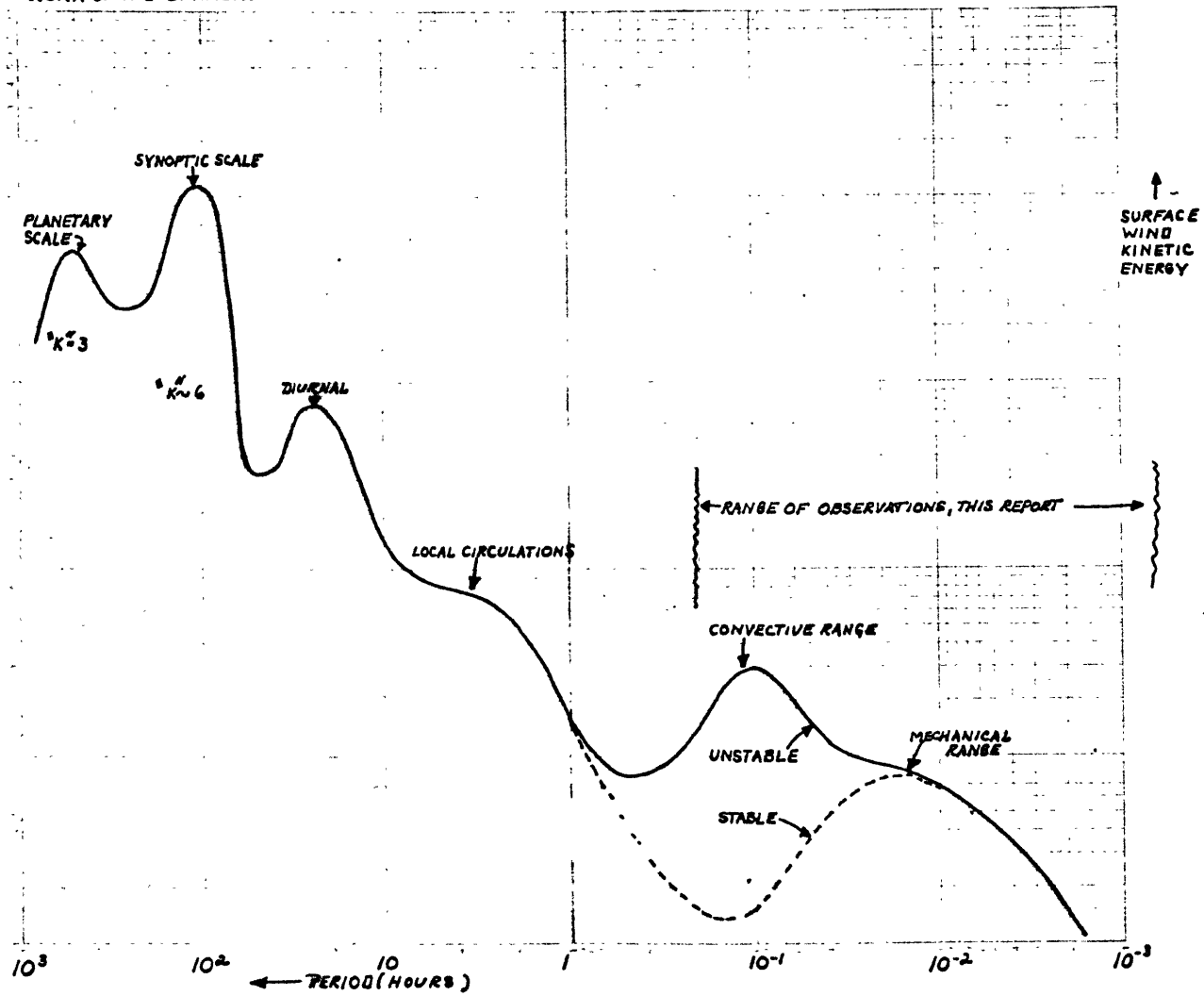
Figure 35.	Power spectra for nine runs in coordinates $\eta S_{KUP, 16}$ versus $\log(\text{period})$ .	99
Figure 36.	Power spectra for nine runs in coordinates $\eta S_{K, 40}$ versus $\log(\text{period})$ .	100
Figure 37.	Power spectra for nine runs in coordinates $\eta S_{V, 40}$ versus $\log(\text{period})$ .	101
Figure 38.	Power spectra for nine runs in coordinates $\eta S_{W, 40}$ versus $\log(\text{period})$ .	102
Figure 39.	Power spectra for nine runs in coordinates $\eta S_{KUP, 40}$ versus $\log(\text{period})$ .	102
Figure 40.	Isotropy ratios as a function of frequency.	103
Figure 41.	Comparison of various theoretical spectral functions with observed data.	123
Figure 42.	Non-dimensional heat flux as a function of the Richardson number.	128
Figure 43.	Period associated with the maximum value of $\eta S(\tau)$ as a function of : a) $\sigma_{\theta}$ and b) $\partial\theta/\partial z$ .	129
Figure 44.	Vertical profiles of temperature, variance of temperature and vertical velocity for free convective runs.	132
Figure 45.	Diagrammatical explanation of the "modified Businger model".	135



## I. INTRODUCTION

Atmospheric turbulence is generally fully developed, with Reynolds numbers of the order of  $10^6$ . The usual situation is that of flow over an aerodynamically rough lower boundary with vertical shear of the horizontal mean wind and buoyancy forces present. The wind and stratification are both strong functions of the time of day and the synoptic situation. In addition, they are interdependent in a complicated manner. At a particular site, the type of regime and intensity of turbulence are highly dependent on the mean wind, its shear and the stratification. From site to site, these characteristics of turbulence are also dependent on the effect of the lower boundary. This effect is variable, depending on the particular turbulence regime that is dominant at the time. Another interesting feature of atmospheric turbulence is that it involves length scales ranging from the planetary scale to scales so small that viscous forces are dominant over inertial forces. In time units, the scales span a range between weeks and very small fractions of a second. Figure 1 demonstrates this situation schematically. Except under very restricted laboratory conditions, a mathematical solution of the equations of motion is out of the question. Before one can even make judicious simplifying assumptions, it is necessary to know something about the spectral distribution of energy sources and sinks, the range of length scales that might be expected to exhibit isotropic conditions, and the general shape of the energy spectral density functions. One must also know something about the general behavior of the heat and momentum fluxes and under what conditions the assumption of horizontal homogeneity is reasonable. The first step,

FIG. 1: QUALITATIVE GRAPH OF KINETIC ENERGY OF SURFACE WINDS AS A FUNCTION OF THE TIME SCALE. INFORMATION SOURCES ARE: SALTZMAN (1957); VAN DER HOVEN (1957) AND UNPUBLISHED WORK OF H.E. CRAMER.



then, becomes the observation of the velocity and temperature fluctuations. The data used in this research consists of fluctuations of the orthogonal velocity components and temperature taken simultaneously by fast response equipment at the 16-meter and 40-meter levels. These measurements were made with the instruments located on a 40-meter tower surrounded by reasonably flat terrain at the Round Hill Field Station (M.I.T.), South Dartmouth, Mass. There are twenty one-hour runs at each level spanning a frequency range between  $n = .0014$  and  $n = .4 \text{ sec}^{-1}$ . From these data, power spectral and cospectral analyses of the orthogonal velocity component and temperature fluctuations are obtained. A more complete description of this data sample is given by Cramer, Record, Tillman and Vaughan (1961), and Cramer, Record and Tillman (1962) and in Section IV of this report. This represents a larger data sample, taken under carefully controlled experimental conditions, than has previously been available. Therefore it is believed desirable to supplement work of other investigators because the results can be stated with greater assurance and the effect of stratification on the power spectral functions and on the heat and momentum fluxes can be better defined. A partial inventory of previous measurements and some analyses of these, includes the following:

1. Great Plains data, consisting of approximately fifty runs of ten minutes length at heights of 1 1/2, 3, 6 and 12 meters. These data are presented and analyzed by Lettau and Davidson (1957) and analyzed by Takauchi (1961) and others.

2. Prairie Grass Data, consisting of approximately fifty runs of twenty minutes in length at a height of 2 meters. These data are presented

by Haugen (1959) and has been analyzed by Panofsky and Deland (1959), Cramer (1960) and others.

3. Numerous runs of about one hour each in length have been taken at the Brookhaven National Laboratory, Upton, N.Y. The basic data are 5 sec. averages of velocity components and include temperature fluctuation data, taken at heights of 23, 46 and 91 meters. These data have been analyzed by Panofsky and Deland (1959), Panofsky and McCormick (1954), Panofsky (1962) and others.

4. There are a number of analyses of smaller data samples. A few of these are: (a) Monin (1962) analyzed w-component data for seven runs of unknown record length at the 1-meter level. (b) Takeuchi (1963) analyzed two runs of 10 minutes duration each at the 16-meter level. (c) Maccready (1953) analyzed five runs, varying in length from 10 minutes to one hour. Blackadar and Panofsky (1964) gave a review of the status of research, concerning atmospheric turbulence and diffusion, in the Soviet Union.

The Round Hill data are of sufficiently long time duration (each run is approximately one hour in length) to evaluate the low frequency convective range with considerable confidence and, at the same time, the rapid response of the wind measuring instruments permits one to measure frequencies high enough to reach the inertial sub-range for most runs. Also, the 16 and 40-meter levels are high enough above ground level so that vertical velocities of considerable size appear in the larger turbulence scales. So it was decided as necessary to evaluate these twenty one-hour runs first; then go on to consider what theoretical works seem to be most successful in explaining the behavior of the power spectral density functions.

Theoretical work, pertinent to atmospheric turbulence, has mainly been in three areas:

1. **Isotropic Turbulence.** Work in this area has been extensive and has led, with the aid of similarity assumptions of various forms, to predictions about the energy spectral density functions for those scales of atmospheric motion that are isotropic. Batchelor (1953) and Lin and Reid (1963) present a comprehensive description of this area of work. Recently Kraichnan (1958), (1959) has introduced modelling in the form of his "direct interaction" approximation first, and then operated mathematically on the resulting equations with the aid of the isotropic assumption.

2. **Similarity Assumptions in the Anisotropic Case.** This development is the work of Monin and Obukhov (1954). They assume that the vertical heat and momentum fluxes are constant in a sufficiently shallow surface layer. Using these assumptions and dimensional analysis, predictions are made about the shape of the vertical wind and temperature profiles; also a means of non-dimensionalizing power spectral density functions is suggested.

3. **Solution of Equations of Motion under very Restricted Conditions,** assuming that the interaction of one perturbation quantity with another is small compared to the interaction of perturbation and mean quantities. The works of Deissler (1961); (1962) are examples of this approach. Some very specialized predictions about the form of the energy spectral density as a function of frequency are obtained.

For a detailed and rather complete indication of the present state of theoretical and observational knowledge in the area of atmospheric turbulence, the following list of books and papers are recommended: Batchelor

(1953), Lin and Reid (1963) and Pasquill (1961), Chapter I. The basis of the spectral and cospectral analyses of variance and covariance functions was provided by Taylor (1938). For a continuation of the discussion, including treatment of the problem with vertical shear and stratification present, see: Frenkiel and Sheppard (1959), Hinze (1959) and Frenkiel (1962). With this knowledge of the nature of atmospheric turbulence in the surface layer and of the state of the art regarding both theory and observations, the problem can be more specifically stated as follows: first, a large data sample should be used to learn more about the general characteristics of atmospheric turbulence. Then one is in a position to apply the present theoretical developments judiciously. For instance, if it were known under what conditions and for what scales that atmospheric turbulence is isotropic, then one could make use of the present theoretical work in this area. Also one would know what simplifying assumptions and modelling are acceptable in treating the problem. Then the plan of attack indicated is to gather data; analyze it; evaluate the available theoretical results; and possibly start the whole cycle over again with some new predictions.

## II. OBJECTIVES OF THE RESEARCH.

The objectives of the research are to analyze and present the experimental data from the twenty runs in a manner which is most convenient for reaching theoretical and observational conclusions. In order to do this, it will be necessary to use several coordinate systems and non-dimensionalizing methods, to find the most appropriate techniques. An associated

problem is the necessity of selecting parameters to express the effects of stratification and lower boundary roughness on the energy spectral density functions of the orthogonal velocity components and temperature. The problem, specifically, is to express the energy density functions as functions of: frequency,  $n$ ; mean wind speed at some height,  $\bar{U}_z$ ; buoyancy expressed as the gradient of potential temperature,  $\frac{\partial \theta}{\partial z}$ ; and surface roughness,  $s_0$ , or some other parameter descriptive of the lower boundary. Although primary emphasis is on the power spectral data, some work, designed to evaluate vertical heat and momentum fluxes, is done. The objective is to choose a minimum number of parameters, which are well behaved, not too difficult to evaluate, and which are pertinent to the physics of the problem. With  $\bar{U}_z$  incorporated in the non-dimensionalizing process, then there are needed two parameters: one to specify the lower boundary effect and the other to specify the stratification. When this point is reached, one has results which can serve two purposes. The results are of engineering value, which yield estimates of power spectral densities, momentum fluxes and heat fluxes when the necessary parameters can be evaluated. The second and far more important result, so far as this research is concerned, is a data sample organized in such a manner that theoretical results can be critiqued. The primary thesis objective can now be attained: that is to choose the theories and models which show the most promise in explaining observational results. The last objective is to develop a composite model, which explains the general shape of the energy spectral density functions and their dependence on thermal stratification and lower boundary effects.

If these energy spectral density functions can be determined with

reasonable accuracy, then the dissipation rate of turbulent kinetic energy,  $\epsilon$ , can be determined. Knowledge of this dissipation rate of energy and its dependence on terrain and meteorological parameters is essential for numerical weather prediction of the larger scales of atmospheric motions. It is also necessary for evaluating the equations of energy balance in the surface layer, where energy exchanges are of prime importance. Estimates of energy spectral density functions are of basic importance in calculating diffusion rates of contaminants in the atmosphere.

### III. A REVIEW OF PERTINENT LITERATURE.

#### A. Brief historical review of research in atmospheric turbulence.

Three papers of G.I. Taylor provide a foundation for the present day mathematical analysis of turbulent motions. In the first two of these (Taylor, 1921; 1935), Taylor recognized that the velocity in a fluid is a continuous function of position and time. Taylor presented the hypothesis that  $x = \bar{U}t$ , if the turbulent energy is small compared to the energy of mean motion ( $x$  is the displacement,  $\bar{U}$  is the mean velocity and  $t$  is the time). He made another very important contribution to the study of turbulent motion in his 1938 paper when he showed that the velocity correlation function,  $\overline{u_i(\vec{x}) u_j(\vec{x} + \vec{r})}$ , and the energy spectral density function,  $\Phi_{ij}(\vec{k})$  are Fourier transforms of each other. Expressed in mathematical symbols, this relationship may be stated as follows:

$$R_{ij}(\vec{r}) = \overline{u_i(\vec{x}) u_j(\vec{x} + \vec{r})} = \int \Phi_{ij}(\vec{k}) e^{i\vec{k} \cdot \vec{r}} d\vec{k} \quad (3.1)$$

$$\text{and } \Phi_{ij}(\vec{k}) = \frac{L}{8\pi^3} \int R_{ij}(\vec{r}) e^{-i\vec{k} \cdot \vec{r}} d\vec{r} \quad (3.2)$$



In 1941, Kolmogoroff introduced the concept of "universal equilibrium" for sufficient by high wave numbers and, with the aid of dimensional arguments, he derived the form of the energy spectral density function in this high wave number region.

Batchelor (1953) in his book, "The Theory of Homogeneous Turbulence", presented a comprehensive review of the mathematical theory of turbulence. The treatment is mostly concerned with isotropic turbulence. The same year he [Batchelor (1953 A)] also showed the importance of the Richardson number in evaluating the dynamic similarity of atmospheric motions.

Commencing with Macready (1953), measurements of velocity fluctuations in the atmosphere became available for the first time for empirical evaluation of the above theoretical predictions. This trend continued with the Great Plains and Prairie Grass experimental programs. For a more complete inventory, see Section I and Section IIIC.

Monin and Obukhov (1954) proposed a similarity theory designed for predicting the details of turbulent motions in the boundary layer under anisotropic conditions. Many of the more recent papers (see Section IIIC) analyze the recently taken data and there is renewed interest in the works of Kolmogoroff, Monin and Obukhov. This is about the situation at present as larger and more satisfactory data samples become available.

Kraichnan (1958; 1959) has been doing important theoretical work by first modelling the atmospheric motions, then operating with mathematical exactness on the simplified system. Other recent theoretical work has involved the solution of "linearized" perturbation equations of motion. Deissler (1961; 1962) and Bolgiano (1962) are examples of this approach.

This section is a brief chronology of the important happenings in atmospheric turbulence studies for the scales of motion considered here. Next, Section III B shows the contrasting approaches to this problem; Section III C and the Appendix give brief resumes of many pertinent papers.

### B. Outline of Various Approaches to the Problem.

Due to the chaotic nature of atmospheric turbulence, one would usually be content to know some statistics of the flow after time,  $t$ , given data at time,  $t = 0$ , the values of the important parameters and the boundary conditions. A number of theoretical approaches have been suggested. The generally accepted equations of motion are

$$\frac{\partial u_i}{\partial x_i} = 0, \quad \text{Non-divergent flow}$$

$$\rho \left\{ \frac{\partial u_i(\vec{x}, t)}{\partial t} + u_j(\vec{x}, t) \frac{\partial u_i}{\partial x_j} \right\} = -\frac{\partial p}{\partial x_i} + \rho \nu \nabla^2 u_i - g_i \rho$$

Navier-Stokes equation (3.3)

When buoyancy forces are treated, the Boussinesq approximation is quite acceptable:  $\rho = \rho_0$ , except when multiplying  $g_i$ , giving:

$$\rho_0 \frac{\partial u_i}{\partial t} + \rho_0 u_j \frac{\partial u_i}{\partial x_j} = -\frac{\partial p}{\partial x_i} + \rho_0 \nu \nabla^2 u_i - g_i \rho_0 \{1 - \alpha T'\} \quad (3.4)$$

where  $g_i = (0, 0, g)$

$\alpha$  = coefficient of thermal expansion

$T'$  = departure of temperature from the value at which  $\rho = \rho_0$

The symbols used in this report have the same meaning as in Batchelor's

book unless they are otherwise described.

This investigation of atmospheric turbulence is confined to the surface layer and the regions immediately adjacent thereto. It is therefore necessary to discuss the depth of this layer. The depth is not only variable because of dependence on meteorological conditions but may also be defined in several ways. The definition of this layer has to be a part of each treatment and is not defined in general terms.

The following is a review of the various theoretical approaches to the problem:

1. Solving as an initial value problem, using a Taylor series.

$$\vec{u}(\vec{x}, t) = \vec{u}(\vec{x}, t_0) + (t - t_0) \left[ \frac{\partial \vec{u}(\vec{x}, t)}{\partial t} \right]_{t=t_0} + \frac{1}{2!} (t - t_0)^2 \left[ \frac{\partial^2 \vec{u}(\vec{x}, t)}{\partial t^2} \right]_{t=t_0} + \dots \quad (3.5)$$

By taking the divergence of the Navier-Stokes equation,

$$\frac{1}{\rho} \nabla^2 p = - \frac{\partial^2 u_i u_j}{\partial x_i \partial x_j};$$

Using a Green's Function,

$$\frac{1}{\rho} p(\vec{x}) = \frac{1}{4\pi} \int \frac{\partial^2 [u_i'' u_j'']}{\partial x_i'' \partial x_j''} \frac{d\vec{x}''}{|\vec{x}'' - \vec{x}|}$$

Next  $\left( \frac{\partial^2 \vec{u}}{\partial t^2} \right)_{t=t_0}$  is evaluated. As  $(t - t_0)$  becomes larger, it is necessary to evaluate higher order derivatives in the series and hence to know more completely the initial velocity distribution function.

2. Using the equations of motion and deriving expressions involving

product-mean values. If initial conditions involve probability functions, then these equations are expressions in joint-probability functions.

$$R_{ij}(\vec{r}) = \overline{u_i(\vec{x}) u_j(\vec{x} + \vec{r})} = \int \Phi_{ij}(\vec{k}) e^{i\vec{k} \cdot \vec{r}} d\vec{k}, \quad d\vec{k} = dk_1 dk_2 dk_3$$

(with suitable restrictions)

$$\text{and } \Phi_{ij} = \frac{1}{(2\pi)^3} \int R_{ij}(\vec{r}) e^{-i\vec{k} \cdot \vec{r}} d\vec{r}$$

$$\text{then } \frac{\partial R_{ij}(\vec{r}, t)}{\partial t} = \frac{\partial}{\partial x_k} [u_i \overline{u_j u'_k} - u_i \overline{u'_k u_j}] + \frac{1}{\rho} \left\{ \frac{\partial \overline{p u'_j}}{\partial x_i} - \frac{\partial \overline{p' u_i}}{\partial x_j} \right\} + 2\nu \nabla^2 R_{ij}(\vec{r}, t), \quad (3.5)$$

In order to evaluate second order product means (say a two point probability function), it is necessary to know the third order product mean terms; and in order to evaluate the third order product mean terms, the fourth order terms are needed. So at this point, one can close the set of equations only by assuming some evaluation of these higher order terms.

Some methods are:

- (a) linear solution, where the third order terms are set equal to zero.
- (b) physical transfer theorems; using the isotropic assumption, one takes the Fourier transform of the Navier-Stokes equation to get:

$$\frac{\partial E(k)}{\partial t} = T(k) - 2\nu k^2 E(k) \quad (3.6)$$

where  $E(k)$  is the spectral density of kinetic energy per unit mass and  $T(k)$  is the defining scalar of the Fourier transform of the complicated

non-linear term.  $E(k)$  is also the defining scalar of  $\overline{\Phi(\vec{k})}$ . See Lin and Reid (1963), p. 449, for a more complete description of these terms, the longitudinal and transverse correlation functions and their relation to each other through the Von Karman-Howarth equation. One makes the equations of motion determinant by assuming  $T(k)$  to be expressible in terms of  $E(k)$ .

(c) quasi-Gaussian assumption: the fourth order terms are expressed as a function of the second-order terms (the value that a Gaussian probability function for the velocity would give), without setting the triple correlation equal to zero.

3. Modify the equations of motion first by modelling primarily to deal with the non-linear term, then operate on the resulting system with mathematical exactness. This is in reverse order to the procedure in Section B and is the technique employed by Kraichnan (1958; 1959). Some of these methods are presented more fully in Section III C and the Appendix. Some other authors, who commence by defining a model are: Thompson (1963), Priestley (1959) and Lettau (1949).

4. Hopf's theory of turbulence (see p. 442-444 of the paper by Lin and Reid). This method starts with a known joint-probability distribution function,  $F(\vec{u})$ , for the velocity, or its Fourier transform,  $\varphi(\vec{\alpha})$ .

$$\varphi(\vec{\alpha}) = \int e^{i\vec{\alpha} \cdot \vec{u}} F(\vec{u}) d\vec{u} = \overline{e^{i\vec{\alpha} \cdot \vec{u}}}$$

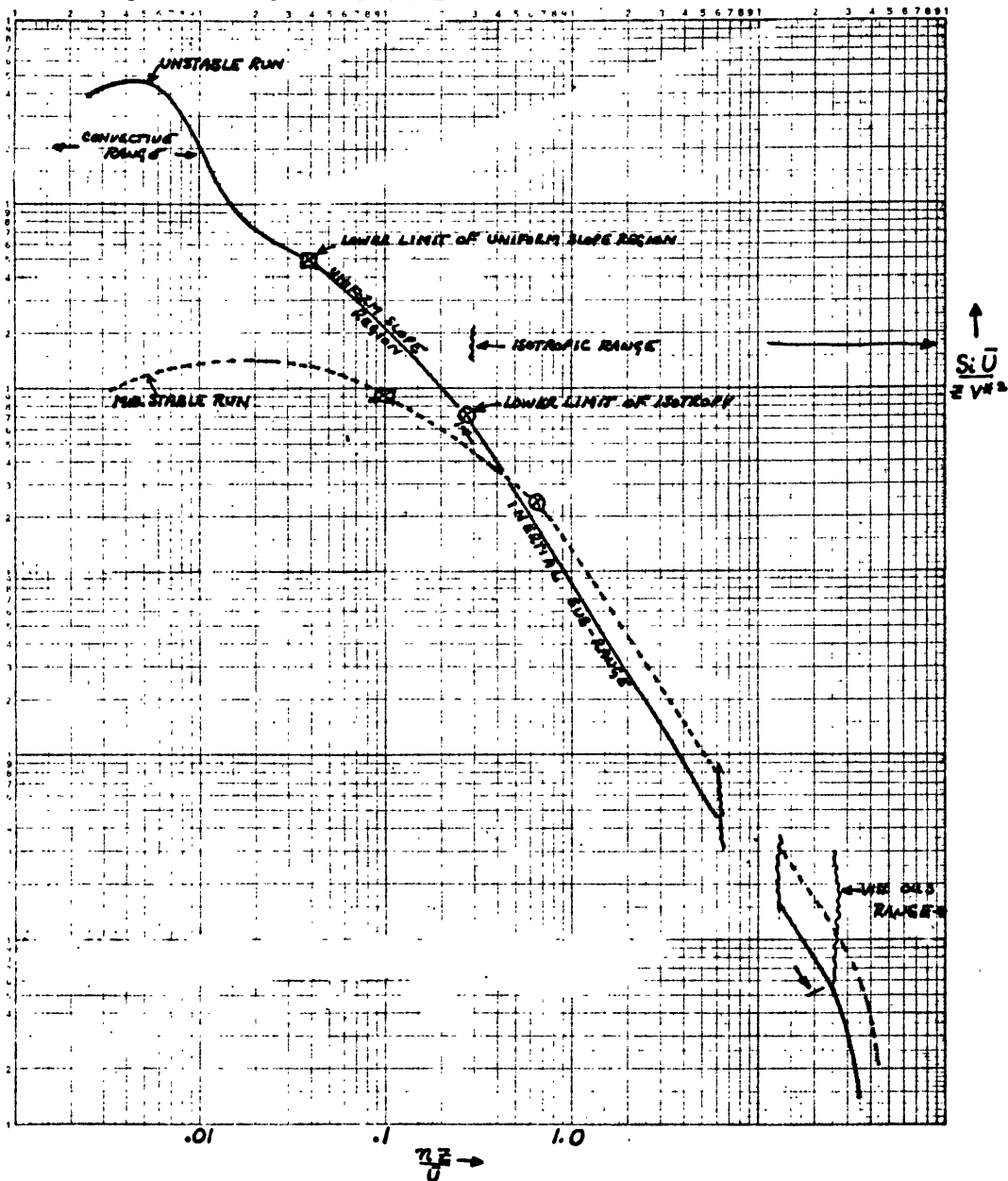
Then express  $\varphi(\vec{\alpha}) = \sum_{m=0}^{\infty} \frac{i^m}{m!} \overline{(\vec{\alpha} \cdot \vec{u})^m}$ , where the coefficients in the series are the complete set of moments of  $\vec{u}$  at a point. Finally use the

dynamical equations to get an expression for  $\varphi(\vec{\alpha})$ . This has not yet been done for homogeneous turbulence.

5. Similarity solutions. In order to use similarity, it is necessary to argue that the turbulence regime must approach some universal state, which is independent of the initial conditions and is only affected by boundary conditions in a very restricted manner. The objective is to be able to describe the flow regime, using a lesser number of physical parameters than was needed to define the solution prior to its approach to the "universal state". The hypothesis of Kolmogoroff (1941) is the most important example of the application of similarity arguments to atmospheric turbulence. He states that at a sufficiently high Reynolds number, a region of isotropic turbulence can be specified in terms of the dissipation rate of kinetic energy,  $\mathcal{E}$ , and the kinematic viscosity,  $\nu$ . If the Reynolds number is sufficiently high (the usual atmospheric case), then the "energy containing" and "dissipative eddies" are sufficiently separated in wave number space to assume that they act independently and are separated by an "inertial sub-range", where  $\mathcal{E}$  is the only important parameter. Using this and dimensional analysis, he derived an expression for the energy spectral density as a function of wave number (or frequency) only. A schematic of the atmospheric case is shown by Figure 2, where the non-dimensional spectral density of energy is plotted against non-dimensional frequency. Log-log coordinates are used for convenience.

In the non-isotropic case, Monin and Obukhov (1954) assumed that the vertical heat flux and momentum flux are constant within a shallow surface layer. From these quantities, using dimensional analysis, a friction

FIG. 2: SCHEMATIC OF ENERGY SPECTRAL DENSITY VS. FREQUENCY IN NON-DIMENSIONAL COORDINATES, SHOWING THE VARIOUS SPECTRAL REGIONS.



velocity,  $V^*$ ; a friction temperature,  $T^*$ ; and a stability length,  $L$ , were formed. Then using the non-dimensional quantity,  $z/L$ , conclusions were derived concerning the diabatic wind and temperature profile. The data used in this investigation are not well suited to a careful evaluation of "profile theorems". The principal significance of this similarity theorem is that it suggests the functions,  $V^{*2}$  and  $T^{*2}$  to non-dimensionalize the power spectra of velocity and temperature respectively. A more detailed explanation of Monin-Obulchov similarity is given in Section III C.

### C. Resumes of selected papers.

In the following review of papers, the selection was determined by the requirement for an adequate description of research activity in each of the several separate approaches to the problem. The papers are grouped according to type of approach and only the most pertinent ones to this investigation are included in this section. Additional resumes are included in the Appendix, Section IX, and a few others are listed only in the bibliography.

Although the atmospheric case is one anisotropy, it is shown later that, under certain conditions, portions of the spectrum are isotropic. In order to derive an expression of the form:  $E(k) = f(k)$ , it is necessary to make certain assumptions about the physics of the problem or about the higher order product-mean terms.

1. Transfer theories. A description is given by Batchelor (1953) and Lin and Reid (1963) of several methods for evaluating the non-linear transfer term,  $T(k)$ , in the equation:

$$\frac{\partial E(k)}{\partial t} = T(k) - 2\nu k^2 E(k)$$



Probably the best known of these is the Heisenberg theory (Lin and Reid [1963]), which states that the mechanism governing energy transfer between wave numbers is similar to the one governing viscous dissipation. In mathematical terms,

$$\int_0^K T(k') dk' = 2\nu_t(k) \int_0^K k'^2 E(k') dk'; \quad \nu_t = K_H \int_K^\infty \sqrt{\frac{E(k')}{k'^3}} dk'$$

The desired equation for  $E(k)$  is:

$$\frac{\partial}{\partial t} \int_0^K E(k') dk' = 2 \left[ \nu + K_H \int_0^\infty \sqrt{\frac{E(k')}{k'^3}} dk' \right] \int_0^K k'' E(k'') dk''.$$

If the following transformations,

$$F(x) = E(k, t) \left[ \frac{t^{1/2} K_H^2}{\alpha^{3/2} \nu^{3/2}} \right]; \quad x = (\alpha \nu t)^{1/2} k$$

based on maintaining self-similarity during initial period decay, are made, then Figure 13 of Lin and Reid (1963) shows the result. This resulting spectrum appears to be quite similar to that observed under known anisotropic conditions (see Figure 41). If it is assumed that the atmosphere is an ensemble of these turbulence cells in various states of decay, and that this transformation is applied to each cell individually, then the space average of the result in  $x - F(x)$  coordinates would be steady state.

2. Quasi-Gaussian assumption. Serious theoretical difficulties arise in using this assumption, as indicated by Ogura (1962), therefore it does not seem worthwhile to consider this approach further.

3. Linear solutions. Two papers by Deissler (1961; 1962) are of particular interest in providing an analysis of the effects of shear of the horizontal mean wind and buoyancy separately on the kinetic energy spectrum of turbulent motion. The approach of Deissler (1962) is to assume no wind shear and a constant stratification expressed by

$$\beta = \frac{1}{\rho} \left( \frac{\partial \rho}{\partial z} \right)_p \quad . \quad \text{The following equation:}$$

$$\frac{\partial u_i}{\partial t} + \frac{\partial}{\partial x_j} (u_i u_j) = -\frac{1}{\rho} \frac{\partial}{\partial x_i} (p - p_{equil}) + \nu \frac{\partial^2 u_i}{\partial x_j \partial x_j} - \beta (\overline{T'} - T_{equil}) g_i$$

is used to derive two point correlation functions such as  $\overline{u_i u_j'}$ ,  $\overline{p u_j'}$ ,  $\overline{u_i T'}$ , etc. Deissler closed the set of equations by setting all triple correlation terms equal to zero and imposed initial conditions at  $t = 0$  of isotropy and no fluctuations of temperature. His conclusions were:

- (a) No steady state was reached
- (b) Dissipation occurred mainly at high frequencies.
- (c) Buoyant energy was fed into or removed from a large range of frequencies and the effect was somewhat stronger at lower frequencies.
- (d) The turbulence is anisotropic at low frequencies.

This paper represents a demonstration of the first approximation of the effect of buoyancy on highly developed turbulence in the absence of shear and without non-linear inertial transfer of energy. The "transfer" that appears here is merely the net result of buoyancy extracting energy at one frequency and putting it in at another and bears no relation to the transfer of energy directly between the degrees of freedom that is going on in the real atmosphere. Deissler's 1961 paper is summarized in the Appendix.

These two papers are instructive, even though the simplification of the problem in each case is severe.

The next paper, Rayleigh (1916) treats convection in an unstably stratified fluid. The model consists of two parallel flat plates of infinite horizontal extent, separated by a distance,  $\mathcal{D}$ . The formulation used is:

(a) Equations of motion without coriolis term, with and without viscosity.

(b) Non-divergent flow.

(c) Boussinesq approximation.

(d) A diffusion term in the thermodynamic equation.

Of particular interest is the identification of the modes of greatest instability. It is inferred that these modes are the ones most likely to be observed in the convective case. In the absence of viscosity, greatest instability occurs when the wave number in the vertical is the least. Then the horizontal wave number,  $\sqrt{\ell^2 + m^2}$ , is given by:

$$\ell^2 + m^2 = \frac{\pi^2}{\mathcal{D}^2} + \frac{\beta' \gamma \mathcal{D}^2}{8 k^2 \pi^2} \quad \left\{ \begin{array}{l} \text{primarily a function of the depth, } \mathcal{D} \\ \text{secondarily a function of the stability, } \beta \end{array} \right.$$

For a fixed depth of fluid, the horizontal wave number of maximum convective energy is expected to be proportional to  $\beta^{1/2}$ . But,  $k$ , the thermal diffusivity, in this case is also dependent on the turbulent intensity and would make the wave number of maximum energy less strongly dependent than  $\beta^{1/2}$ .

If  $\ell = m$ , then  $\lambda$ , the horizontal wave length of maximum instability,  $= 2\sqrt{2} \mathcal{D}$

4. Approaches which involve analysis after a model is defined.

The most important papers are Kraichnan (1958; 1959) and Kraichnan and Spiegel (1962). The approach here is to model the atmosphere in such a way that the equations of motion give a closed set of equations. The model is the "direct interaction approximation" which replaces the non-linear term in the equations of motion. This approximation states that, for three Fourier components  $(p, q, r)$  giving the sides of a triangle in two dimensional wave number space (forming a "triad"), the inertial transfer of energy can be determined by the direct transfer between these components. The "indirect transfers", those interactions involving an intermediate mode, are neglected. This is justified by pointing out that as the region and therefore the number of permissible Fourier components is increased, the interaction between any three modes (triple correlations), becomes smaller, but, there are many more of these interactions, and thus the total effect of the inertial terms remains important. Also, it is safer to neglect the indirect interactions. In the inertial sub-range, this approximation gives:

$$E(k) \propto \epsilon^{1/2} k^{-3/2}$$

In the Kraichnan theory, direct interactions are possible between "energy containing" modes and those of very high wave number, whereas the Kolmogoroff theory relies on the "cascade" of energy on a more local scale between neighboring modes in k-space. Kraichnan suggests that, in the region of wave numbers below the inertial subrange, the direct interaction model may

be comparatively better than those depending on local transfer. This is the region where one can expect some interaction between the turbulent cells and the advecting flow (flow of relatively much lower wave number).

Thompson (1963) used a model of convection between two parallel infinite planes with thermal gradients in a thin boundary layer near each plate separated by a deep region where  $\partial\theta/\partial z \approx 0$ . He also imposed statistical stationarity of heat, momentum and vorticity transfer. In addition, he employed non-divergence and the Boussinesq approximation.

Thompson's results include the following:

(a) The thickness of the "boundary layer" is proportional to  $[Ra]^{-1/4}$ , where  $Ra$  is the Rayleigh number =  $g\beta l^4 (\frac{\partial T}{\partial z})^* / \nu^2$  used in Thompson (1963).

(b) The thickness of the boundary layer is independent of the total depth.

(c) The heat flux is proportional to  $(\Delta T_{emp})^{4/3} f(g, \alpha, \nu, k)$

(d) The variance of temperature reaches a maximum at the top of the boundary layer while the vertical velocity reaches a maximum in the middle of the region. This model has much in common with Herring (1963)'s results.

Lettau (1949) "generalized" mixing length theory to include the diabatic case by defining three parameters of turbulence:

(a)  $l = f(z, z_0)$

(b)  $u^* = f(\text{geostrophic wind}), u^* = l \frac{\partial u}{\partial z}$ , where  $u^0 = l' \frac{\partial u}{\partial z}$

(c)  $w^*$ ,  $u^* w^* = \overline{u^0 w^0}$ ,  $\overline{l^0 w^0} = l w^*$

With these three parameters ( $l, u^*, w^*$ ), a number of identities

are written, which helps explain their meaning. These identities are:

$$\tau = \rho l' \overline{w'} \frac{\partial u}{\partial z} = A \frac{\partial u}{\partial z} ; A = \rho l w^*$$

For isotropic turbulence,  $u_a^* = w_a^*$ ; the subscript, a indicates neutral stability. Then  $\tau_a = \rho \kappa_a^{*2}$ ,  $l_a = K(z+z_0)$ ,  $\frac{\partial u_a^*}{\partial z} \approx 0$

Lettau uses the heat flux, H, rather than  $\partial\theta/\partial z$  as the parameter of stratification.

$$H = -c A \frac{\partial \theta}{\partial z} ; A = \rho l' \overline{w'} = \rho l w^*$$

A is assumed to be the same for any air property.

For non-isotropic conditions,  $u^* \neq w^*$ . Lettau made the following assumptions:

$$(a) \frac{w^*}{l} = f\left(\frac{\partial \theta}{\partial z}\right); \text{ then } \frac{w^*}{l} = \frac{w_a^*}{l_a} \text{ and } \frac{w^*}{w_a^*} = \frac{l}{l_a}$$

(b) The buoyant acceleration influences directly only the vertical turbulence parameters. Then using  $\frac{w^{*2}}{l_a} = \text{vertical component of turbulent acceleration gives:}$

$$\frac{w^{*2}}{l} = \frac{w_a^{*2}}{l_a} - \frac{g l}{\theta} \frac{\partial \theta}{\partial z}$$

with this basis, he defined,

$$x = \frac{g}{\theta} \frac{\partial \theta / \partial z}{\left(\frac{\partial u_a}{\partial z}\right)^2} = \frac{\left(\frac{\partial u}{\partial z}\right)^2 Ri}{\left(\frac{\partial u_a}{\partial z}\right)^2}$$

Other associated identities are:

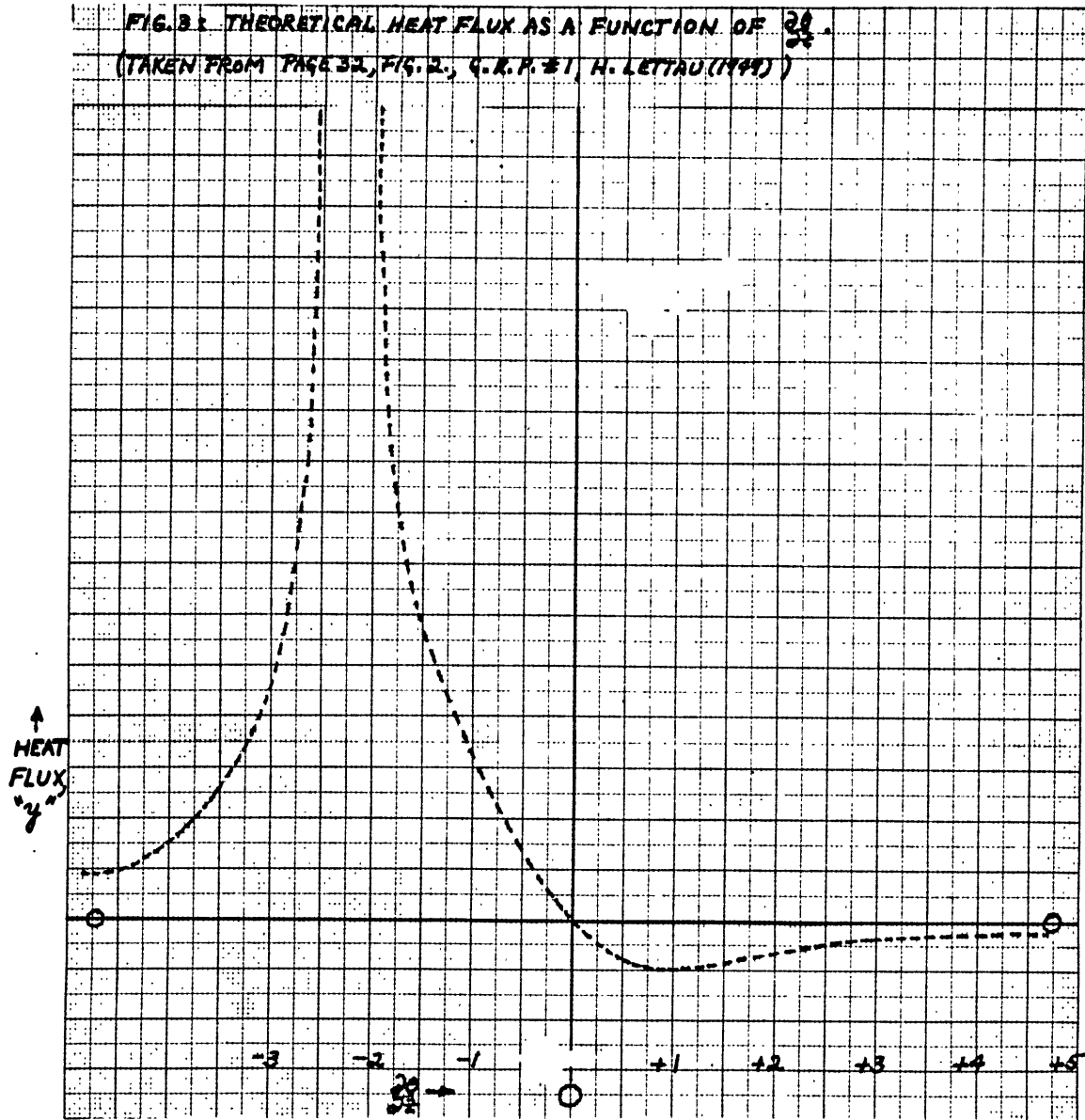
$$Q = \frac{ka}{1+x} ; \omega^* = \frac{\omega_a^*}{1+x} ; A = \frac{Aa}{(1+x)^2} ; H = \frac{c_p Aa \frac{\partial \theta}{\partial z}}{(1+x)^2}$$

Next he defined,  $y = \frac{gHk(z+z_0)}{c_p \rho \omega_a^* \omega}$ , giving  $y = \frac{-x}{(1+x)^2}$

Lettau described this system as follows: "y is defined proportional to the heat flux and independent of the gradient of potential temperature; x is defined proportional to the gradient of potential temperature and independent of the heat flux." This leads to the interesting result that  $y = \frac{-x}{(1+x)^2}$  (see p.32 of Lettau [1949]) which is reproduced as Figure 3 to show the predicted behavior of the heat flux, H. This figure indicates that a maximum of heat flux occurs at a moderately unstable value and that the heat flux decreases as the atmosphere becomes more unstable. There is also a negative maximum of heat flux in the slightly stable atmosphere (see Figure 20).

5. Similarity. Kolmogoroff (1941) postulated that, in the universal equilibrium range, the statistics of turbulence are definable as functions of  $\nu$  and  $\epsilon$  (see Section III B). From these, he formed a length scale,  $\eta = (\nu^3/\epsilon)^{1/4}$ , and a velocity scale,  $v = (\nu\epsilon)^{1/4}$ . Then by dimensional analysis he showed  $E(k) = v^2 \eta \phi(k\eta)$ , where k is wave number and  $\phi$  is a universal function of a dimensionless argument,  $k\eta$ . In the inertial sub-range,  $\nu$  is not important, thus  $E(k) = f(k)$  only. Using dimensional arguments once more, he concluded that  $E(k) \propto \epsilon^{2/3} k^{-5/3}$ .

Monin and Obukhov (1954) proposed a similarity theorem designed to





apply under conditions of non-isotropy in the surface layer (again see Section III B). They assumed the following parameters are constant in this layer:

- (a)  $g/\theta$  , buoyancy
- (b)  $g/c_p\rho = \omega^2 \tau'$  , heat flux
- (c)  $u^2 \omega' = \tau/\rho = v_*^2$  , momentum flux

From these, and using dimensional analysis, the following quantities were formed:

(a) Friction temperature,  $\tau^* = -\frac{L}{K v_*} \omega^2 \tau'$  ,  $K = \text{Von}$

Karman constant.

(b) Stability length,  $L = -v_*^3 / K \frac{g}{\theta} \omega^2 \tau'$

These can be used to derive expressions for non-dimensional shear and temperature gradient:

$$\frac{Kz}{v_*} \frac{dv}{dz} = \phi_1(z/L) \quad ; \quad \frac{z}{\tau^*} \frac{dT}{dz} = \phi_2(z/L)$$

If the exchange coefficients for momentum and heat are equal,  $\phi_1 = \phi_2 = \phi$  a universal dimensionless function. Also, it is shown that  $1/L = (\partial Ri / \partial z)_{z=0}$

The difficulties arising from the necessity of evaluating the above expression

at  $z = 0$ , are avoided by Neumann (1961), who defined the Richardson by the

expression,  $Ri = \alpha z/L + \beta (z/L)^2 + \dots$

. A series expansion of

$\phi(z/L)$  is chosen appropriate for the stability (or size of  $z/L$ ) and

upon integration, the following forms are obtained:

$$v(z) = \frac{v_*}{K} \left[ f(z/L) - f\left(\frac{h_0}{L}\right) \right] \quad h_0 = \text{height where } v = 0$$

$$\text{and } T(z) - T(z_0) = T^* \left[ f\left(\frac{z}{L}\right) - f\left(\frac{z_0}{L}\right) \right], \quad f = \int^z \frac{d(\epsilon)}{\epsilon} dz$$

$$\text{if } \frac{z}{L} \ll 1, \quad f\left(\frac{z}{L}\right) = \log\left(\frac{z}{L}\right) + C$$

$$\frac{z}{L} < 1, \quad f\left(\frac{z}{L}\right) = \log\left(\frac{z}{L}\right) + \beta \frac{z}{L}$$

$$\frac{z}{L} \gg 1, \text{ stable, } f\left(\frac{z}{L}\right) = \frac{z}{Ri L} + C, \text{ for } Ri < Ri_{\text{CRITICAL}}$$

$$\frac{z}{L} \ll -1, \text{ unstable, } f\left(\frac{z}{L}\right) = C \left(\frac{z}{L}\right)^{-1/3} + C$$

Batchelor (1953 A) showed that if the boundary permits a similarity transformation, then having the same Richardson number is a sufficient condition for dynamic similarity. He pointed out that a "bulk" rather than a "local" value for the Richardson number, is the appropriate one.

The analysis of Panofsky and Deland (1959) is based on Prairie Grass data. Normalized spectral analyses were given and there was also a comparison of these data with similar Brookhaven data. They used  $\frac{\eta S_i(w)}{U^2}$  versus  $\eta$  as coordinates ( $i = u, v, w$ ) and compared the energy spectral density of the three components under night (stable) and day (unstable) conditions; the height dependence of the turbulent energy was also examined. More detailed energy spectral density data are given in the papers immediately following.

Cramer (1960) analyzed the Prairie Grass data and presented these plots:  $\left\{ \begin{array}{l} \log \frac{S_{u,v}}{U^2} \text{ versus } \log \eta \\ \log \frac{S_{u,v}}{U^{2/3}} \text{ versus } \log \frac{\eta}{U} \end{array} \right\}$  and analyzed the stability dependence of

the normalized energy spectral densities. The stability was expressed in terms of the standard deviation of the azimuth angle (see his Figure 2). He concluded that the u-spectral energy density (in the log-log coordinates used above) approximates a -4/3 slope at high frequency.

Cramer, Record, Tillman and Vaughan (1961) and Cramer, Record and Tillman (1962) gave a description of the experimental technique used in collecting the Round Hill data and presented the power spectral and cospectral data for the u, v, and w components and temperature for fourteen one-hour runs at the 16-meter level and six one-hour runs at the 40-meter level. They expressed their results in many forms; those most closely associated with the present investigation are shown in their Figures 6a, b; 7a, b; 8a, b and 9a, b, which are based on:  $\log \frac{S_i \bar{U}}{U^2}$  versus  $\log \frac{n}{U}$   $i = u, v, \text{ and } w$ ;  $\log S_i \bar{U}$  versus  $\log \frac{n}{U}$ . These figures generally support a slope of approximately -5/3 at high frequency and a stability dependence at low frequency similar to that shown by Cramer (1960).

In addition to an evaluation of Monin-Obukhov and other profile theorems, Takeuchi (1961) plotted the Great Plains data in the following non-dimensional coordinates, using six twenty minute runs:

$\log \frac{\bar{U} S_i}{z U^2}$  versus  $\log \frac{n z}{U}$ ;  $n = \text{frequency}$ ,  $\bar{U} = \text{mean wind}$ ,  $S_i = \text{energy spectral density for } i = u, v \text{ and } w$ . (See his Figures 19a, b, and c).

For two ten minute runs at 16 meters height, Takeuchi (1963) gave the following plots:  $\log F_A$  versus  $\log n$ , where  $F_A = \text{variance of the azimuth angle} (\cong S_v / \bar{U}^2)$ , and also presented these in the form:

$$\log \frac{\bar{U}^3 F_A}{z U^2} \quad \text{versus} \quad \log \frac{n z}{U}$$

In general, both of these works showed spectra approximating

$c\eta^{-5/3}$  at high frequencies and stability dependence at lower frequencies.

Shiotani (1963) took data at 26 meters and obtained (after smoothing) plots of  $S_u(\eta)$  versus  $\eta$  and  $S_w(\eta)$  versus  $\eta$ . He compared  $S_u$  and  $S_w$  as a check of local isotropy, which gave on the average  $nz/\bar{U} = .46$  for the lower limit of isotropy. His spectral density functions are very close to  $c\eta^{-5/3}$  at high frequency. The analysis involved 6-15 runs.

Priestley (1959 A) obtained  $nz/\bar{U} = .6$  for the lower limit of isotropy.

Gurvich (1960) obtained as the lower limit of isotropy:  $nz/\bar{U} = .4$  for unstable case;  $nz/\bar{U} = .7$  for neutral;  $nz/\bar{U} = 1.9$  for the stable case.

Monin (1962) presented data in support of his universal function, derived by similarity in 1954. He also gave a plot of the power spectra of the temperature and w-components for six runs as a function of the Richardson number. His coordinates are:

$$\log \frac{S_w \bar{U}}{v_*^2 z} \text{ VERSUS } \log \frac{\eta z}{\bar{U}} ; \log \frac{\bar{U} S_T}{\eta_*^2 z} \text{ VERSUS } \log \frac{\eta z}{\bar{U}}$$

These coordinates are also used by Takauchi and later in this research.

Panofsky (1962) treated the turbulent energy budget and the vertical flux of turbulent kinetic energy, using the 23, 46 and 91-meter levels for 9 runs. The equation he considered is:

$$\frac{d\bar{E}}{dt} = \overline{u'w'} \frac{\partial \bar{U}}{\partial z} (1 - Rf) - \frac{\partial \overline{E'w'}}{\partial z} - \frac{1}{\rho} \frac{\partial \overline{p'w'}}{\partial z} - \varepsilon$$

Rf = flux form of the Richardson number.

He showed that the vertical divergence of turbulent kinetic energy is important in unstable cases.

Obukhov (1958) evaluated the validity of the following "structure" function forms (from similarity):

$$(\overline{\Delta V})^2 = B_V^2 l^{2/3}, \quad B_V = c, \quad c^{1/3} \quad \text{Evaluation gives } c, \approx 1.1$$

$$(\overline{\Delta T})^2 = B_T^2 l^{2/3}, \quad B_T = k \bar{N}^{1/2} \epsilon^{-1/6} \quad \text{where } \bar{N} = \chi (\overline{\sigma T})^2$$

$\chi$  = eddy thermal diffusivity.

By using  $\sigma_T \approx l \frac{d\bar{T}}{dz}$  and assuming  $\bar{T}(z) = T^* \log z + C$ , he derived

$B_T = c_2 \chi^{2/3} z^{-1/3} T^*$ . His evaluation gives  $c_2 \approx 2.4$ ; his Figure 7 gives a plot of  $B_T$  versus  $\chi^{2/3} z^{-1/3} T^*$ .

The second part of Obukhov's paper is concerned with the distribution functions of the oscillations. He graphed  $T^0$  values versus the probability density of occurrence; also he graphed stability versus

$$\frac{\sigma_{TEMP}}{\Delta T \text{ (evaluated between } z_1 \text{ and } z_2 \text{ )}}$$

Some results are:  $\sigma_T = .54 (T_1 \text{ meter} - T_4 \text{ meters})$

$$\sigma_w \approx 0.1 \bar{u}_2$$

and  $\sigma_w = .83 v^*$  (independent of height).

The standard deviation of the elevation angle and particularly the standard deviation of the azimuth angle ( $\sigma_A$ ) were dependent on stratification:

$\sigma_A = 5^\circ$  for unstable conditions;  $\sigma_A = 2.5^\circ$  for stable conditions.

#### IV. DATA COLLECTION AND PROCESSING TECHNIQUES.

##### A. Detailed description of the measurements.

The measurements were taken at Round Hill Field Station (M.I.T.), South Dartmouth, Mass. The tower on which the instruments were mounted is 143 ft. in height. The area immediately surrounding the tower is covered with beach grass, trimmed to 5-10 cm. height. The adjacent land area is covered with a mixture of grass, low shrubs and some small cedar trees. Buzzard's Bay borders the area to the south and east; 1100 ft. to the west is a wooded area and about 3/4 mile west of the tower is a north-south oriented ridge with a maximum elevation of 88 ft.

In this data sample there are twenty one-hour runs, taken simultaneously at 16 and 40 meters, of the fluctuations of the orthogonal velocity components and temperature, spanning a frequency range from  $N = .0014$  to  $N = .4 \text{ sec}^{-1}$ . The time spacing between measurements is 1.2 sec. In addition to the 60 lag analysis, a 10 lag analysis was done for high frequencies and a 30 lag analysis (each data point is an average of 10 points, giving a spacing of 12 sec.) was done for low frequencies. Power spectral and cospectral analyses for the three orthogonal velocity components and temperature and the possible combinations of these were obtained by digital computer analysis. Also total variance and co-variance statistics for these same elements are available, together with the vertical profile data for the mean wind and temperature associated with each run.

The fluctuations of wind were measured by heated bead thermistor anemometers (speed) and lightweight mechanical bivanes; the temperature fluctuations were measured by the change of resistance in platinum wire probes.

The output of each transducer is fed into an amplifier-filter circuit. An analog-to-digital encoder takes the circuit output and converts it to binary number representation. Finally, a programmer samples the encoder output once per second (represented by a number between 1 and 256) and prints the data on a punched paper tape. See Section III of Cramer, Record, Tillman and Vaughan (1961) for details of this data acquisition system. In decoding, this information is converted to decimal data, put on IBM punched cards or magnetic tape and fed into a computer for spectral and cospectral analysis.

#### B. Explanation of the data processing.

Prior to spectral and cospectral analysis, the wind speed and bivariate measurements are converted into orthogonal velocity components. The following procedure is used: commencing with a set of approximately 3600 data points, consisting of a velocity,  $V_i$ ; an azimuth angle,  $A_i$ ; and an elevation angle,  $E_i$ , these are converted into fluctuations of each component about its mean value. It is necessary to define a virtual mean azimuth angle,

$$A^* = \frac{\sum_{i=1}^N V_i \cos(E_i - E^*) \sin A_i}{\sum_{i=1}^N V_i \cos(E_i - E^*) \cos A_i}, \quad N \approx 3600$$

and a virtual mean elevation angle,  $E^* = \frac{\sum_{i=1}^N V_i \sin E_i}{\sum_{i=1}^N V_i \cos E_i}$

Then the velocity component fluctuations become:

$$u_i = U_i - \bar{U}$$

$$V_i = V_i \cos(E_i - E^*) \sin(A_i - A^*)$$

$$w_i = V_i \sin(E_i - E^*)$$

where

$$\bar{U} = \frac{1}{N} \quad U_i, \text{ and } U_i = V_i \cos(E - E^*) \cos(A_i - A^*)$$

and  $\bar{u}, \bar{v}$  and  $\bar{w} = 0$

The data is smoothed by a 601 point running mean and this mean is subtracted from the unaveraged record, in order to remove long period fluctuations and drifts in the mean value. This differenced data forms the input to the computer. Variance spectra calculations follow procedures described by Blackman and Tukey (1958). First an auto-covariance function,  $A_L$  is computed.

$$A_L = \left[ \frac{1}{N-L} \sum_{i=L+1}^N X_{i-L} X_i \right] - \left[ \frac{1}{(N-L)^2} \sum_{i=L+1}^N X_{i-L} \sum_{i=L+1}^N X_i \right]$$

where  $N$  = total number of observations

$L$  = the lag number

$M$  = maximum number of lags

Then the following equations are used to obtain smoothed power spectral estimates:

$$X_0 = \frac{1}{2M} \left[ A_0 + \sum_{L=1}^{M-1} A_L \cos \frac{KL\pi}{M} \left( 1 + \cos \frac{L\pi}{M} \right) \right]$$

$$X_k = \frac{1}{M} \left[ A_0 + \sum_{L=1}^{M-1} A_L \cos \frac{KL\pi}{M} \left( 1 + \cos \frac{L\pi}{M} \right) \right]; \quad 1 \leq k \leq M-1$$

where  $1 + \cos \frac{L\pi}{M}$  is a cosine weighting factor.

$$X_M = \frac{1}{2M} \left[ A_0 + \sum_{L=1}^{M-1} A_L \cos \frac{KL\pi}{M} \left( 1 + \cos \frac{L\pi}{M} \right) \right]$$



These smoothed values are in units of variance per unit frequency interval,  $\Delta K = \frac{1}{2M\Delta t}$ . The quantity,  $\Delta t$ , is the time interval between observations and equals about 1.2 sec.

Cospectral estimates are derived in a similar manner by replacing  $x_i$  by  $y_i$  in the equation for  $A_L$ . For a description in complete detail, refer to Cramer, Record, Tillman and Vaughan (1961).

### C. Data reliability.

In analyzing the lowest frequencies, the initial data set is reduced tenfold by taking consecutive block averages of each ten points. This results in a new  $\Delta t$  of 12 sec; the maximum number of lags used is 30. Advantage has been taken of symmetry so that cosine functions up to periods of 720 sec. can be evaluated. As shown by Panofsky and Brier (1958), the number of degrees of freedom for a moving lag window is  $\frac{2N-m/2}{m}$ , where N is the total number of observations, m is the maximum number of lags, and S is the spacing of data points. Then the degrees of freedom, df, for the 30 lag analysis (S = 12sec.) is 19.5 and for 60 lag analysis (S = 1.2 sec.) is 99.5. There is an 80 per cent chance that the observed values, for 30 lag analysis, are between .62 and 1.41 times the true value (Tukey and Blackman [1958]).

For simplicity and also for desirable smoothing the high-frequency spectral and cospectral estimates ( 60 lag analysis) have been combined into the following list of wave number groups:

K (wave number of original data)	K (adjusted)
7 - 8	7.5
9 - 11	10
12 - 15	13.5
16 - 20	18
21 - 27	24
28 - 36	32
37 - 47	42
48 - 60	54

In the digitally analyzed time series, thought has to be given to: distortion of spectral data at the high frequency end of the spectrum and to errors in the spectral density at  $n = 1/360 \text{ sec}^{-1}$  and  $n = 1/720 \text{ sec}^{-1}$  resulting from those fluctuations in the time series of periods longer than 720 sec (maximum period that the lag window can see), which has not been completely filtered out.

Aliasing at high frequencies is usually relatively easy to identify due to the effect on the shape of the energy spectral density function. At high frequency this function (in log-log coordinates) usually has a uniform slope of about  $-5/3$ , hence aliasing would give a nearly flat horizontal graph. Then an abrupt transition from a  $-5/3$  slope to a much less slope in going from lower to higher frequencies is an indication of high frequency aliasing.

Then only the low frequency end of the spectrum has to be considered further. The data-processing techniques have the effect of a band-pass filter [see Chapter I of Pasquill (1962)]. This filtering action is represented by the expression (variance seen by the system)

$$= (\text{True variance}) \int_0^{\infty} \left[ 1 - \frac{\sin^2 \pi n \tau}{(\pi n \tau)^2} \right] \frac{\sin^2 \pi n s}{(\pi n s)^2} \left[ 1 - \frac{\sin^2 \pi n T}{(\pi n T)^2} \right] F(n) \, dn$$

where  $F(n)$  = Fourier transformed normalized covariance function,  
 $S$  = sampling interval,  $\tau$  = maximum lag, and  $T$  = overall record length.  
 The nature of this function is seen in Figure 4, below.

The low-frequency range difficulty arises in determining where the analysis distributes that variance of periods in excess of 720 sec., which the system should not observe. Without including the computational work, an estimate of the "low frequency aliasing" was made by assuming a spectral energy density function,  $E(n) \propto n^{+c}$  and taking  $c = -5/3$  and  $c = +1/3$  as including the range of  $E(n)$  functions at low frequency.

A numerical integration was carried out and the results are listed below:

1.  $T = 720$  sec.

- (a)  $c = -5/3$ , True value is 83 per cent of observed value.
- (b)  $c = +1/3$ , True value is 124 per cent of observed value.

2.  $T = 360$  sec.

- (a)  $c = -5/3$ , True value is 132 per cent of observed value.
- (b)  $c = +1/3$ , True value is 102 per cent of observed value.

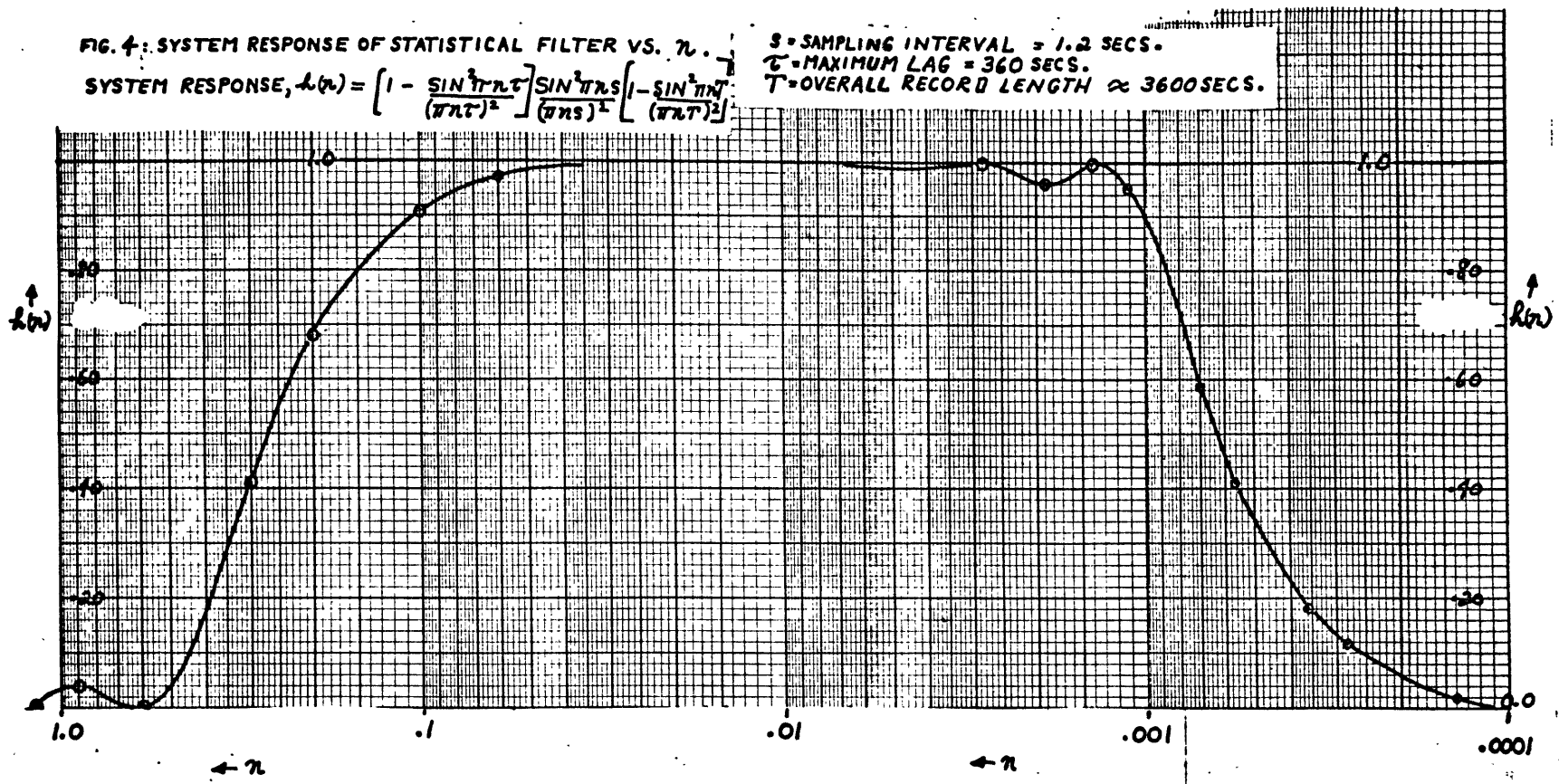
There is some error in these, since a more exact evaluation would apply to individual data points rather than the assumed smooth function. In comparing the results above to the spread permitted by the 80 per cent confidence limits, it is seen that a correction to the data at  $T = 360$  and  $720$  sec. is not necessary.

For several reasons, it is very difficult to do anything about increasing the reliability of the data without taking simultaneous time series measurements at several points or resorting to measurements over

FIG. 4: SYSTEM RESPONSE OF STATISTICAL FILTER VS.  $\omega$ .

$$\text{SYSTEM RESPONSE, } h(\omega) = \left[ 1 - \frac{\sin^2 \pi \omega T}{(\pi \omega T)^2} \right] \frac{\sin^2 \pi \omega S}{(\pi \omega S)^2} \left[ 1 - \frac{\sin^2 \pi \omega T}{(\pi \omega T)^2} \right]$$

S = SAMPLING INTERVAL = 1.2 SECS.  
 T = MAXIMUM LAG = 360 SECS.  
 T = OVERALL RECORD LENGTH  $\approx$  3600 SECS.



a space network and evaluating  $\overline{u_i(\vec{x}, t) u_j(\vec{x} + \vec{r}, t)}$ . To increase the number of degrees of freedom for a single time series at a point one would either have to shorten the span of the lag window and thus cut down the maximum observable period, or increase the total length of record. If record lengths of more than an hour are used, then changes of the meteorological parameters,  $\bar{u}$  and  $\partial\theta/\partial z$ , may be expected and the observational result would be a combination of more than one turbulence regime. Also, at the longest time scales, Taylor's hypothesis ( $x = \bar{u}t$ ) is less dependable. It appears there is no choice left but to measure space correlation functions of the fluctuations. Even then difficulty arises because, although horizontal homogeneity may be a good assumption for stable stratification and forced convective regimes, it is probably a poor one for free convective regimes (in the very low frequency range). One can imagine semi-permanent "thermals" over terrain features such as bare surfaces next to wooded or water areas. Here horizontal fluxes and the lack of horizontal homogeneity would be important. Despite all these difficulties, if one had a homogeneous lower boundary, it seems that the average value of the spectral density of energy at a point would be a reasonable first estimate of its spatially averaged value. Then the low frequency observations here should be reasonable, including the occurrence of a maximum of convective energy at low frequencies, as shown in Figures 8 - 15, 24, 25, 26 and 27. Most of these observations were taken under northwest flow patterns at Round Hill, where the effect of sea proximity on horizontal homogeneity is minimized. The light wind cases with convection and those having sea trajectories, or trajectories parallel to the shore

are more difficult to evaluate.

## V. DESCRIPTION OF THE RESEARCH

### A. Method of approach.

The investigation proceeds in the following order:

1. Definition and explanation of the necessary derived statistics.
2. Presentation of the pertinent statistics for the twenty runs in tabular form.
3. A discussion of the choice of parameters to express the effects of thermal stratification and the lower boundary.
4. Presentation of the power spectral data in Monin-Obukhov similarity coordinates.
5. Presentation of the empirical results, including the identification of the isotropic range.
6. A comparison of these empirical results with those obtained by other investigators.
7. A comparison of empirical results with those predicted by theory and a selection of those theories which are in best agreement with the analyzed data.
8. A suggested model for energy spectral density functions.

### B. Definition of derived turbulence statistics.

The following is a list of some of the derived statistics used in the data analysis. Additional statistics are either defined in the

TABLE 1: SAMPLE COMPUTATION SHEET FOR THE MONIN-OBUKHOV SIMILARITY NORMALIZATION (1 OF 40)

RUN 67A  
16 METERS

$$\bar{U}_{16} = 5.74 \text{ m/sec}$$

$$V^* = .456$$

$$T^* = -\frac{1}{K V^*} \bar{w} T' = .171^\circ\text{C}$$

$$\frac{z}{U_*} = 2.79$$

$$\bar{w} T' = -.2085$$

[DOWNWARD]

$$\bar{w} T' = -.0312$$

[DOWNWARD]

$$\frac{\bar{U}_{16}}{V^{*2z}} = 1.722$$

$$\frac{\bar{U}_z}{T^{*2z}} = 12.3$$

$$\bar{S}_i = \frac{S_i \bar{U}}{V^{*2z}}$$

$$\bar{S}_T = \frac{S_T \bar{U}}{T^{*2z}}$$

ENERGY  
S<sub>i</sub> = SPECTRAL DENSITY

PERIOD [SECS]	S <sub>u x n</sub>	S <sub>u</sub>	S <sub>u</sub>	S <sub>v x n</sub>	S <sub>v</sub>	S <sub>v</sub>	S <sub>w x n</sub>	S <sub>w</sub>	S <sub>w</sub>	S <sub>T x n</sub>	S <sub>T</sub>	S <sub>T</sub>	$\eta = \frac{z/\bar{U}}{T'(\text{SECS})}$
7.20	.0302	21.8	37.6	.00205	1.475	2.54	.00133	.957	1.65	.000831	.599	7.36	.00387
3.60	.0909	32.7	56.3	.00765	2.75	4.73	.00394	1.42	2.44	.00263	.946	11.6	.00775
2.40	.124	29.8	51.3	.0152	3.65	6.28	.00452	1.085	1.87	.00240	.624	9.67	.01162
1.80	.169	30.4	52.4	.0272	4.90	8.44	.00493	.887	1.53	.00248	.446	5.49	.0155
1.44	.193	27.8	47.8	.0391	5.625	9.68	.00807	1.162	2.00	.00362	.521	6.40	.0194
1.20	.152	18.96	32.6	.0481	5.77	9.93	.0122	1.462	2.52	.00338	.406	5.00	.0232
1.03	.112	11.53	19.9	.0520	5.35	9.21	.0161	1.66	2.86	.00203	.209	2.57	.0271
.90	.174	15.68	27.0	.0516	4.65	8.00	.0185	1.67	2.87	.00254	.229	2.82	.0310
.72	.342	25.1	43.2	.0853	6.14	10.6	.0215	1.55	2.67	.00631	.455	5.59	.0387
.55.4	.353	19.6	33.8	.107	5.93	10.2	.0372	2.06	3.55	.00631	.350	4.30	.0508
.36	.331	11.9	20.5	.158	5.69	9.80	.0527	1.90	3.27	.00578	.208	2.56	.0775
.28	.342	9.57	16.5	.182	5.09	8.76	.0693	1.94	3.34	.00625	.175	2.15	.0996
.24	.398	7.15	12.3	.157	3.77	6.49	.0852	2.045	3.52	.00605	.145	1.79	.1162
.20.67	.242	4.98	8.58	.160	3.29	5.66	.0946	1.945	3.35	.00598	.123	1.51	.136
.14.4	.219	3.15	5.42	.159	2.29	3.94	.0809	1.165	2.01	.00574	.083	1.02	.194
10.67	.220	2.35	4.05	.163	1.74	3.00	.0946	1.01	1.74	.00613	.065	.804	.262
.8	.196	1.57	2.70	.196	1.57	2.70	.0905	.724	1.25	.00492	.0394	.484	.349
.6	.152	.912	1.57	.137	.822	1.42	.103	.618	1.065	.00438	.0263	.323	.465
.4.5	.128	.576	.912	.117	.527	.907	.108	.486	.836	.00366	.0165	.203	.620
.3.43	.099	.340	.576	.105	.360	.620	.098	.336	.578	.00258	.00885	.109	.813
.2.67	.083	.248	.427	.089	.237	.408	.084	.226	.388	.00197	.00526	.065	1.045

TABLE 2: SAMPLE COMPUTATION SHEET FOR THE MONIN-OBUKHOV SIMILARITY  
 NORMALIZATION ( 1 OF 40 )

RUN 67A  
 40 METERS

$$U_{40} = 7.62 \text{ M/SEC}$$

$$V_{*} = .450$$

$$T_{*} = -\frac{1}{K V_{*}} \overline{w'T'} = .186^{\circ}\text{C}$$

$$\frac{z}{U_{40}} = 5.25$$

$$\overline{w'w'} = -2.032 \text{ (DOWNWARD)}$$

$$\frac{\overline{U}_{40}}{V_{*}^2} = .939$$

$$\frac{\overline{U}_{40}}{T_{*}^2} = 5.54$$

$$\overline{S}_i = \frac{S_i \overline{U}}{V_{*}^2 z} = \text{NORMALIZED ENERGY SPECTRAL DENSITY}$$

PERIOD (SECS)	$S_{u \times \tau}$	$S_u$	$\overline{S}_u$	$S_{v \times \tau}$	$S_v$	$\overline{S}_v$	$S_{w \times \tau}$	$S_w$	$\overline{S}_w$	$S_{T \times \tau}$	$S_T$	$\overline{S}_T$	$\tau = \frac{z(\overline{U})}{T'}$ (SECS)		
7.20	.0211	15.2	14.3	.00412	2.96	2.79	.00177	1.275	1.20	.000605	.436	2.92	.00729		
360	.0457	16.4	15.4	.0134	4.82	4.53	.00594	2.14	2.01	.00144	.578	2.87	.0146		
240	.0503	12.1	11.4	.0229	5.50	5.17	.00897	2.03	1.91	.00152	.365	2.02	.0219		
180	.0861	15.5	14.6	.0276	4.96	4.66	.00957	1.72	1.62	.00229	.412	2.28	.0292		
144	.130	18.7	17.6	.0275	3.96	3.72	.0140	2.02	1.89	.00291	.418	2.32	.0365		
120	.171	20.5	19.3	.0245	2.94	2.76	.0164	1.97	1.85	.00369	.443	2.46	.0438		
103	.199	20.5	19.3	.0290	2.99	2.81	.0139	1.43	1.34	.00529	.545	3.02	.0570		
90	.205	18.5	17.3	.0441	3.97	3.73	.0146	1.32	1.24	.00557	.502	2.78	.0583		
72	.226	16.3	15.3	.0689	4.96	4.66	.0212	1.53	1.44	.00425	.306	1.70	.0729		
55.4	.216	12.0	11.3	.0749	4.15	3.90	.0456	2.53	2.38	.00672	.372	2.06	.0947		
36	.242	8.71	8.27	.161	5.80	5.45	.0544	1.96	1.84	.00721	.260	1.44	.146		
28	.264	7.39	6.94	.177	5.00	4.70	.0689	1.93	1.82	.00815	.228	1.26	.188		
24	.245	5.88	5.53	.165	2.96	3.72	.0789	1.89	1.78	.00822	.197	1.09	.219		
20.57	.225	4.62	4.33	.173	3.56	3.34	.0933	1.92	1.80	.00710	.146	.808	.255		
14.4	.204	2.94	2.76	.180	2.59	2.43	.123	1.77	1.66	.00590	.078	.481	.365		
10.67	.152	1.62	1.52	.206	2.20	2.07	.145	1.55	1.46	.00560	.060	.332	.472		
8	.162	1.30	1.22	.174	1.39	1.31	.124	.992	.931	.00455	.036	.202	.656		
6	.121	.726	.682	.161	.966	.907	.112	.672	.631	.00329	.0198	.109	.875		
4.5	.104	.468	.440	.131	.590	.554	.103	.463	.435	.00307	.0138	.0765	1.167		
3.43	.081	.277	.260	.120	.412	.387	.100	.343	.322	.00204	.00700	.0388	1.63		
2.67	.073	.196	.184	.085	.227	.217	.0833	.223	.209	.00142	.00379	.0210	1.97		

48



TABLE 3: GENERAL STATISTICS FOR THE RUNS, PART A.

+ AFTER 601 RUNNING MEAN FILTER

RUN	U M/SEC	TA DEGREES	-U'W' M/SEC <sup>2</sup>	V* M/SEC	W'T1 M °C/SEC	T* °C	z/L	g/θ M/SEC <sup>2</sup> °C	ΔTEMP. SPC-8M. °C	16-40M. ΔWIND M/SEC	KEYPS# °C	σ <sub>a</sub> DEGREES
66D 16m	4.01	6.9	.0778	.278	-.0178	+1.59	+1.87	.0346	+2.6 °C	1.92		3.7
+ 40m	5.93	5.5	.0710	.277	-.0198	+1.78	+1.516					2.7
66E 16	4.30	5.4	.0501	.224	-.0126	+1.40	+2.18	.0347	+2.5	1.99		3.1
⊙ 40	6.29	4.8	.0774	.278	-.0184	+1.66	+4.79					2.4
66F 16	5.14	6.2	.1176	.342	-.0292	+2.13	+1.65	.0348	+1.5	1.89		3.4
⊖ 40	7.03	5.4	.1571	.388	-.0316	+2.04	+3.05					2.9
67A 16	5.74	6.5	.208	.456	-.0312	+1.71	+1.05	.0349	+1.5	1.88		3.8
∞ 40	7.62	5.5	.203	.450	-.0334	+1.85	+2.09					2.9
67B 16	5.89	7.3	.265	.514	-.0328	+1.59	+1.05	.0349	+1.1	1.74	.14	4.6
X 40	7.63	5.6	.254	.503	-.0373	+1.85	+1.66					3.3
67C 16	6.23	8.4	.333	.577	-.0075	+0.324	+0.089	.0349	-0.2	.88	.22	6.3
* 40	7.11	7.7	.387	.622	-.0049	+0.198	+0.114					5.6
67D 16	7.39	12.6	.360	.600	+0.0674	-.281	-.0717	.0344	-1.6	.68	.38	10.4
△ 40	8.07	10.8	.407	.637	+0.0893	-.350	-.180					9.0
67E 16	9.58	14.4	.623	.789	+0.133	-.420	-.062	.0342	-2.0	1.06	.64	12.0
∇ 40	10.64	12.8	.865	.729	+0.182	-.491	-.119					10.3
67G 16	9.49	14.7	.678	.772	+0.155	-.501	-.0757	.0339	-3.0	.98	.66	11.8
⊙ 40	10.47	13.7	.930	.963	+0.245	-.637	-.157					10.8
31 16	3.55	12.7	.150	.388	+0.0039	-.0248	-.0149	.0352	0.0	.74	.08	9.9
○ 40	4.29	11.8	.209	.458	+0.0042	-.0228	-.0245					8.6
32 16	6.27	14.6	.387	.622	+0.104	-.418	-.0985	.0349	-1.1	.40	.28	12.4
□ 40	6.67	12.3	.869	.933	+0.133	-.356	-.0933					9.5
33 16	5.54	17.2	.216	.465	+0.0990	-.532	-.208	.0345	-2.0	.27	.23	10.4
▽ 40	5.81	14.5	.555	.745	+0.159	-.532	-.215					12.0
34 16	4.70	18.2	.231	.481	+0.0857	-.446	-.159	.0342	-1.5	.35	.16	14.6
⊖ 40	5.05	18.5	.279	.529	+0.117	-.551	-.414					14.5
35 16	1.04	3.4	.0083	.091	-.0035	+0.099	+1.021	.0344	+3.0	2.45		1.4
■ 40	6.50	2.3	.0021	.046	-.0001	+0.061	+5.01					0.9
36 16	4.55	4.7	.0138	.118	-.0060	+0.128	+0.808	.0343	+2.2	2.59		1.6
● 40	7.19	4.4	.0023	.047	-.0010	+0.054	+5.245					1.3
38 16	6.12	18.3	.240	.490	+0.117	-.598	-.225	.0349	-2.1	.36	.31	14.8
⊙ 40	6.48	17.9	.568	.754	+0.142	-.472	-.182					12.9
39 16	5.81	15.1	.316	.562	+0.0424	-.189	-.0548	.0346	-1.0	.88	.21	10.6
⊖ 40	6.69	14.7	.533	.730	+0.0697	-.239	-.0999					10.4
40 16	3.67	4.7	.0255	.160	-.0080	+0.125	+0.356	.0350	+2.2	1.81		2.9
● 40	5.98	3.5	.0408	.202	-.0108	+0.134	+0.735					2.0
41 16	5.03	7.0	.0949	.308	-.0219	+0.178	+1.59	.0351	+1.4	1.58		4.0
▽ 40	6.61	6.5	.126	.355	-.0321	+0.216	+0.373					3.6
42 16	4.21	7.3	.106	.325	-.0225	+0.173	+1.49	.0352	+1.6	1.59		4.7
▲ 40	5.80	6.0	.128	.358	-.0290	+0.202	+0.351					3.4

49

TABLE 4: GENERAL STATISTICS FOR THE RUNS, PART B.

RUN	1-4 METERS		4-32 METERS		16-40 METERS		H*		
	$\frac{20}{32}$	Ri	$\frac{20}{32}$	Ri.	$\frac{20}{32}$	Ri.			
66D 16M	+0.366	+0.203	+0.039	+0.194	+0.025	+0.135	-0.043		
+ 40M							-0.017		
66E 16	+0.333	+0.163	+0.046	+0.227	+0.029	+0.147	-0.031		
⊙ 40							-0.015		$Ri = \frac{20}{32} \frac{20}{32}$
66F 16	+0.167	+0.080	+0.036	+0.165	+0.021	+0.117	-0.090		$(\frac{24}{32})^2$
⊙ 40							-0.035		
67A 16	+0.167	+0.033	+0.025	+0.160	+0.017	+0.095	-0.170		
∞ 40							-0.048		
67B 16	+0.133	+0.043	+0.018	+0.100	+0.017	+0.111	-0.310		$H* = \frac{W' \pi}{(9/16)^{1/2} (\frac{20}{32})^{3/2} 2^2}$
X 40							-0.058		
67C 16	-0.033	-0.010	+0.004	+0.045	+0.004	+0.109	+0.079		
* 40							-0.162		
67D 16	-0.200	-0.044	-0.011	-0.117	-0.008	-0.356	+1.57		
Δ 40							+0.437		
67E 16	-0.230	-0.030	-0.018	-0.110	-0.012	-0.218	+1.115		
∇ 40							+0.370		
67G 16	-0.300	-0.032	-0.021	-0.161	-0.012	-0.254	+1.046		
◇ 40							+0.573		
31 16	-0.067	-0.146	+0.007	0.0	+0.004	+0.154	→+∞		
⊙ 40							+0.050		
32 16	-0.167	-0.063	-0.007	-0.107	0.0	0.0	+3.61		
□ 40							→+∞		
33 16	-0.300	-0.142	-0.007	-0.175	0.0	0.0	+3.44		
∇ 40							→+∞		
34 16	-0.230	-0.157	-0.004	-0.142	0.0	0.0	+8.48		
⊙ 40							→+∞		
35 16	+0.400	+0.143	+0.100	+0.275	+0.050	+0.164	-0.0027		
⊙ 40							-0.00003		
36 16	+0.333	+0.142	+0.097	+0.224	+0.050	+0.146	-0.0042		
⊙ 40							-0.0003		
38 16	-0.230	-0.076	-0.018	-0.178	0.0	0.0	+1.40		
⊙ 40							→+∞		
39 16	-0.133	-0.045	0.0	0.0	+0.004	+0.108	→+∞		
⊙ 40							+0.975		
40 16	+0.300	+0.136	+0.046	+0.297	+0.025	+0.154	-0.019		
⊙ 40							-0.009		
41 16	+0.167	+0.071	+0.025	+0.141	+0.017	+0.135	-0.117		
∇ 40							-0.058		
42 16	+0.200	+0.113	+0.025	+0.169	+0.017	+0.134	-0.138		
▲ 40							-0.044		

TABLE 5: GENERAL STATISTICS FOR THE RUNS (AUXILIARY DATA).

\* DATA DOUBTFUL  
+ AFTER 601 RUNNING MEAN

RUN	U	O <sub>A</sub>	-W/W'	W/T <sub>1</sub>	ΔTEMP	ΔWIND	16-40M.		4-32M.		R <sub>i</sub>	z/L	O <sub>A</sub> + DEGREES
							M/SEC	DEGREES	M/SEC	DEGREES			
7B	16	4.78	12.0	.135	+.086	-1.4	.37	-.012	-.200	0.0	0.0	-.381	3.4
8	16	3.82	5.4	.018	-.004	+2.1	2.07	+.045	+.300	+.029	+.135	+.365	3.5
9	16	5.92	11.6	.246	-.006	+0.1	.73	+.006	0.0	0.0	0.0	+.0110	8.7
10	16	4.19	7.9	.049	-.007	+2.9	1.41	+.035	+.400	+.017	+.173	+.145	4.0
12	16	4.42	7.0	.059	-.016	+2.3	2.12	+.052	+.367	+.037	+.168	+.254	3.3
14	16	4.05	19.8	.057	+.075	-1.9	.14	-.012	-.233	-.004	-4.20	-1.26	13.4
15	16	3.76	11.7	.082	+.011	-0.1	.32	0.0	0.0	-.004	-.800	-.107	8.1
16	16	8.20	14.2	.577	+.056	-1.2	.84	-.008	-.167	-.004	-.113	-.027	10.7
20	16	5.53	7.7	.156	-.024	+1.6	1.78	+.038	+.167	+.025	+.153	+.034	8.9
	40	7.31	5.7	.106	-.026							+.394	5.4
63A	16	8.08	16.3	.492	+.163	-2.9	.65	-.018	-.300	*-.004	-.185	-.103	12.7
	40	8.74	15.8	.732	+.197							-.171	11.1
63B	16	8.27	16.0	.522	+.168	-2.9	.59	-.014	-.300	*-.004	-.224	-.096	13.8
	40	8.86	14.4	.634	+.215							-.230	12.4
64A	16	8.41	14.1	.496	+.141	-2.8	.60	-.018	-.367	*-.008	-.442	-.090	10.7
	40	9.01	12.9	.863	+.240							-.165	9.3
64B	16	9.42	15.5	.696	+.194	-2.9	.60	-.018	-.333	*.008	-.441	-.074	14.9
	40	10.02	13.8	.981	+.257							-.147	13.2
65A	16	9.10	15.3	.500	+.166	-3.0	.54	-.018	-.267	*.004	-.270	-.103	14.1
	40	9.64	13.9	.724	+.200							-.178	12.1
65B	16	9.62	18.9	.622	+.121	-2.1	.62	-.004	-.233	*.004	-.204	-.056	11.4
	40	10.24	17.1	.968	+.129							-.072	10.4
66A	16	7.93	14.1	.437	+.011	-0.1	.56	+.006	0.0	*0.0	0.0	-.008	9.7
	40	7.99	13.3	.706	+.011							-.010	8.5
66B	16	6.25	11.3	.320	-.045	+1.3	.78	+.017	+.133	*+.008	+.258	+.056	7.1
	40	7.03	10.3	.388	-.012							+.028	6.3
66C	16	3.65	8.5	.030	-.004	+4.0	1.80	+.045	+.500	*+.029	+.178	+.161	3.5
	40	5.45	7.5	.022	-.012							+.089	2.2
67F	16	10.45		*.235	-.118*	-2.7	1.09	-.022	-.267	*.008	-.133	*	3.4
	40	11.54		*.318	-.125*							*	3.0
68	16	3.67	21.7	.067	+.052	-1.9	.21	-.008	-.167	*+.004	+.178	-.650	16.0
	40	3.88	18.4	.032	+.094							-.890	13.4
69A	16	7.27	8.8	*.072	-.098	-4.1	.61	0.0*	-.600	*+.008	+.425	*	4.2
	40	7.88	7.0	*.016	-.034							*	3.2
69B	16	8.72	7.4	*.137	-.021	-3.7	.75	+.016	-.533	*+.017	+.410	*	3.3
	40	9.47	4.4	*.069	+.003							*	2.0
84A	16	5.02		.373	+.028	-0.4	.87	0.0	-.033	-.008	-.216	-.028	7.7 (1)
	40	5.89		.195	+.009							-.060	6.7
84B	16	5.02		.195	+.009	-0.2	.54	0.0	0.0	-.004	-.282	-.024	4.7
	40	5.56		.394	+.015							-.054	7.4

51

TABLE 6: VERTICAL PROFILE DATA FOR MEAN TEMPERATURE AND MEAN HORIZONTAL WIND.

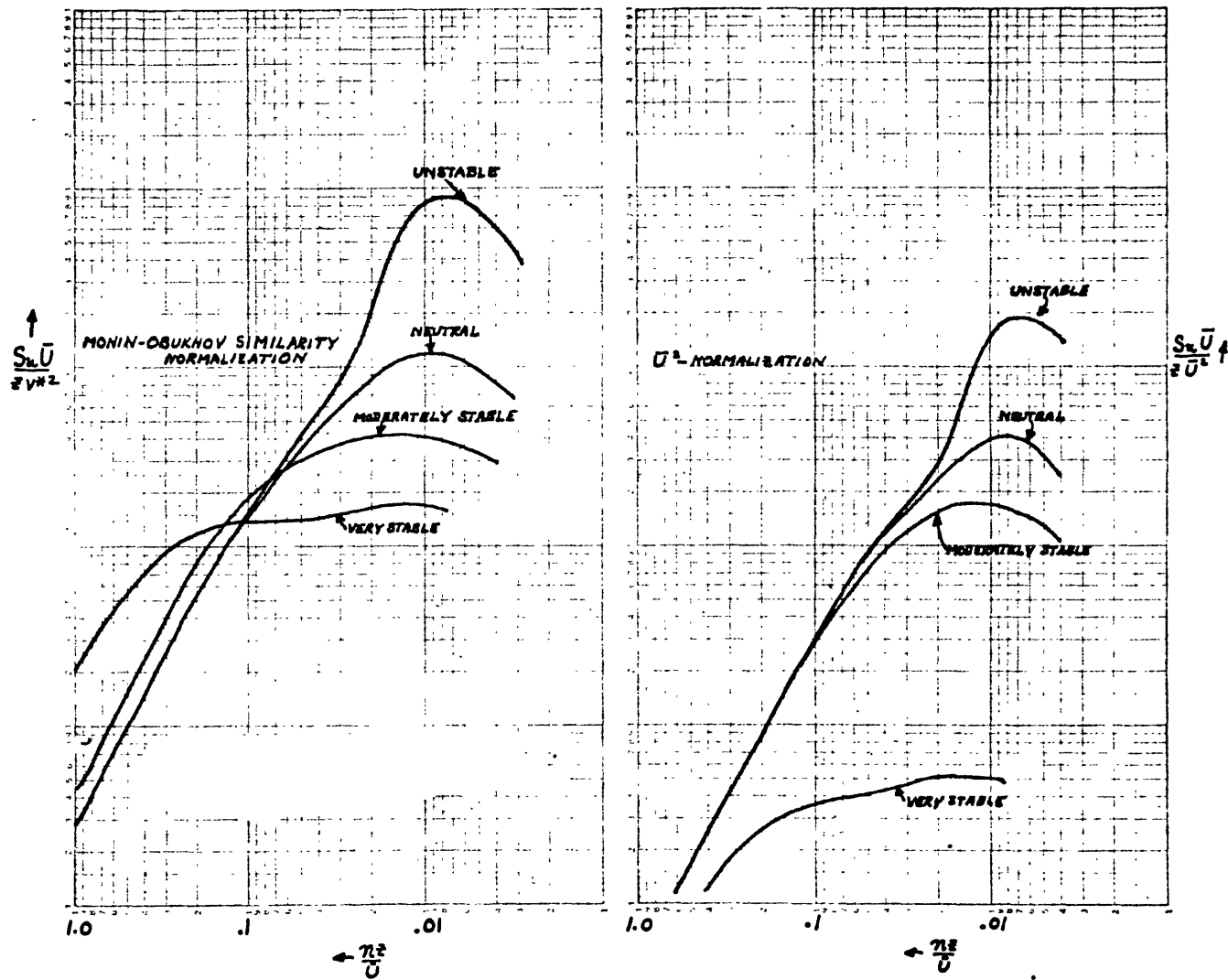
RUN	LEVEL (METERS)	.25	.5	1	2	4	8	16	32	40	.12
66D	WIND - M/SEC	7.9	8.3	2.13	2.50	2.88	3.28	4.01	5.22	5.93	7.6
+	TEMP - °C			8.8	9.4	9.9	10.2	10.5	10.8	10.9	
66E	W	6.4	6.8	2.19	2.52	2.98	3.58	4.30	5.34	6.29	6.2
⊙	W			7.2	7.7	8.2	8.7	9.0	9.3	9.5	
66F	W	7.0	7.2	2.96	3.31	3.77	4.36	5.14	6.20	7.03	6.8
⊙	W			7.5	7.7	8.0	8.3	8.5	8.8	8.8	
67A	W	6.4	6.7	3.51	3.98	4.78	4.98	5.74	6.86	7.62	6.2
∞	W			7.0	7.2	7.5	7.7	7.8	8.0	8.0	
67B	W	6.5	6.7	3.76	4.26	4.74	5.19	5.89	6.94	7.63	6.4
X	W			7.0	7.2	7.4	7.5	7.6	7.7	7.8	
67C	W	9.4	9.4	4.28	4.80	5.29	5.70	6.23	6.76	7.11	9.4
*	W			9.3	9.3	9.2	9.2	9.1	9.1	9.0	
67D	W	13.6	13.3	5.16	5.76	6.34	6.82	7.39	7.87	8.07	13.8
Δ	W			13.0	12.6	12.4	12.2	12.1	11.9	11.7	
67E	W	15.6	15.2	6.64	7.44	8.17	8.77	9.58	10.25	10.64	15.8
Y	W			14.8	14.4	14.1	13.8	13.7	13.4	13.2	
67G	W	19.2	18.5	6.55	7.52	8.25	8.83	9.49	10.13	10.47	19.7
◇	W			17.9	17.4	17.0	16.7	16.4	16.2	15.9	
31	W	5.4	5.4	2.48	2.71	2.86	3.18	3.55	4.00	4.29	5.2
○	W			5.4	5.3	5.2	5.2	5.2	5.2	5.1	
32	W	9.2	9.1	4.37	4.87	5.28	5.79	6.27	6.63	6.67	9.3
□	W			9.0	8.8	8.5	8.2	8.0	7.9	7.8	
33	W	13.0	12.7	3.93	4.37	4.74	5.10	5.54	5.79	5.81	13.2
▽	W			12.3	11.8	11.4	11.2	11.1	11.0	10.9	
34	W	15.1	14.9	3.36	3.75	4.03	4.38	4.70	4.85	5.05	15.3
○	W			14.6	14.2	13.9	13.8	13.7	13.6	13.5	
35	W	8.7	8.9	1.48	1.88	2.41	3.19	4.04	5.54	6.50	8.4
■	W			9.3	9.7	10.5	11.5	12.3	13.1	13.3	
36	W	9.3	9.5	1.90	2.29	2.75	3.66	4.58	6.15	7.14	9.0
◆	W			9.8	10.2	10.8	11.6	12.5	13.3	13.5	
38	W	10.1	9.8	4.29	4.77	5.26	6.66	6.12	6.27	6.48	10.5
▣	W			9.4	9.0	8.7	8.4	8.2	8.0	8.0	
39	W	10.6	10.5	4.00	4.49	4.96	5.30	5.81	6.31	6.69	10.8
◇	W			10.3	10.1	9.9	9.8	9.8	9.7	9.7	
40	W	4.5	4.8	1.78	2.08	2.61	3.03	3.67	4.68	5.48	4.3
●	W			5.2	5.6	6.1	6.5	6.9	7.2	7.3	
41	W	5.0	5.3	2.90	3.26	3.76	4.20	5.03	5.97	6.61	4.8
▽	W			5.5	5.7	6.0	6.2	6.4	6.5	6.6	
42	W	4.0	4.3	2.41	2.74	3.16	3.50	4.21	5.18	5.80	3.8
▲	W			4.6	4.9	5.2	5.4	5.6	5.7	5.8	

52

TABLE 7: TOTAL VARIANCE OF  $U, V, W,$  AND  $T$  BEFORE AND AFTER FILTERING (HIGH-PASS).

RUN	TOTAL				AFTER 601-POINT RUNNING MEAN FILTER			
	$\overline{U'^2}$	$\overline{V'^2}$	$\overline{W'^2}$	$\overline{T'^2}$	$\overline{U'^2}$	$\overline{V'^2}$	$\overline{W'^2}$	$\overline{T'^2}$
66D 16M.	.531	.232	.086	.0321	.446	.179	.086	.0245
+ 40M.	.539	.313	.102	.0357	.362	.236	.102	.0257
66E 16	.507	.177	.062	.0910	.300	.149	.062	.0198
⊙ 40	.536	.267	.093	.106	.329	.212	.092	.0198
66F 16	.785	.378	.136	.0346	.749	.327	.135	.0331
⊙ 40	.708	.434	.189	.0311	.651	.394	.188	.0294
67A 16	1.075	.609	.241	.0282	1.035	.476	.240	.0220
⊙ 40	.801	.581	.285	.0281	.778	.496	.284	.0219
67B 16	1.238	.694	.296	.0296	1.189	.676	.294	.0207
X 40	1.128	.616	.340	.0250	1.077	.606	.340	.0214
67C 16	1.665	.977	.422	.295	1.564	.946	.420	.0040
* 40	1.614	.981	.610	.289	1.536	.946	.601	.0032
67D 16	2.818	2.720	.508	.208	2.288	2.444	.499	.0563
Δ 40	2.535	2.370	.830	.217	2.056	2.165	.805	.0470
67E 16	4.983	6.309	.769	.155	3.773	5.221	.766	.133
√ 40	5.024	6.452	1.307	.154	3.733	4.413	1.294	.102
67G 16	3.501	5.994	.752	.231	3.278	4.505	.753	.190
⊙ 40	4.093	5.771	1.257	.232	3.654	4.360	1.260	.175
◇ 16	.879	.652	.242	.258	.642	.514	.240	.0084
○ 40	1.005	.672	.374	.0928	.842	.597	.369	.0026
32 16	2.578	2.553	.709	.302	1.745	2.299	.703	.0980
□ 40	3.882	1.909	1.064	.245	2.899	1.696	1.070	.0558
33 16	1.586	2.484	.453	.322	1.461	2.110	.455	.131
▽ 40	2.402	1.909	.665	.230	2.236	1.625	.663	.123
34 16	1.721	2.017	.369	.100	1.433	1.627	.366	.0835
⊙ 40	2.098	1.961	.618	.117	1.429	1.508	.604	.0776
35 16	.180	.060	.009	.0255	.063	.026	.009	.0138
■ 40	.106	.062	.004	.0144	.072	.014	.004	.0069
36 16	.270	.141	.018	.0638	.104	.052	.018	.0225
◆ 40	.338	.251	.009	.102	.063	.036	.009	.0910
38 16	2.130	4.042	.479	.224	1.823	2.704	.457	.141
▢ 40	2.751	4.090	.946	.202	2.251	2.437	.939	.0917
39 16	2.357	2.222	.438	.0550	1.769	1.484	.437	.0381
⊙ 40	2.936	2.545	.702	.0480	2.117	1.728	.702	.0404
40 16	.188	.107	.051	.0197	.147	.099	.051	.0111
● 40	.260	.119	.053	.0301	.221	.108	.052	.0131
41 16	.700	.332	.150	.0363	.497	.276	.149	.0255
▽ 40	.646	.467	.207	.0333	.602	.385	.206	.0253
▲ 16					.474	.244	.133	.0207
▲ 40					.565	.323	.190	.0221

FIG. 5: GENERAL FUNCTIONAL FORM OF THE DEPENDENCE OF NON-DIMENSIONAL ENERGY SPECTRAL DENSITY ON NON-DIMENSIONAL FREQUENCY AND STABILITY.



tables and figures where they appear or in the resumes of the papers of Section III and the Appendix.

1. Standard deviation of the azimuth angle,  $\sigma_A$  where  $\tan^2 \sigma_A = \frac{S_k}{U^2}$  and  $\sigma_A^2 \approx S_v / U^2$  for small angles.

2. Vertical gradient of potential temperature,  $\frac{\partial \theta}{\partial z}$

3. Richardson number,  $\frac{g/\theta}{(\partial v / \partial z)^2}$ , computed for several layers in an effort to see if a single representative "bulk" value really exists.

4. Friction velocity,  $V^* = (-\overline{u'w'})^{1/2}$

5. Friction temperature,  $T^* = -\frac{1}{kV^*} \overline{w'T'}$ , where

$k$  = the von Karman constant.

5. Similarity stability parameter,  $z/L$ , where  $L = \frac{-V^{*3}}{k \frac{g}{\theta} \overline{w'T'}}$

These and many more general statistics are tabulated by run in Tables 3-7. Tables 1 and 2 are samples of the calculation procedure used in putting the power spectral estimates into the following similarity coordinates:

$$\log \frac{S_i \bar{U}}{z V^{*2}} \quad \text{versus} \quad \log \frac{nz}{U} \quad , \quad \text{where } i = u, v \text{ and } w$$

and

$$\log \frac{S_T \bar{U}}{z T^{*2}} \quad \text{versus} \quad \log \frac{nz}{U} \quad , \quad \text{where } T = \text{temperature and}$$

$S_i$  and  $S_T$  are power spectral density estimates. See Figures 8-15 for the data in this coordinate system. These are the same coordinates as used by Takauchi (1961) and Monin (1962).

C. Choice of parameters describing effects of stratification and the lower boundary.

Figure 5 shows the general form of the power spectral density

functions (in non-dimensional log-log coordinates) for both similarity and  $\bar{U}^2$ -normalization. Figures 8-15 and 24 and 25 show the data in these coordinate systems. In qualitative terms, it can be seen that there are three spectral regions.

1. A high-frequency region of fairly uniform slope, where the normalized spectral density =  $f(n)$  only. This is called the mechanical and isotropic range.

2. A low-frequency region, where the normalized spectral density is an increasingly strong function of stratification with decreasing frequency.

3. A transition region between these two.

At a particular site (implying constant roughness or lower boundary effect), one has the empirical problem of expressing  $S_i$ , the energy spectral density, as a function of  $\bar{U}_z$ ,  $n$ , and stratification. This function is complicated by the interdependence of  $\bar{U}_z$  and the stratification. At this point it is necessary to choose descriptive parameters representative of the stability and roughness.

Batchelor (1953 A) indicated the appropriateness of the Richardson number in specifying the effect of stratification on turbulence but, as seen in Tables 3-6, this number is quite variable with height and is also difficult to evaluate with sufficient accuracy.

The stability parameter,  $z/L$ , has the disadvantage of requiring that the gross statistics,  $\overline{u^2 w^2}$  and  $\overline{w^2 T^2}$ , be known. The approach adopted in the present work is to use the more easily measured quantities in determining the power spectral functions and the gross statistics. Although

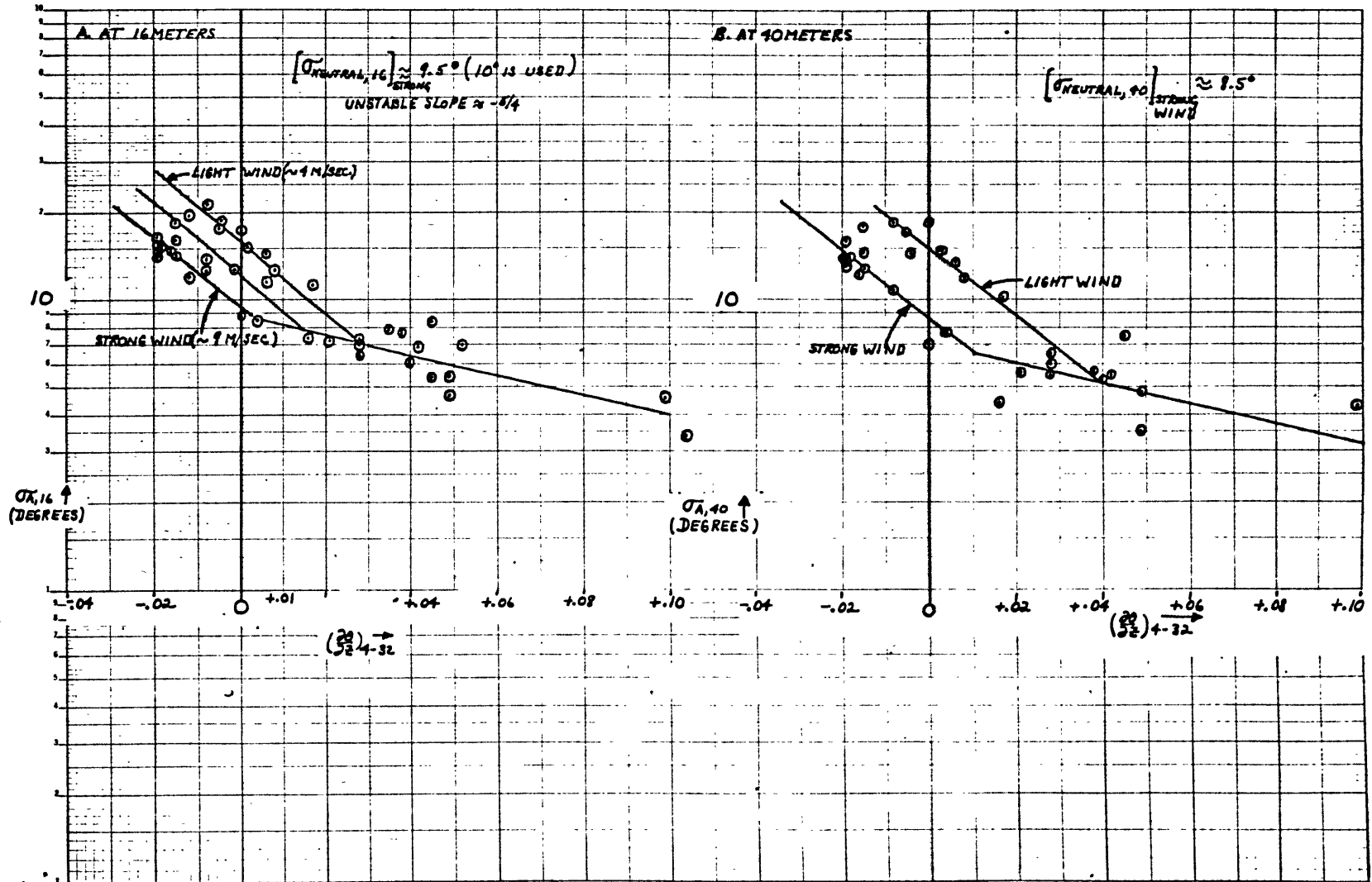


it is necessary to use the momentum and heat flux values later, it is desirable to keep their use to a minimum so that the errors in the power spectral density functions, occurring as a result of errors in these flux values can be isolated.

The gradient of potential temperature can be used, if care is taken in evaluating it. Most of the thermal gradient occurs near the surface below a height of 4 meters, thus, the levels between which  $\frac{\partial \theta}{\partial z}$  is measured, are critical. Additionally, in an unstable atmosphere, small differences in thermal gradient may indicate large differences in the scale and intensity of turbulence.

The standard deviation of the azimuth angle,  $\sigma_A$ , is a sensitive parameter of stability, as shown by Cramer (1957; 1960), Takeuchi (1963), Shiotani (1963) and Inoue (1959). Inoue found an empirical relation between  $\sigma_A$  and stability for the Prairie Grass data; a value of 6.5 degrees was found for near neutral stratification. The quantity,  $\sigma_A$ , is a very weak function of height,  $z$ , and is nearly independent of  $z$  in very unstable conditions. Using data from about sixty runs, Figure 6 shows the relation between  $\sigma_A$  and  $\frac{\partial \theta}{\partial z}$ . For very unstable conditions,  $\sigma_A$  is a better indicator of the relative difference in turbulence scales and intensities than is  $\frac{\partial \theta}{\partial z}$ . Under very stable conditions, when the scales are small and the regime is more localized,  $\frac{\partial \theta}{\partial z}$  may be a better measure of the stratification (in the absence of filtering), because the value of  $\sigma_A$  is sensitive to the effects of long waves not directly related to turbulence. Using Figure 6, a modified stability parameter,  $(\frac{\partial \theta}{\partial z})^*$ , can be defined. In the moderately stable and very stable region,  $\frac{\partial \theta}{\partial z} = (\frac{\partial \theta}{\partial z})^*$ ; in the near neutral and unstable region (using the "strong

FIG. 6 : STANDARD DEVIATION OF AZIMUTH ANGLE VS.  $\frac{\sigma_z}{z}$  BETWEEN 4 AND 32 METERS.



wind" curve),  $(\partial\theta/\partial z)^*$  could be the  $\frac{\partial\theta}{\partial z}$  obtained by placing  $\sigma_A$  on the strong wind curve and reading the abscissa. This function is designed to incorporate the best behavior of each ( $\sigma_A$  and  $\partial\theta/\partial z$ ) parameter in their respective regions of superiority. A modified  $\sigma_A$  can just as easily be obtained, using the same curves, and is more convenient to use. The evaluation difficulties of  $\partial\theta/\partial z$  are also felt in the Richardson number calculations, aggravated by the taking of a ratio of two small and not accurately determined quantities,  $(\partial v/\partial z)^2$  and  $\partial\theta/\partial z$ , especially under neutral and unstable conditions and at a distance from the lower boundary. It is just under these conditions that the Richardson number is so critical in defining the regime. On a purely empirical basis, the stability is defined as  $\sigma_N/\sigma_A$ , where  $\sigma_N$  is the standard deviation of the azimuth angle under neutral conditions. The quantity,  $\sigma_N$ , is then used as the description of the roughness or lower boundary effect. By defining  $\sigma_N^2 = \int_0^\infty \sigma_N^2(n) dn$ , the lower boundary effect is expressed in terms of the frequencies it excites or,  $\sigma_N^2(\bar{U}/x)$  gives the roughness in terms of length scales. This assumes that Taylor's hypothesis is valid in the "mechanical" range (Panofsky, Rao and Cramer [1958]). The quantity,  $\sigma_A$ , should emphasize the larger roughness elements and varies from 2-3 degrees for a very smooth site or sea surface to 15-20 degrees for very rough sites, such as hilly, wooded areas. This variability is compared to the three orders of magnitude or more variation for the friction length,  $z_0$ , as shown by Sutton (1949), p. 103. Also  $\sigma_N$  is not as sensitive as  $z_0$  to small changes in the lower boundary (see Cramer [1960] and Obukhov [1958]). From the following identities,

$$\frac{\sigma_V^2}{\bar{U}^2} = T \tan^2 \sigma_A ; \sigma_V^2 = \text{total } v\text{-variance} = \int_0^\infty S_V(n) dn \quad (5.1)$$

it is seen that,

$$\sigma_n^2(n) = \frac{S_V(n)}{\bar{U}^2} \text{ and } \sigma_n^2 = \frac{1}{\bar{U}^2} \int_0^\infty S_V(n) dn = \int_0^\infty n S_V(\text{normalized}) d\left(\frac{n}{\bar{U}}\right) \quad (5.2)$$

which is equal to the area under the curve of the semi-log plot.

The quantity,  $\sigma_A^2$ , is approximately the ratio of the v- component energy to the kinetic energy of the mean flow and  $\sigma_N^2$  gives this ratio under neutral conditions. Then  $\sigma_n^2$  gives this ratio from site to site and supplies an estimate, under neutral conditions, of the v-component variance in terms of  $\bar{U}^2$ .

If  $n = l$ , where  $l$  is known to be in the inertial sub-range,

$$E_l = \alpha \varepsilon^{2/3} n_l^{-5/3} \quad (\text{see Pasquill and Panofsky [1963] for an evaluation$$

of this constant of proportionality), and  $\varepsilon = \left[ \frac{E_l n_l^{+5/3}}{\alpha} \right]^{3/2}$ .

If the level of turbulent kinetic energy is steady,  $\frac{\partial \overline{u_i u_i}}{\partial t} = 0$ , then

$$\varepsilon = \frac{\tau}{\rho} \frac{\partial \bar{u}}{\partial z} + \frac{g}{\theta} \overline{w' T'} - \frac{\partial}{\partial z} (\overline{w' E'}) \quad , \text{ where } E = \text{turbulent kinetic}$$

energy per unit mass summed over the components and  $E_l =$  the same quantity

at frequency,  $n = l$ . And if  $\frac{g}{\theta} \overline{w' T'}$  and  $\frac{\partial}{\partial z} (\overline{w' E'})$  are assumed

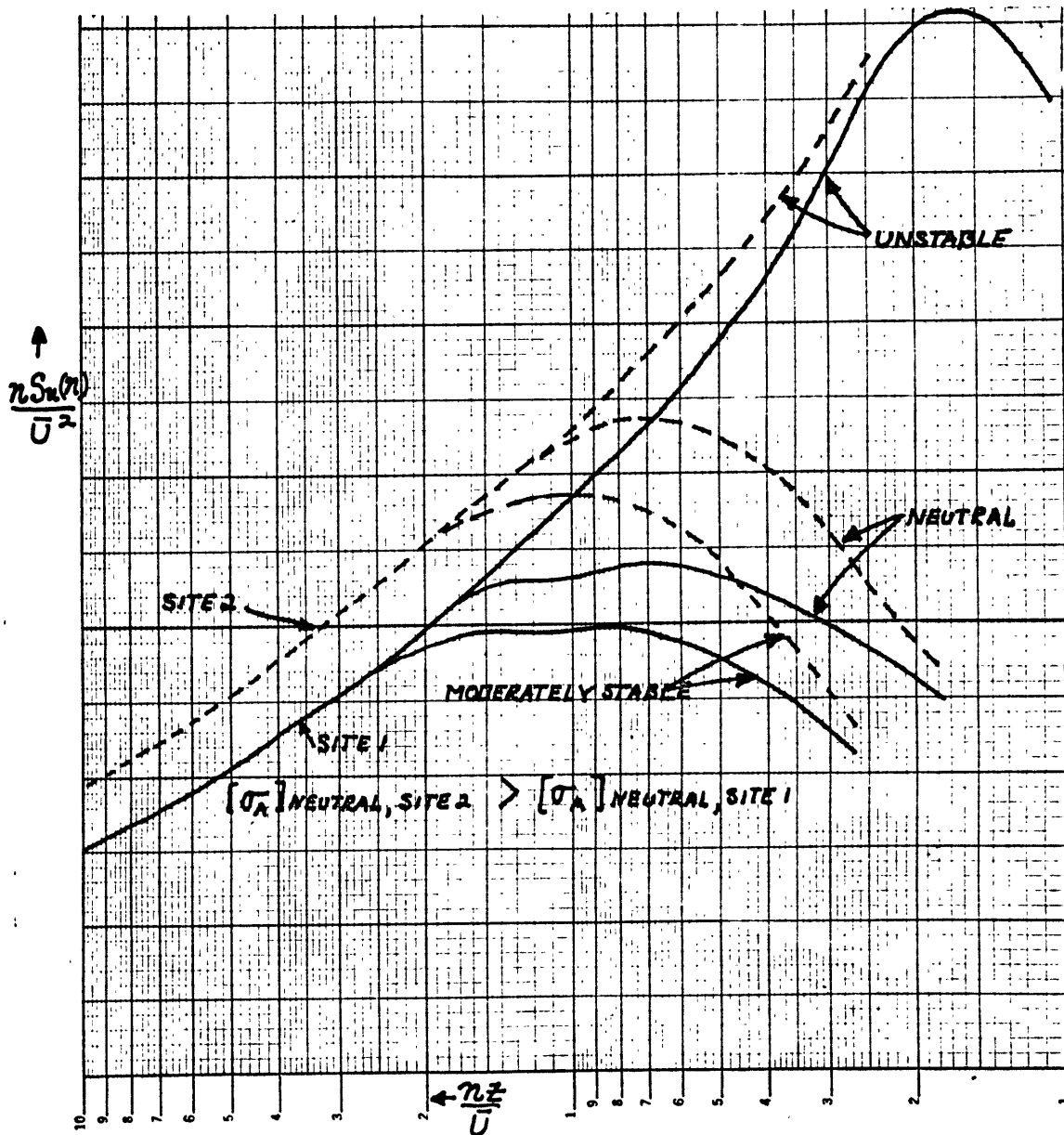
small, except under unstable condition when they tend to counterbalance

each other (Taylor [1961], and Panofsky [1962]), then:

$$\varepsilon \cong \frac{\tau}{\rho} \frac{\partial \bar{u}}{\partial z} \text{ and } \tau = \frac{\rho}{\partial u} \left[ \frac{E_l n^{5/3}}{\alpha} \right]^{3/2}$$

This permits one to establish the relation between the dissipation rate,  $\varepsilon$ ,

FIG. 7: SCHEMATIC OF  $\pi S_{\alpha}(\pi)/U^2$  VS.  $\log \pi z/D$  AT THE SAME HEIGHT FOR TWO SITES OF DIFFERENT ROUGHNESS, EXPRESSED IN TERMS OF THE STANDARD DEVIATION OF THE AZIMUTH ANGLE UNDER NEUTRAL CONDITIONS,  $\sigma_N$ .



and the stress,  $\tau$ . It is suggested that  $\tau_A^2$  could be expressed in terms of two functions, one that is stability dependent and one that is only frequency dependent. A somewhat different approach is taken in the following paragraph.

Businger (1961) considered the resulting spectrum if turbulence were isotropically introduced at two discrete frequencies (a low frequency for convective energy and a high frequency for mechanical energy) and then "cascaded" to higher frequencies as described by the Kolmogoroff hypothesis. A generalization of this idea is used below:

Let  $\mathcal{E}(n_i)$  be an increment of energy introduced at frequency,  $n_i$ . If a "power law" of some form for the energy spectral density function is obtained from assumptions about the inertial energy transfer, then an increment of energy, introduced at  $n_i$ , produces an increment of energy,  $\mathcal{E}(n_j)$  at  $n_j$ , which is 
$$\mathcal{E}(n_j) = \mathcal{E}(n_i) \left(\frac{n_i}{n_j}\right)^c, \quad \text{for } j \geq i$$

$$= 0, \quad \text{for } j < i,$$

where  $c = + 3/2$  for the Kraichnan model and  $c = + 5/3$  for the Kolmogoroff hypothesis. The total energy at  $n_j$  is

$$E(n_j) = \sum_{i \leq j} \mathcal{E}(n_i) \left(\frac{n_i}{n_j}\right)^c \quad (5.3)$$

$\mathcal{E}(n_i)$  may be thought of as a source strength and  $(n_i/n_j)^c$  can be considered as an influence function for  $n_j$  relative to  $n_i$ . Let  $E_\ell$  be a value for  $E$ , where  $\ell$  is in the inertial sub-range. Then define

$$I_1 = E_\ell = \int_{i \leq \ell} \mathcal{E}(n_i) \left(\frac{n_i}{n_\ell}\right)^c dn_i \quad (5.4)$$

In practice, the integration over the  $n_i$ 's may be over a very restricted range if one particular roughness element is dominant. Next define the total energy

$$I_2 = \int_{\text{all } j} \int_{i \leq j} \mathcal{E}(n_i) \left(\frac{n_i}{n_j}\right)^c dn_i dn_j \quad (5.5)$$

The relation between  $I_1$  and  $I_2$  is difficult to handle, especially under convective conditions. These difficulties can be avoided if the roughness effect is thought of in terms of energy introduction; this idea suggests convective "excitation" as a variable roughness. These ideas are formally expressed as:

$$\left. \begin{aligned} R(n) &= \mathcal{E}(n)/\bar{U}^2 && , \text{ mechanical roughness} \\ A(n, \frac{\partial \theta}{\partial z}) &= \mathcal{E}(n)/\bar{U}^2 && , \text{ convective excitation} \end{aligned} \right\} \quad (5.6)$$

$$\text{Then } \sigma_A^2(n_j) = \int_i R(n_i) \left(\frac{n_i}{n_j}\right)^c dn_i \int_{n_i} A(n, \frac{\partial \theta}{\partial z}) \left(\frac{n_i}{n_j}\right)^c dn_i, \quad (5.7)$$

for  $i \leq j$

$$\text{and } \sigma_A^2 = \int_j \sigma_A^2(n_j) dn_j \quad (5.8)$$

This discussion is expanded in Section V $\zeta$  and more is said about this model.  $R(n)$  and  $A(n, \frac{\partial \theta}{\partial z})$  are the fractional portion of the mean energy,  $\bar{U}^2$ , extracted at each Fourier component and is associated with an actual physical length scale of the elements of the lower boundary roughness.

#### D. Presentation of power spectra in similarity coordinates.

Tables 1 and 2 show the calculations needed to put power spectral density data into this coordinate system. Figures 8 - 15 give the plotted result of putting this twenty run data sample into the Monin-Obukhov similarity coordinates. These data are analyzed in Section V E 1, and elsewhere under empirical results. Although other investigators have used this coordinate system, it is believed that the quality and size of the present data sample permit a much more comprehensive evaluation than has previously been possible. The data introduced here is the basis of the results to follow.

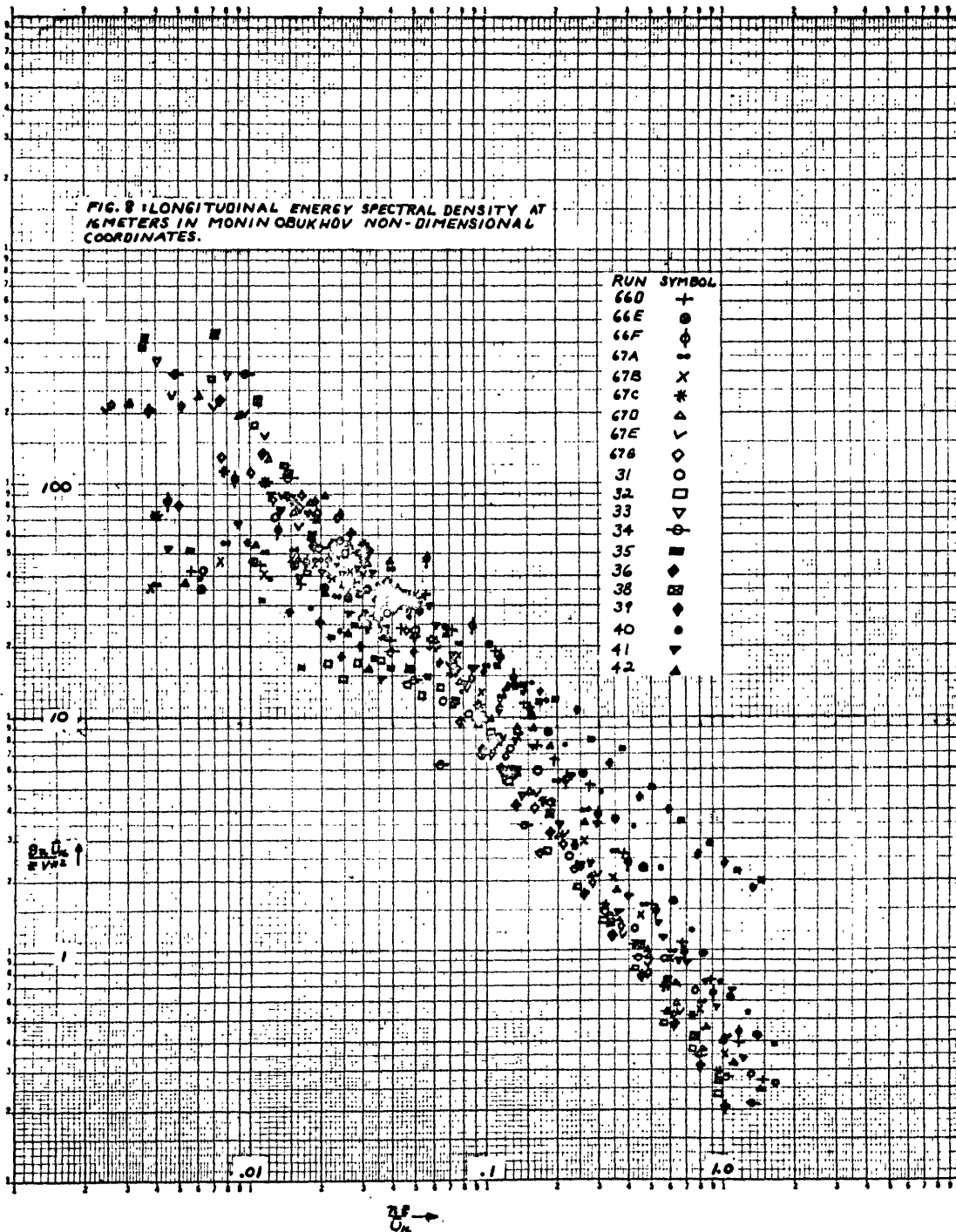
### E. Results.

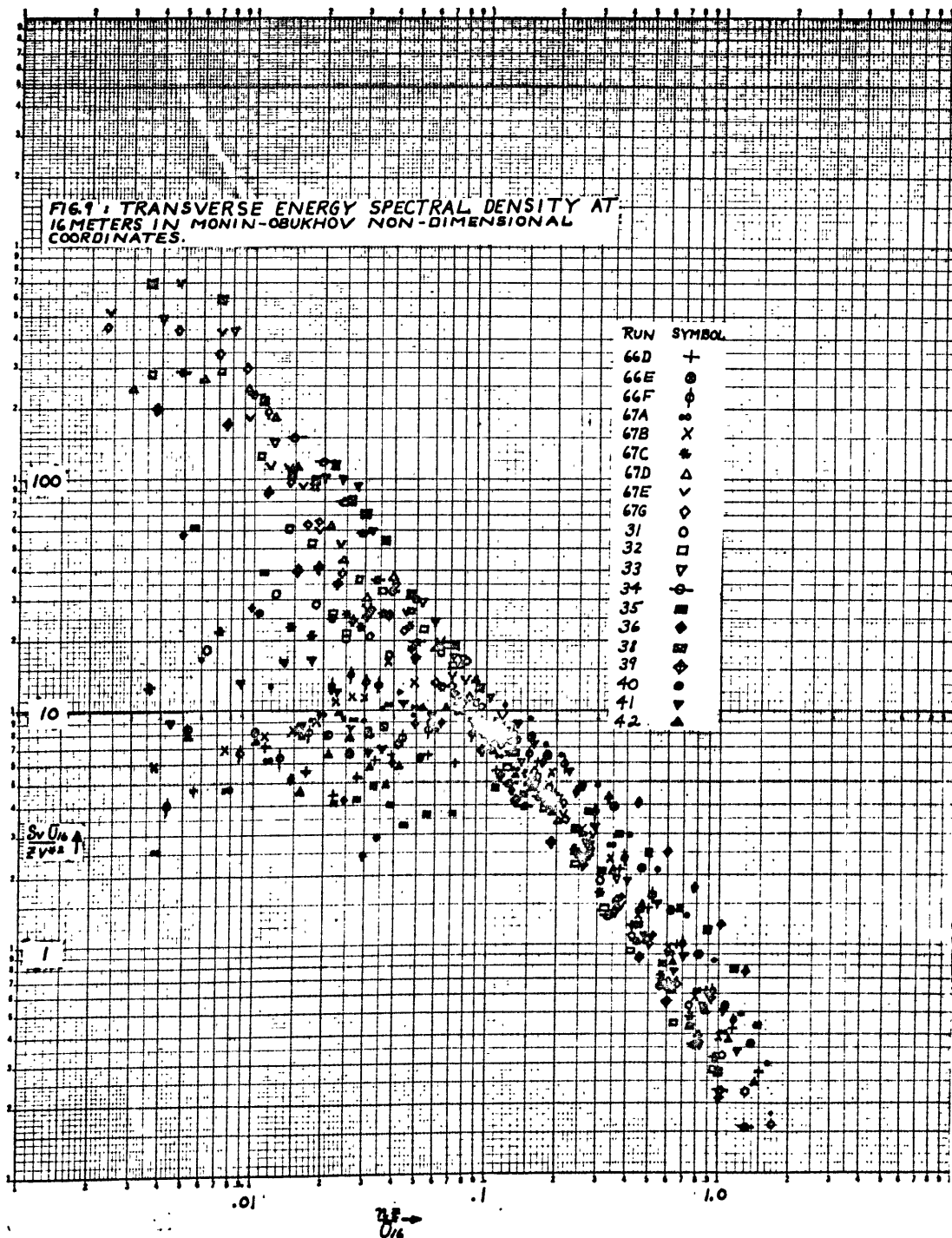
The results are given in several different forms and then are compared. Each of these forms is a means of evaluating the energy spectral density functions, if the meteorological parameters of mean wind and stratification are given and the geometrical values of roughness and  $z$  are known. The first approach is to express the non-dimensional energy spectral density,  $\frac{S_i \bar{U}}{z U_*^2}$  or  $\frac{S_i \bar{U}}{z T_*^2}$  as a function of  $\bar{U}$ ,  $\sigma_A$  or  $(\frac{\partial \theta}{\partial z})^*$ ,  $\sigma_N$ ,  $n$  and  $z$ , where the coordinates are those of Figures 8 - 15 and as schematically represented in Figure 5.

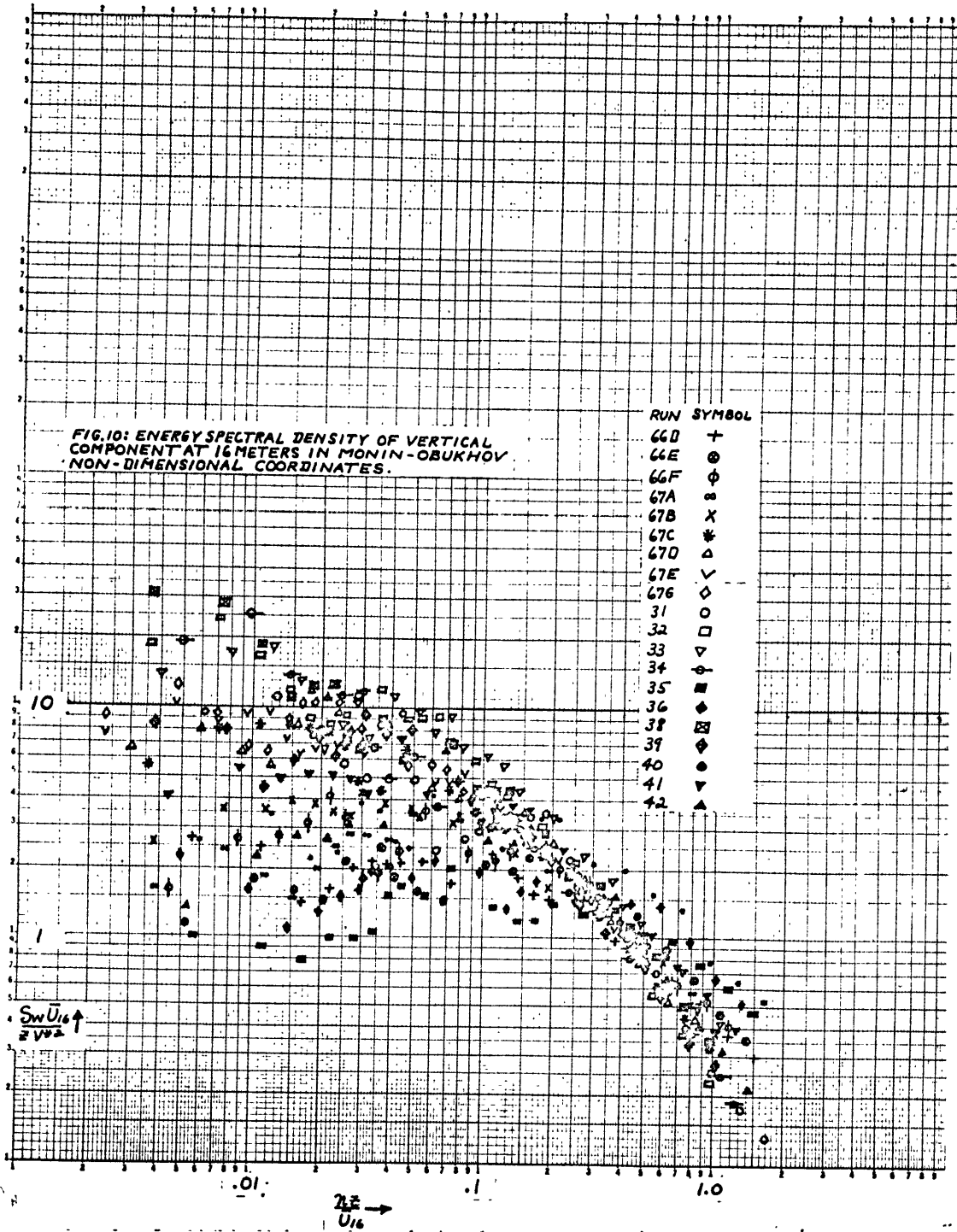
1. Algebraic expressions for energy spectral density functions in similarity coordinates.

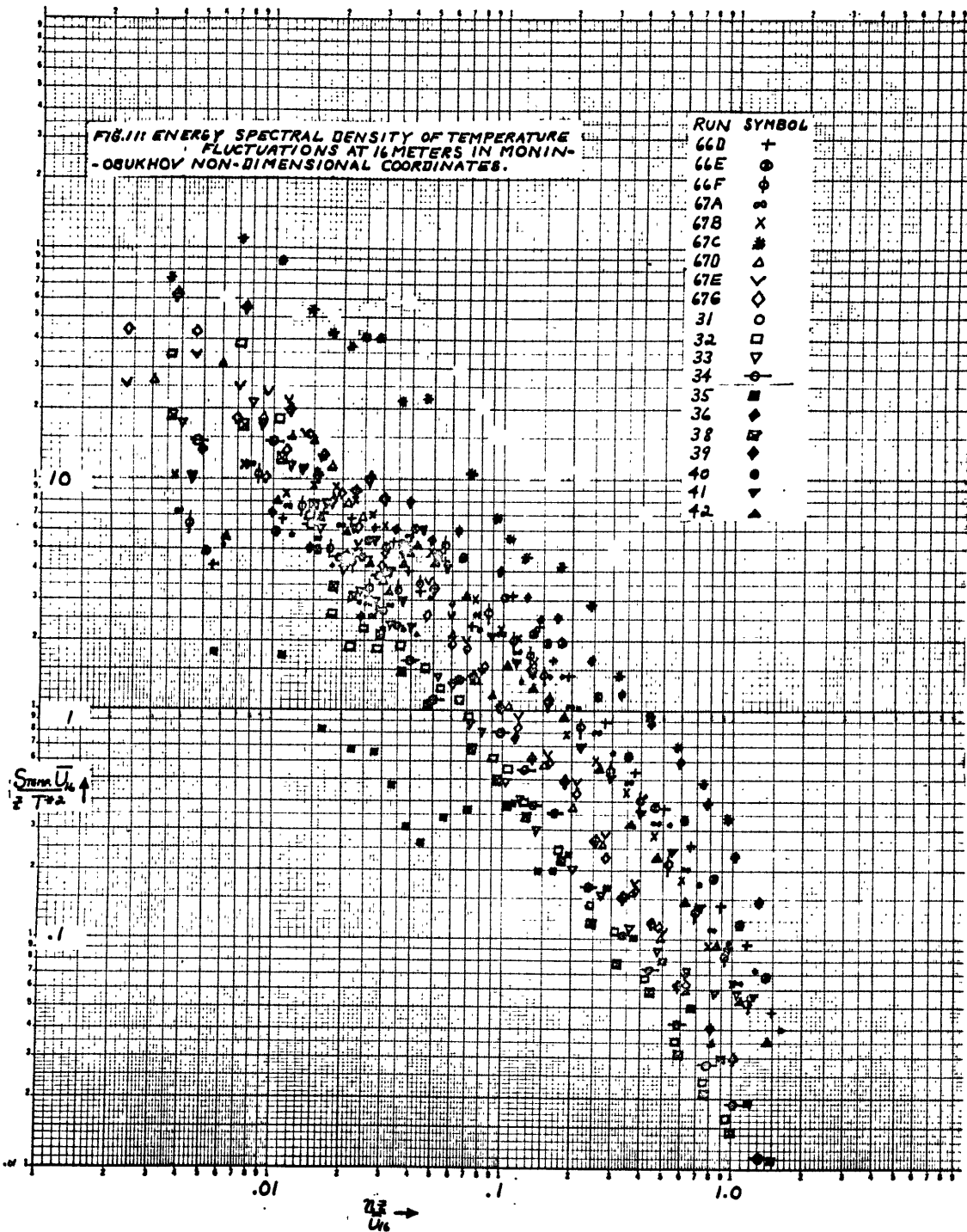
The approach here is to express these functions as algebraic equations; then to use these equations to reproduce curves for the spectral densities,  $S_i = f(\sigma_A, n)$ , for a given velocity component or temperature at a given level for a given site. The next step is to use any one of a variety of ways to estimate  $\overline{u'w'}$  and  $\overline{w'T'}$  (see the next section), assuming

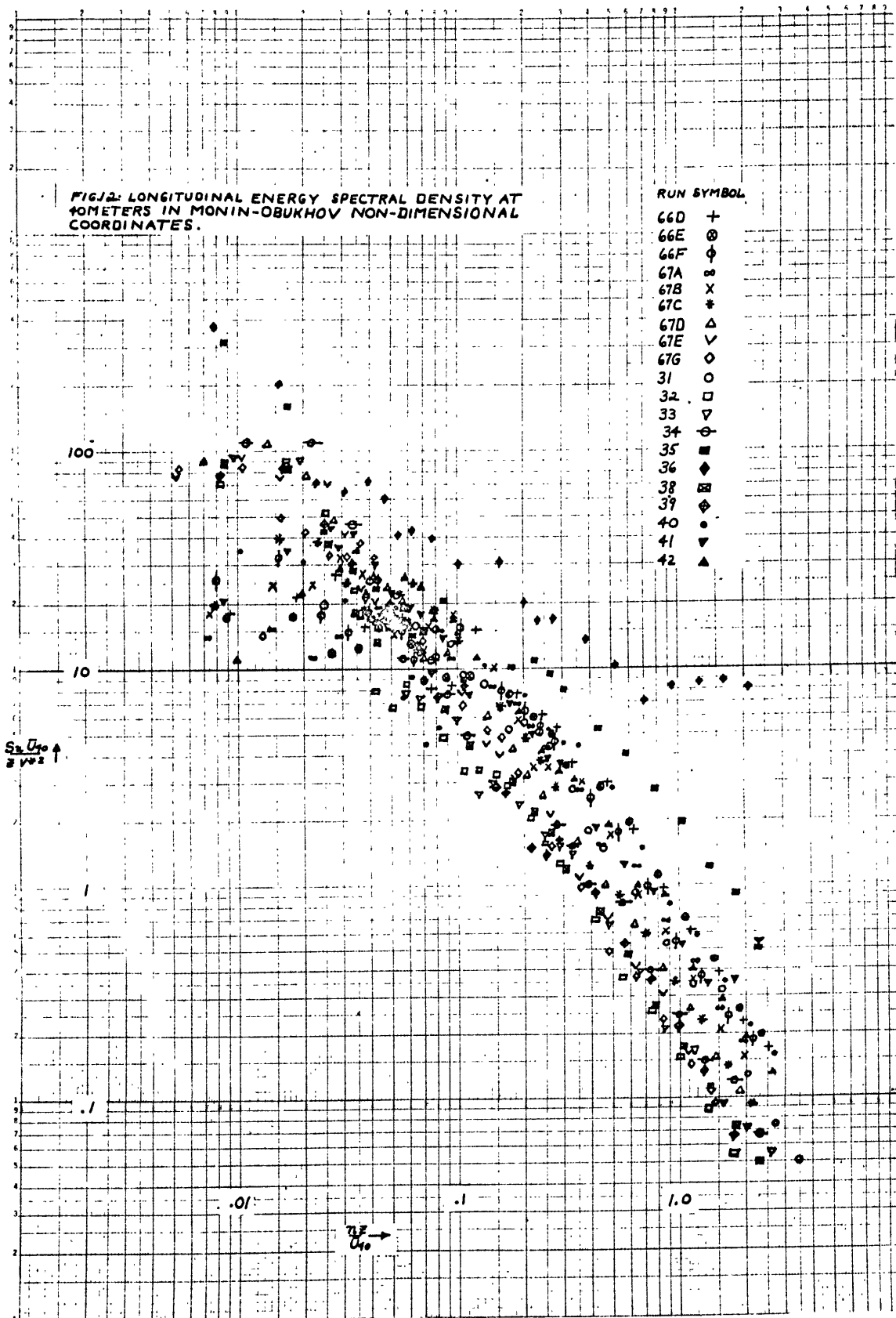


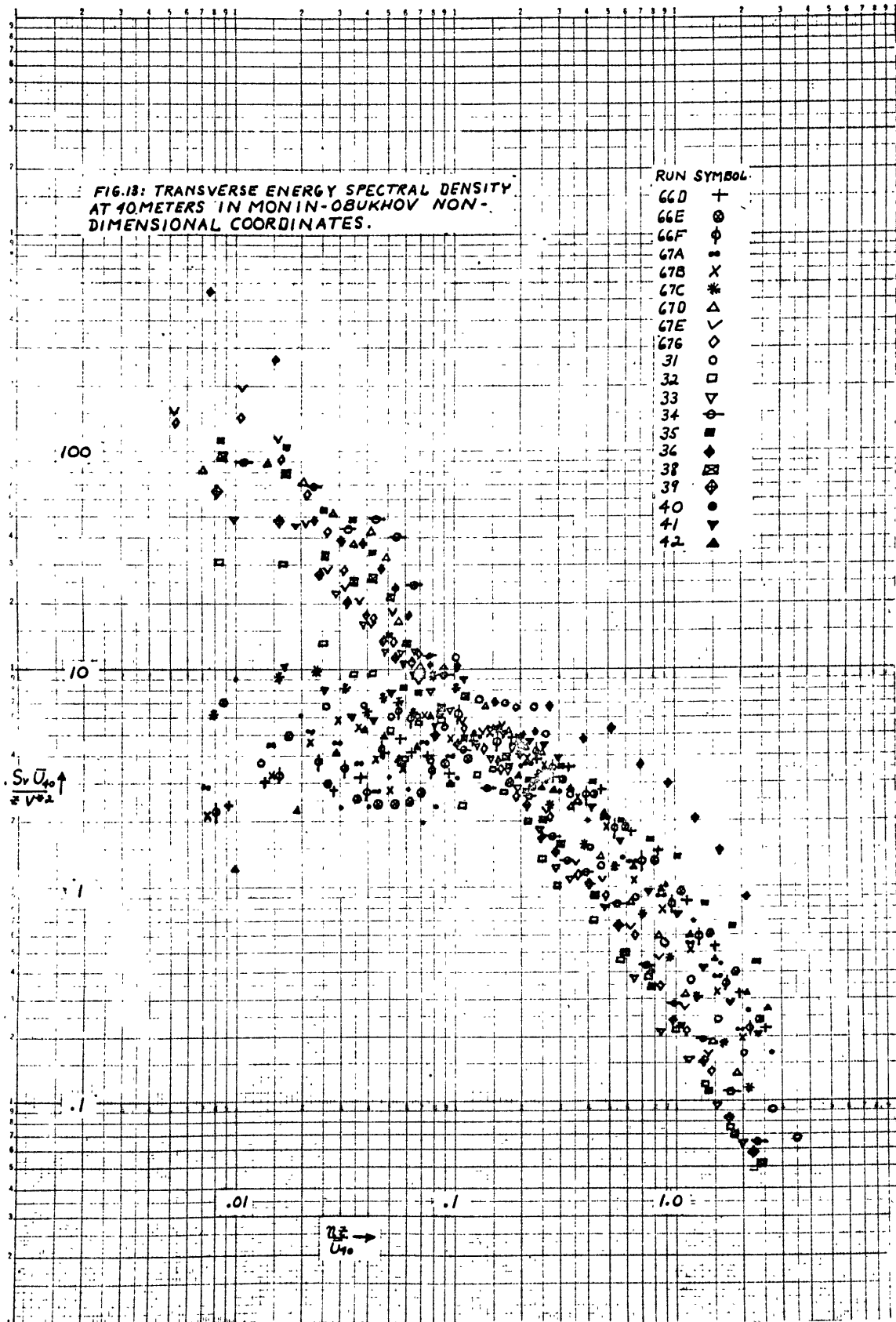


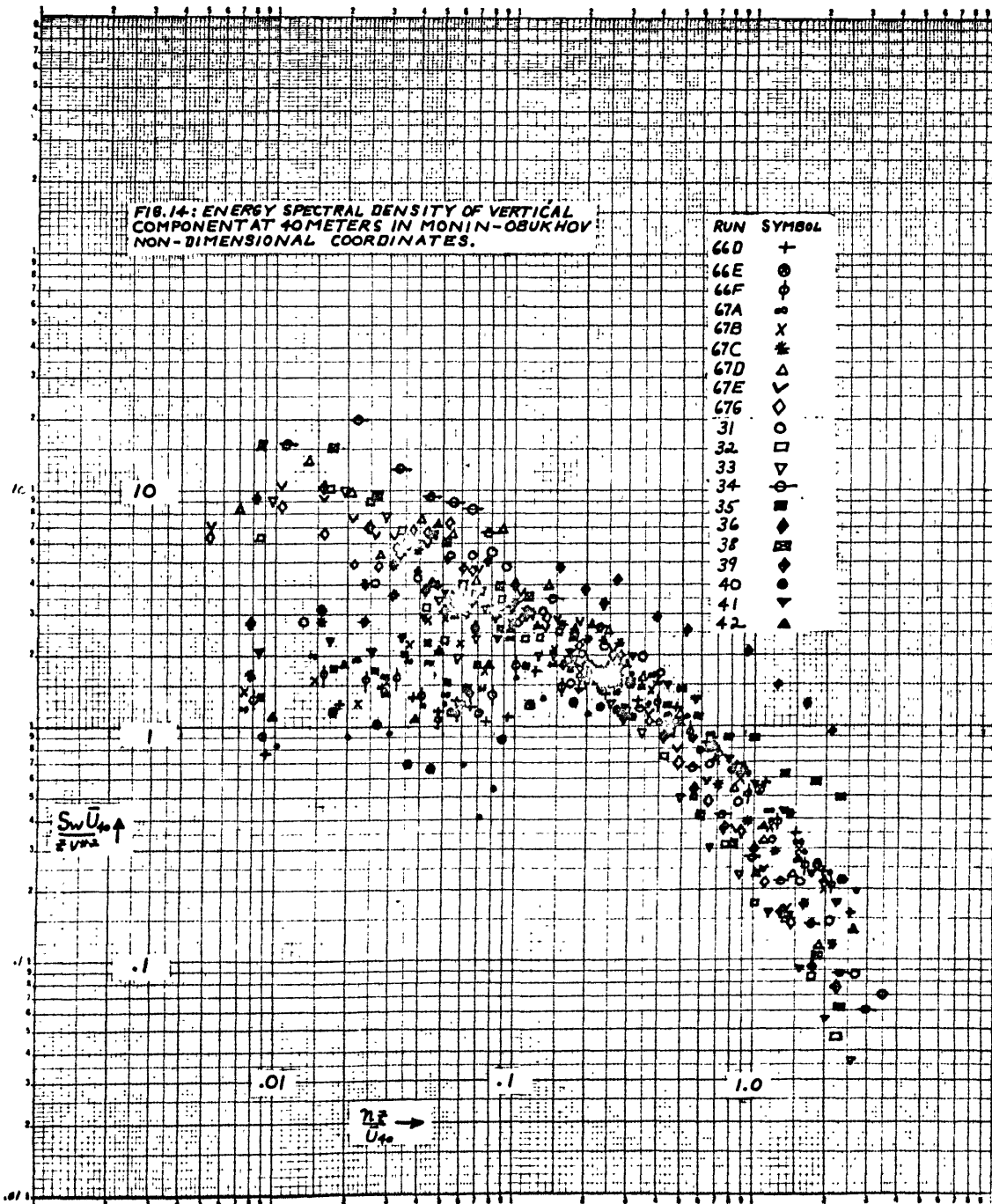


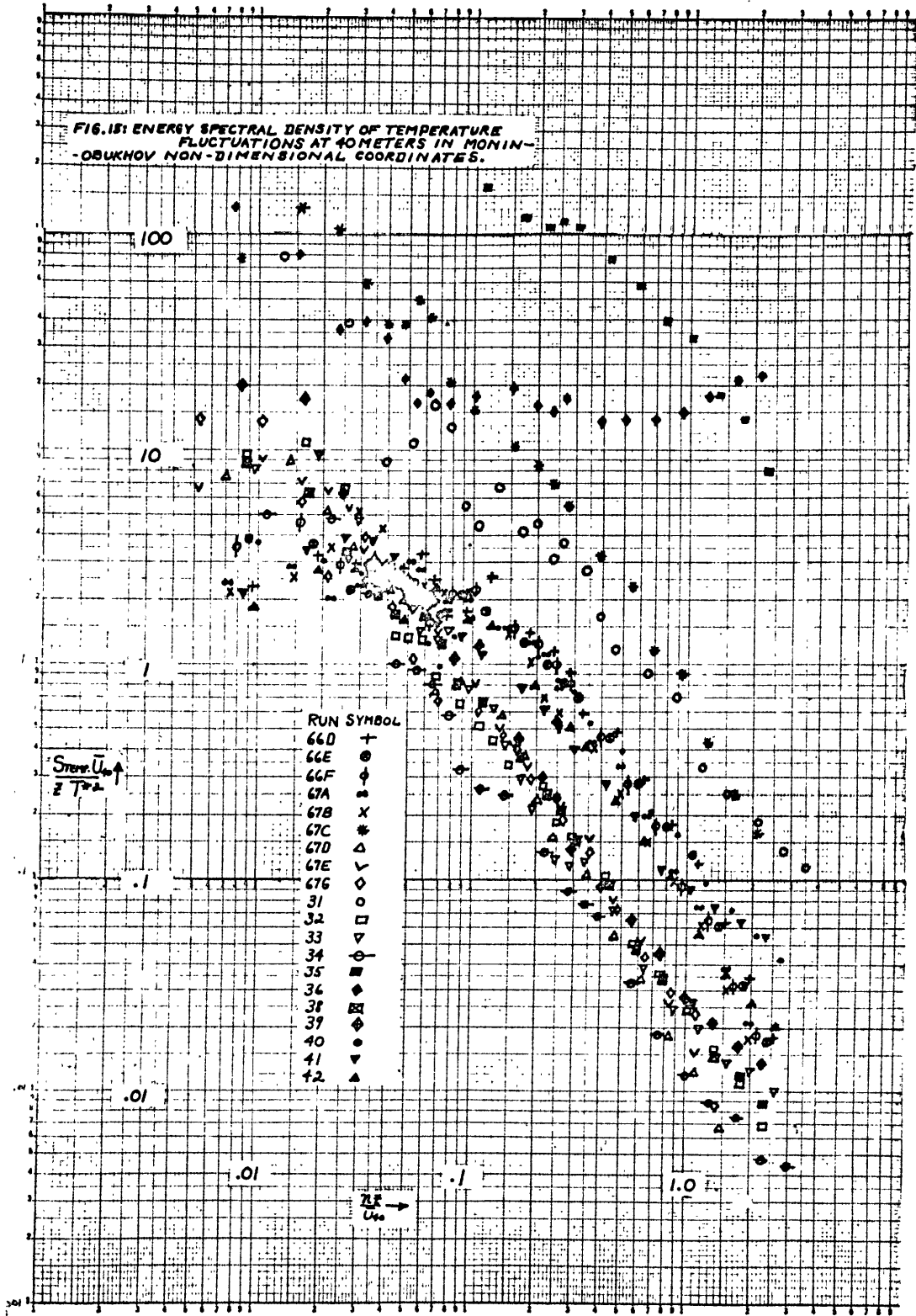














that they are not available, to return to dimensional coordinates and thus to give the desired engineering estimate.

As shown in Figure 5, if the high frequency dependence of  $S_1$  is expressed as a function of  $\sigma_A$ , there is an asymptotic approach to a uniform slope at high frequencies and a suggested asymptotic approach to a different uniform slope at low frequencies, with a relatively smooth transition and a single maximum in between these regions. It will be shown later that this is an over simplification. However this approach provides results, although it does not contribute much enlightenment. After experimenting with a number of functions, the following function was found to perform this "match" of low to high frequencies in the desired manner:

$$\left[ S_i \right]_{\text{NON-DIMENSIONAL}} = \frac{a n^b F}{1 + \frac{c}{n^d} \left( \frac{\sigma_N}{\sigma_A} \right)^e},$$

where  $F$  is a linear function of  $\left( \frac{\partial \theta}{\partial t} \right)^*$

and  $\frac{\sigma_N}{\sigma_A}$  is also used as a stability parameter.

a  $S_1$  at  $n = 1.0$  for the neutral case and serves to position the ordinate,  $S_1$ , at high frequency.

n actually stands for  $\frac{n^2}{D}$  here

b is the slope value at high frequency

c is determined by the value of  $S_1$  at a selected low frequency, say  $n = .01$

b plus d is the slope of  $S_1$  as n approaches zero.

e is determined by the low frequency stability dependence of  $S_1$

F is determined by the high frequency stability dependence of  $S_1$ .

These constants were then determined, using the data in Figures 8 - 15. Then using selected values of  $\sigma_A = 4, 5, 8, 10, 12$  and 18 degrees, where  $\sigma_A = 10$  degrees is the neutral case, and using the corresponding values of  $(\partial\theta/\partial z)^*$ , the results are shown in Figures 16 and 17 and by the algebraic expression in part B of the Appendix.

The most serious deficiency of these empirical functions seems to be in the transition (between  $\frac{\eta z}{U} = .02$  and  $.07$ ) in unstable cases. Here, it looks as if a separation occurs between the mechanically and the convectively introduced turbulence. Compare Figures 8 - 15 with Figures 16, 17, 24 and 25. If one could tolerate a 50 per cent error, then for a large part of the higher frequency scale ( $\frac{\eta z}{U} > .1$ ), the same function can be used for either 16 or 40 meters. This can be seen either from Figures 8 - 15, 16 and 17 or the algebraic expressions. Additionally, under near-neutral and unstable conditions,  $S_u$  and  $S_v$  are interchangeable with less than a 50 per cent error. In this region, there are about one hundred degrees of freedom in the data, so that 90 per cent of the time, the true value should be within 15 - 20 per cent of the observed value. This difference between the 16 and 40-meter curves is apparently significant and the use of the more simplified functions would be a matter of accuracy requirements. In order to return to dimensional quantities, the stress,  $\tau$ , and the heat flux,  $\overline{w'T}$ , must be used.

## 2. Various methods of estimating stress and heat flux.

See part C of the Appendix for a number of methods of determining the stress and heat flux which are suggested by recent papers.

As an alternative to these methods, the stress and heat flux data

FIG. 16: GRAPHS FOR ENERGY SPECTRAL DENSITY IN SIMILARITY COORDINATES. (ALGEBRAIC EXPRESSIONS)

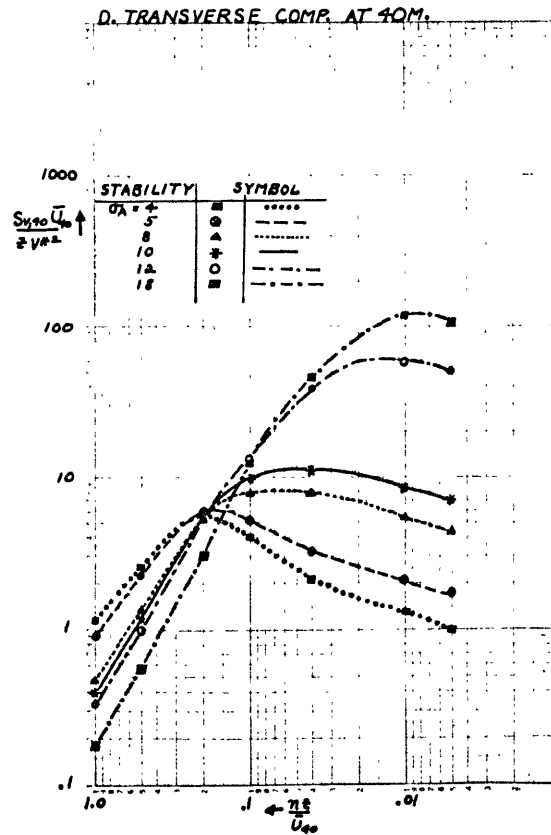
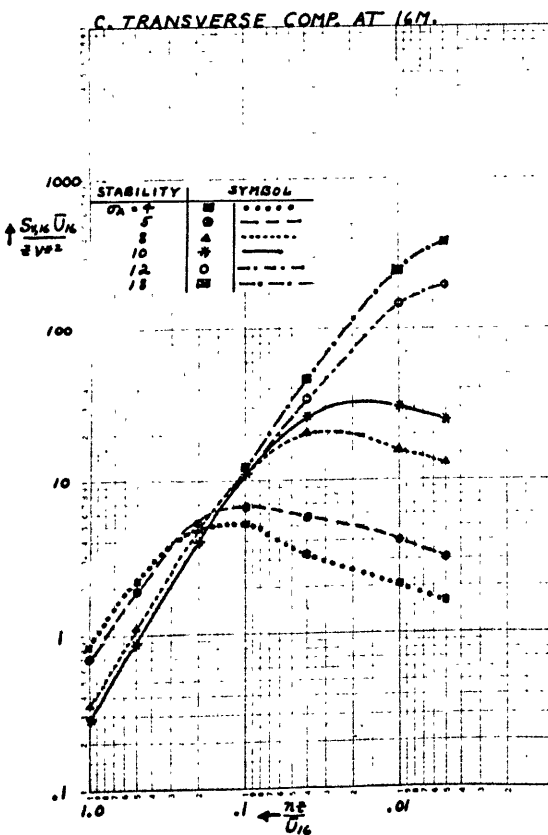
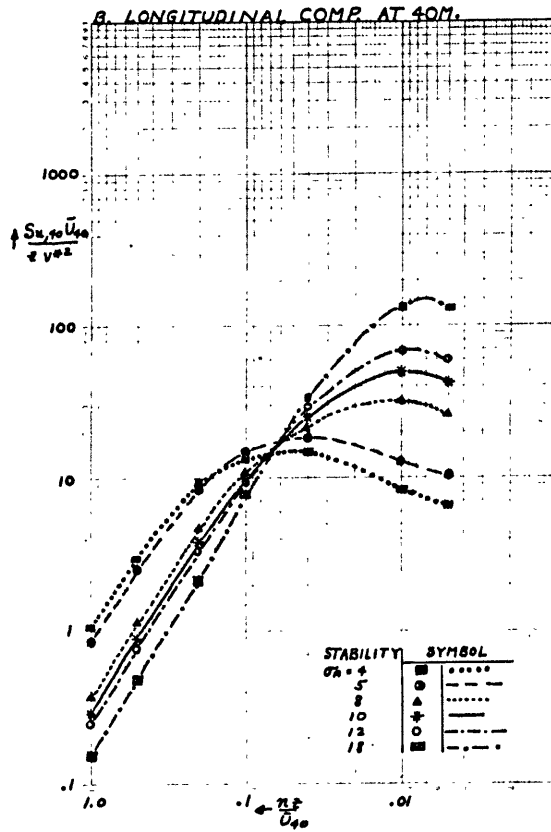
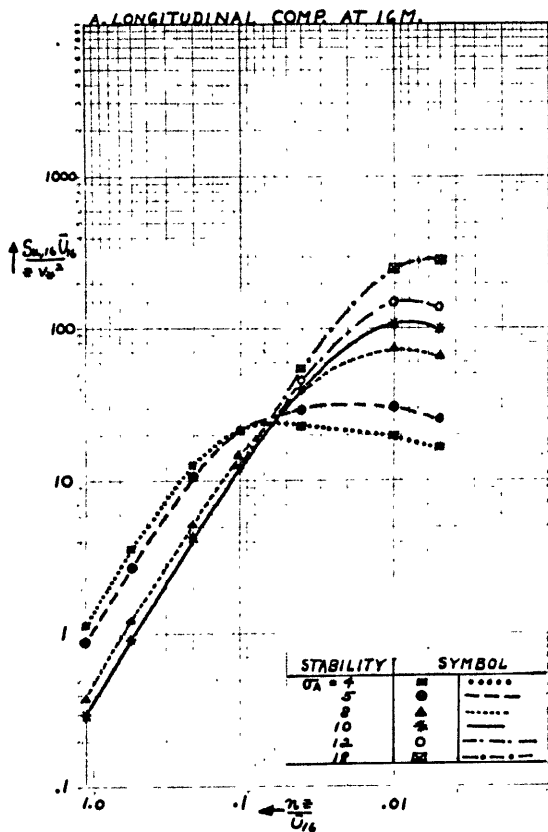
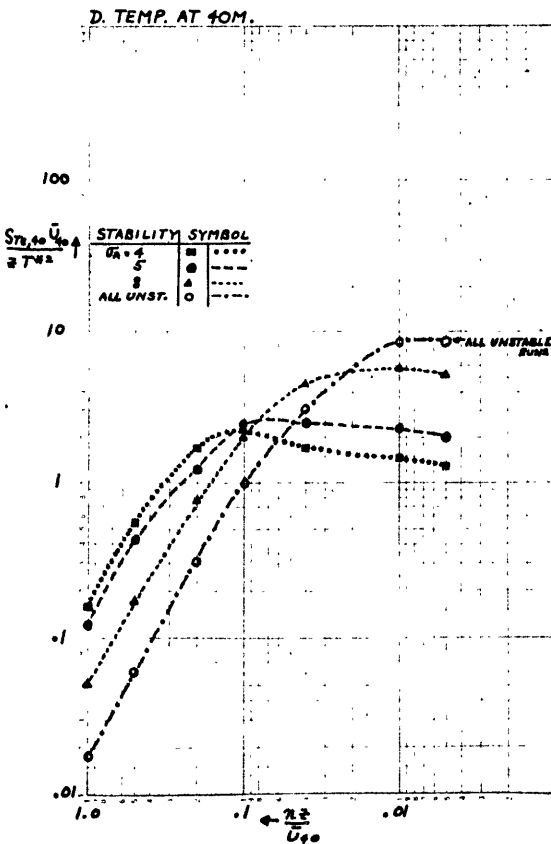
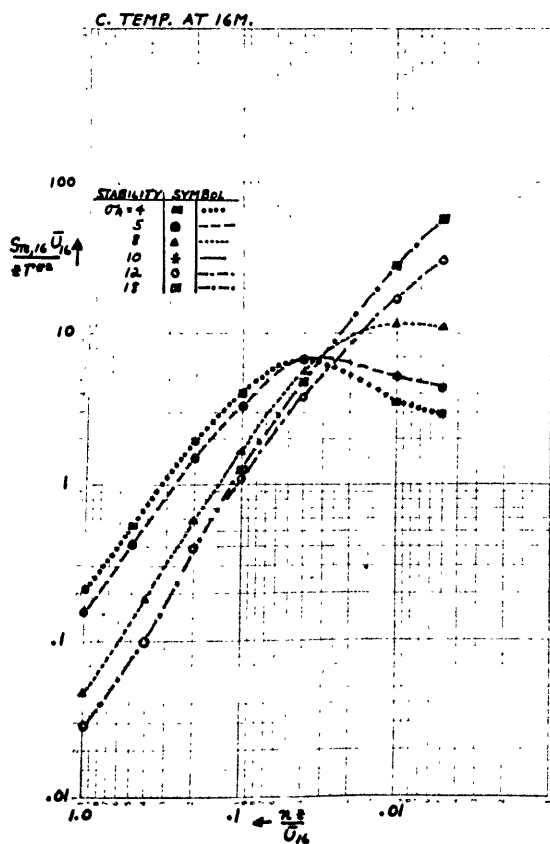
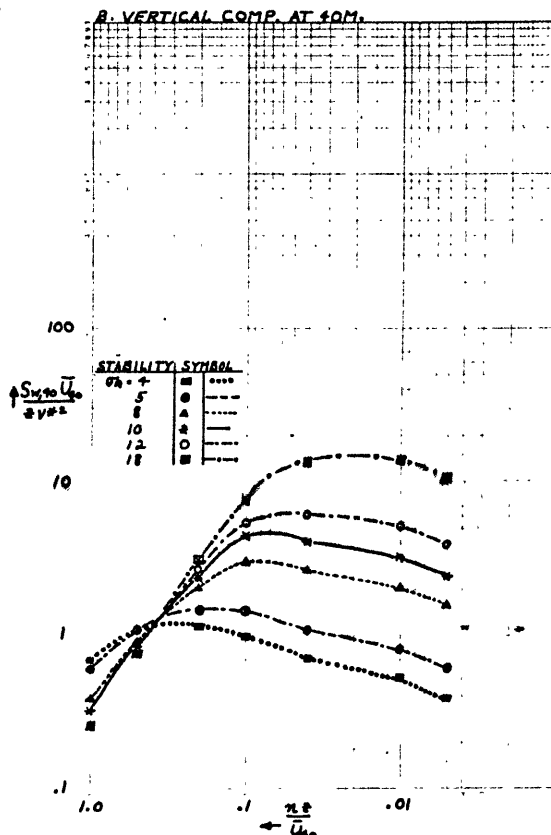
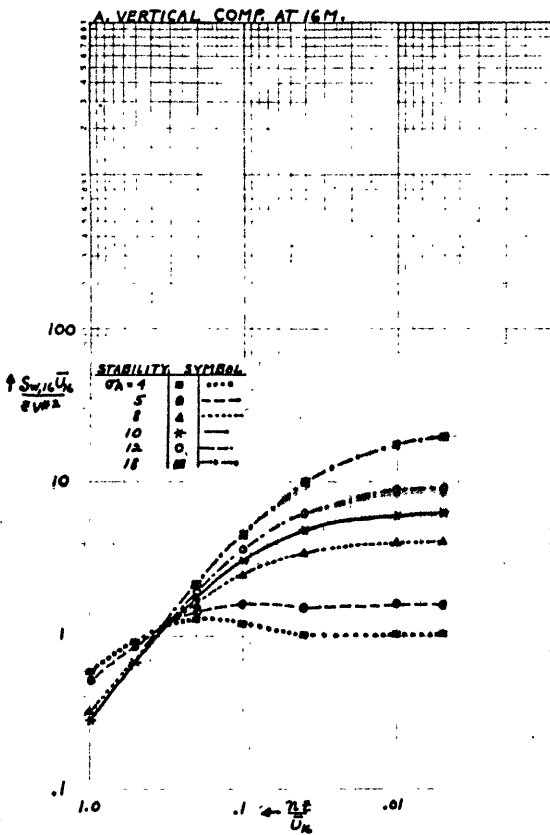


FIG. 17: CONTINUATION OF ALGEBRAIC EXPRESSIONS IN SIMILARITY COORDINATES



for about sixty runs, have been plotted and analyzed. The results are presented in Figures 18, 19, 20 and 21. This method would require a new set of figures for each site; if the functional relationships of the fluxes to the site parameters are well behaved, these figures may be quite predictable, after the accumulation of more data on the site variability and its effects. In Figure 21, the .05 labels of divergence of heat flux between 16 and 40 meters could be relabelled as cooling rates of approximately ten degrees centigrade per hour.

### 3. Regression analysis of power spectra.

The power spectral data for the twenty runs in similarity coordinates were multiplied by  $\frac{V^* \bar{U}}{\bar{U}^2}$  or by  $\frac{\bar{U} \bar{T}^* \bar{z}}{(\Delta T)^2}$  as appropriate. The quantity,  $(\Delta T)$ , is measured between the surface and 16 or 40 meters as required. Then at each of twelve selected frequencies ( $nz/\bar{U} = .007, .01, .015, .02, .03, .04, .07, .1, .2, .5, \text{ and } 1.0$ ), a regression graph of  $\sigma_n^2$  versus  $\frac{S_i \bar{U}}{z \bar{U}^2}$  or  $\frac{S_T \bar{U}}{z (\Delta T)^2}$  for each velocity component and temperature at each level was made. A simple curve, usually a straight line, was chosen by eye to best represent the data. See Table 8 and Figures 22 and 23.

Next, for each velocity component and temperature for each of the twelve frequencies, a value of  $S_{i,16,40} = \frac{S_{i,16,40} \bar{U}}{z \bar{U}_{16,40}^2}$  or  $\frac{S_{T,16,40} \bar{U}}{z (\Delta T)_{16,40}^2}$  was read, from the regression curves for each of six stabilities ( $\Lambda = 4, 5, 8, 10, 12, 18$ ) and recorded as shown in Table 9. From the derived data of Table 9, for each velocity component and temperature at each level,  $\log S_i$  or  $\log S_T$  vs.  $\log nz/\bar{U}$  was plotted, giving two figures of the energy spectral density of the component fluctuations with stability as a parameter. See Figures 24 - 27. These same data are also shown in appropriate semi-log

FIG. 18: HEAT AND MOMENTUM FLUX AS A FUNCTION OF THE MEAN WIND SPEED AND  $(\partial\theta/\partial z)^*$ , MODIFIED STABILITY PARAMETER.

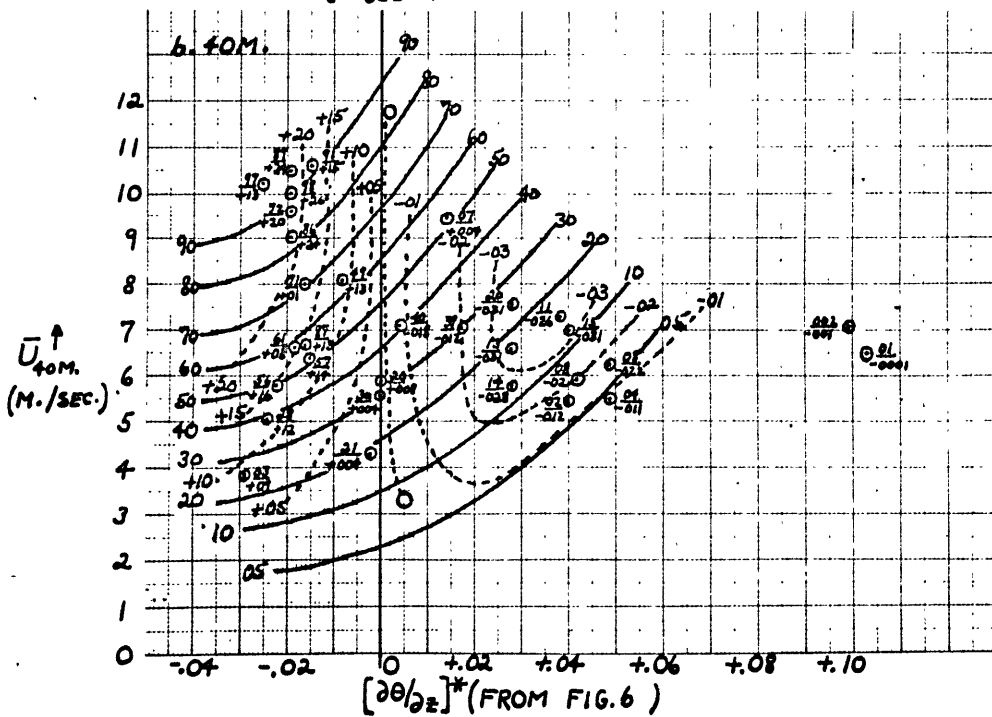
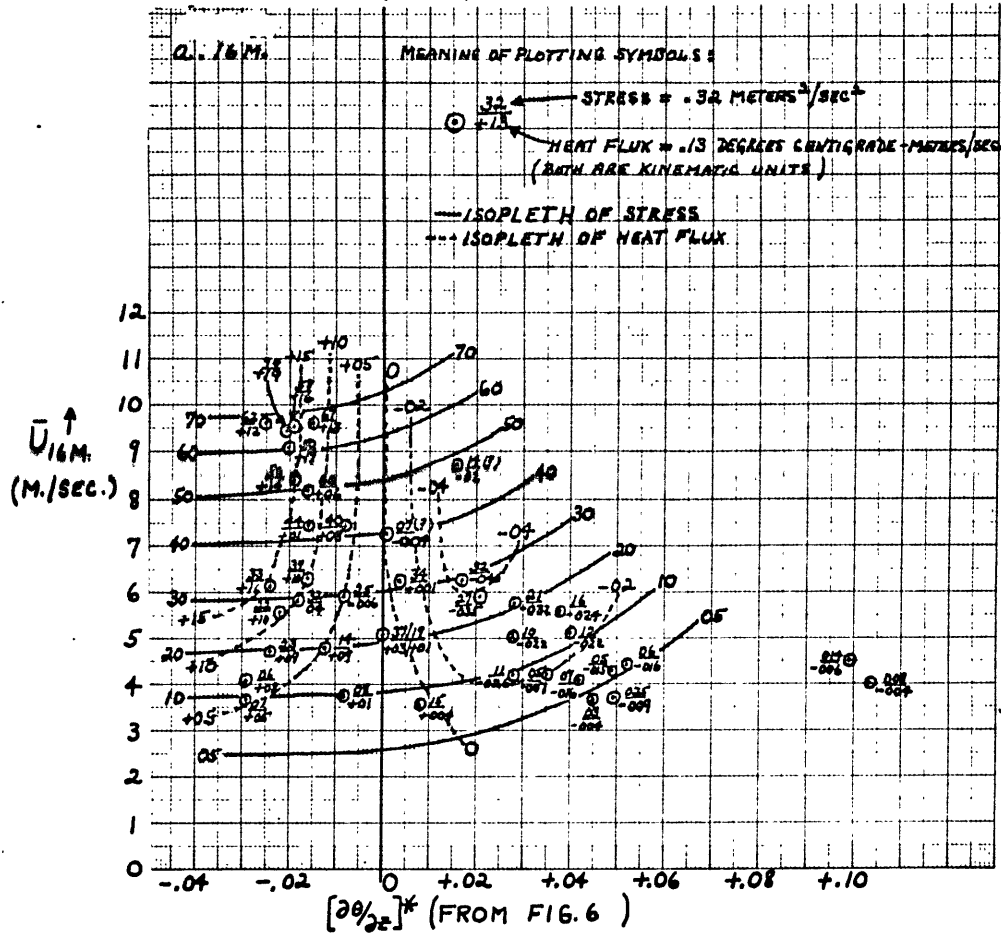


FIG. 19A: 16M. STRESS AND 40M. STRESS AS FUNCTIONS OF THE MEAN WIND SPEED AT 16M. AND THE TEMP. DIFFERENCE BETWEEN THE SURFACE AND 8M.

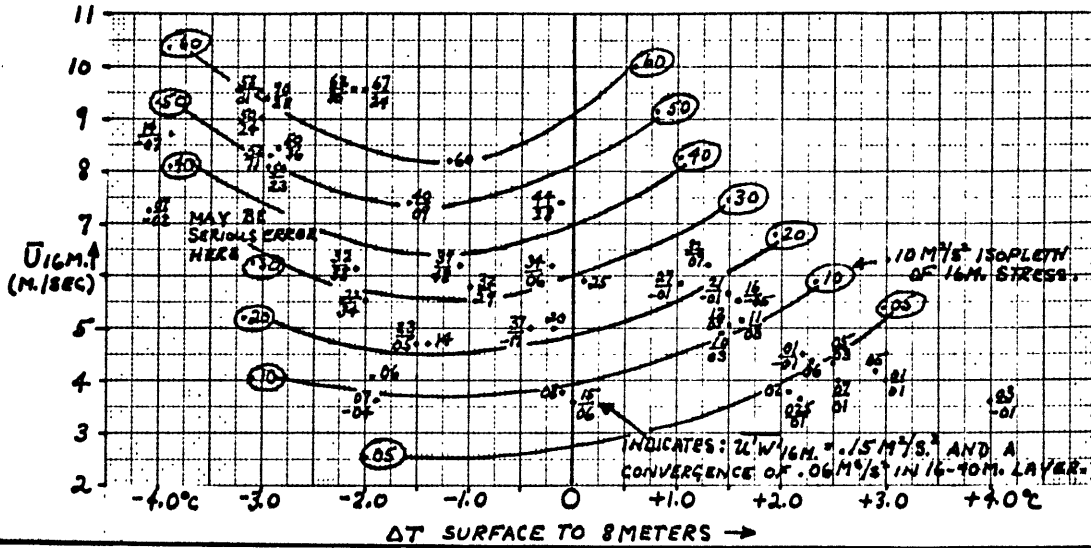


FIG. 19B: STRESS AS A FUNCTION OF WIND SHEAR AND THE TEMP. DIFFERENCE SURFACE TO 8M.

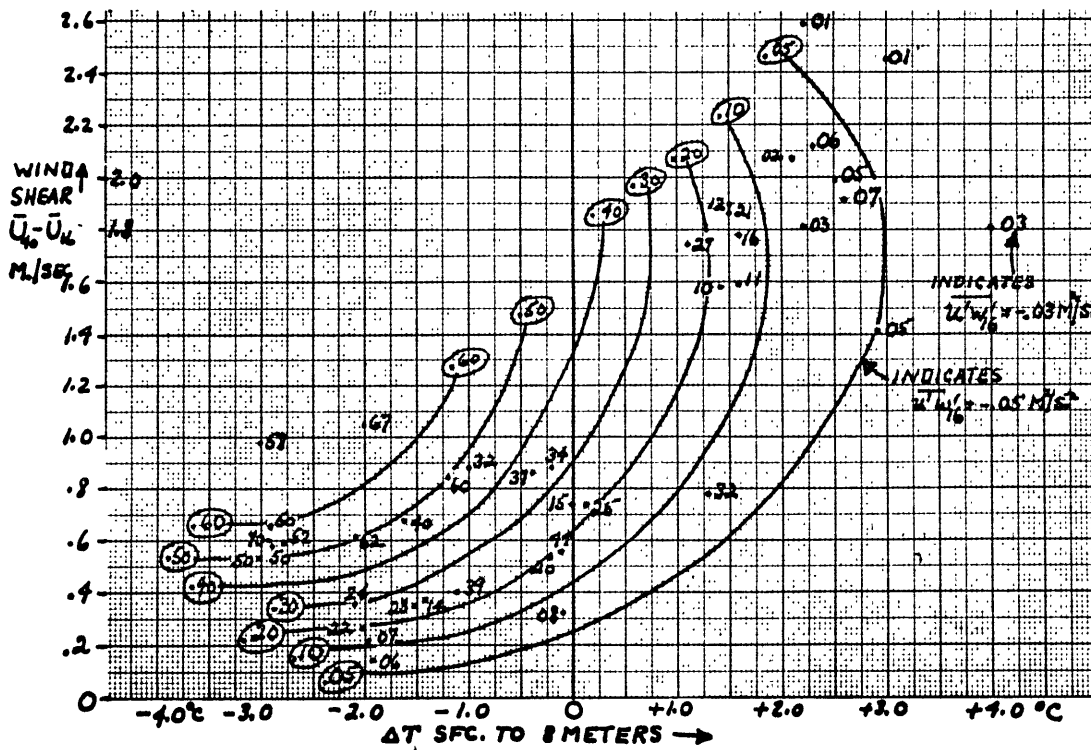


FIG. 20: HEAT FLUX AS A FUNCTION OF  $\frac{\partial \theta}{\partial z}$

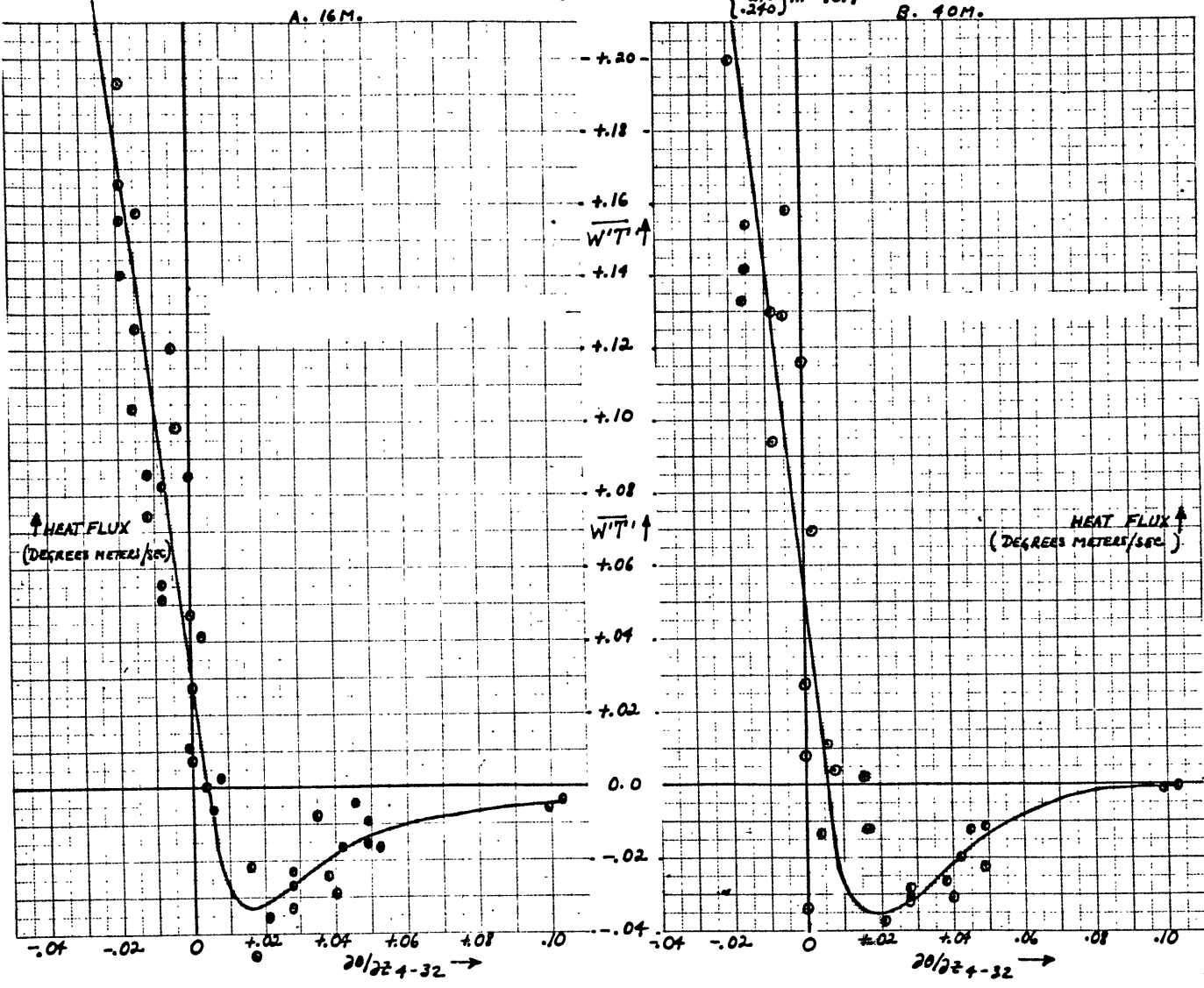




FIG. 21: HEAT FLUX AT 16M. AND FLUX DIVERGENCE IN 16-40M. LAYER AS A FUNCTION OF  $\bar{U}_{16}$  AND  $\Delta\text{TEMP. SFC-8M.}$

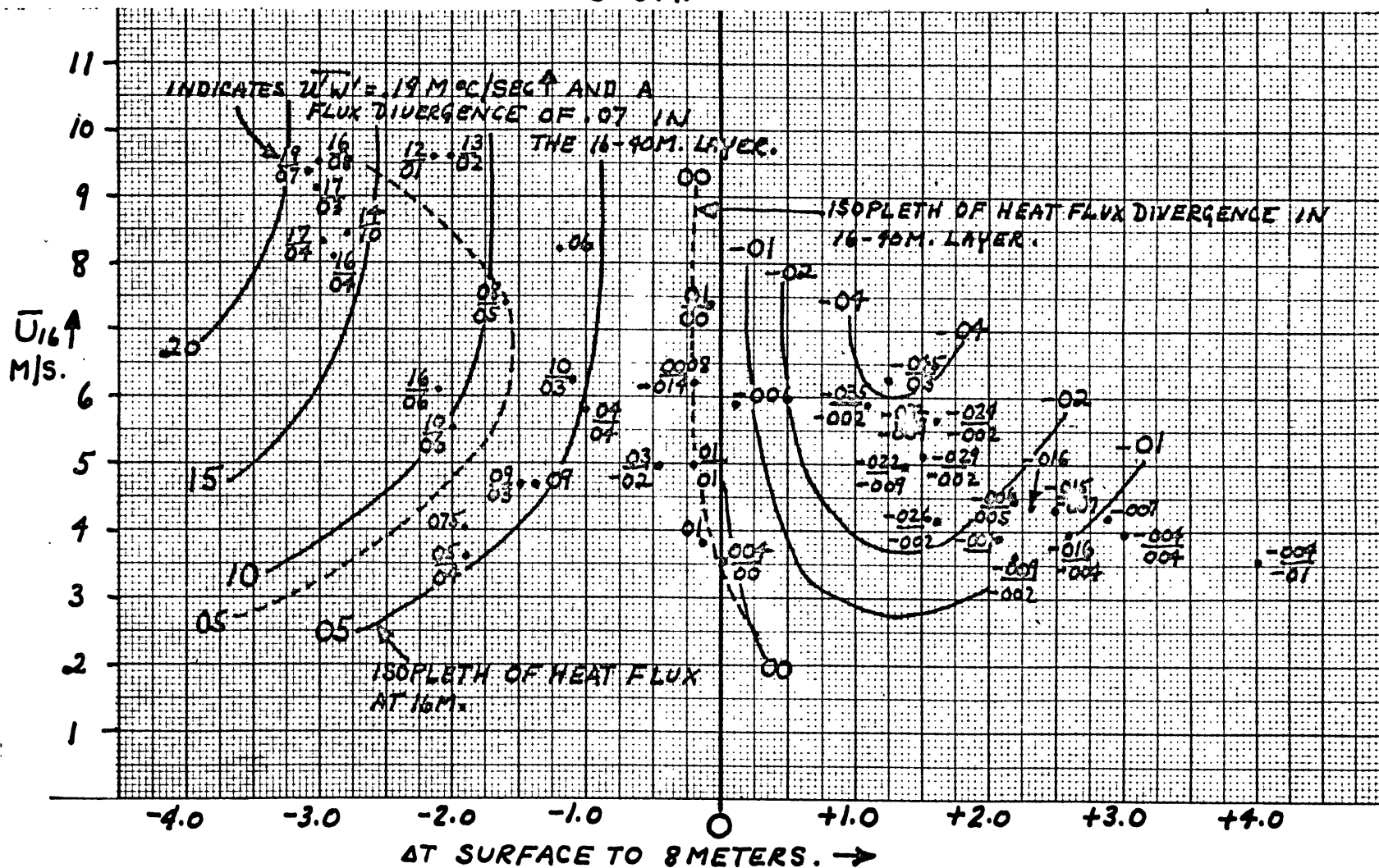


FIG. 22: SAMPLE OF REGRESSION GRAPHS FOR INDIVIDUAL FREQUENCIES (6 OF 96), V-COMR, 16M.

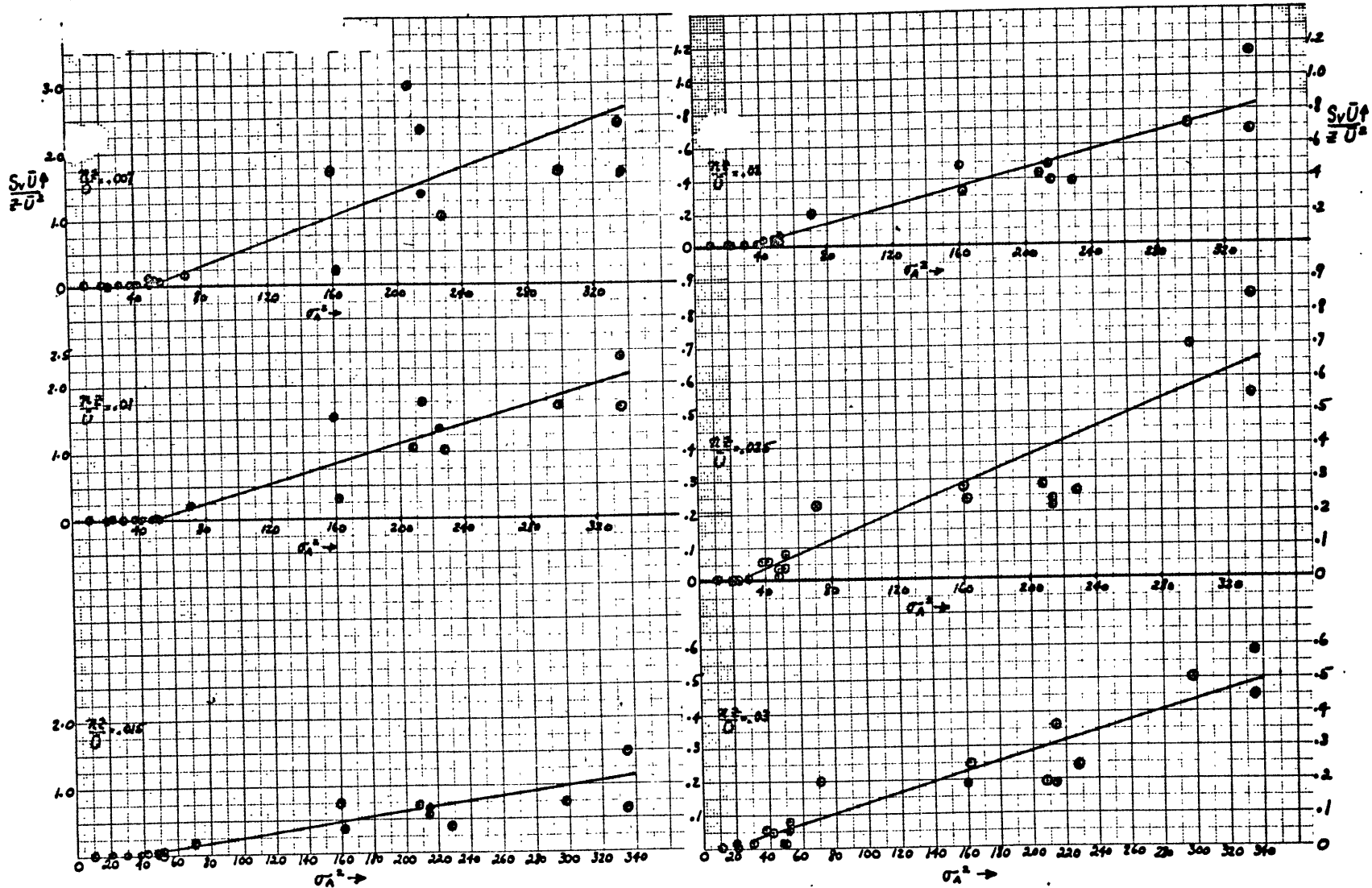


FIG. 23: CONTINUATION OF FIG. 22.

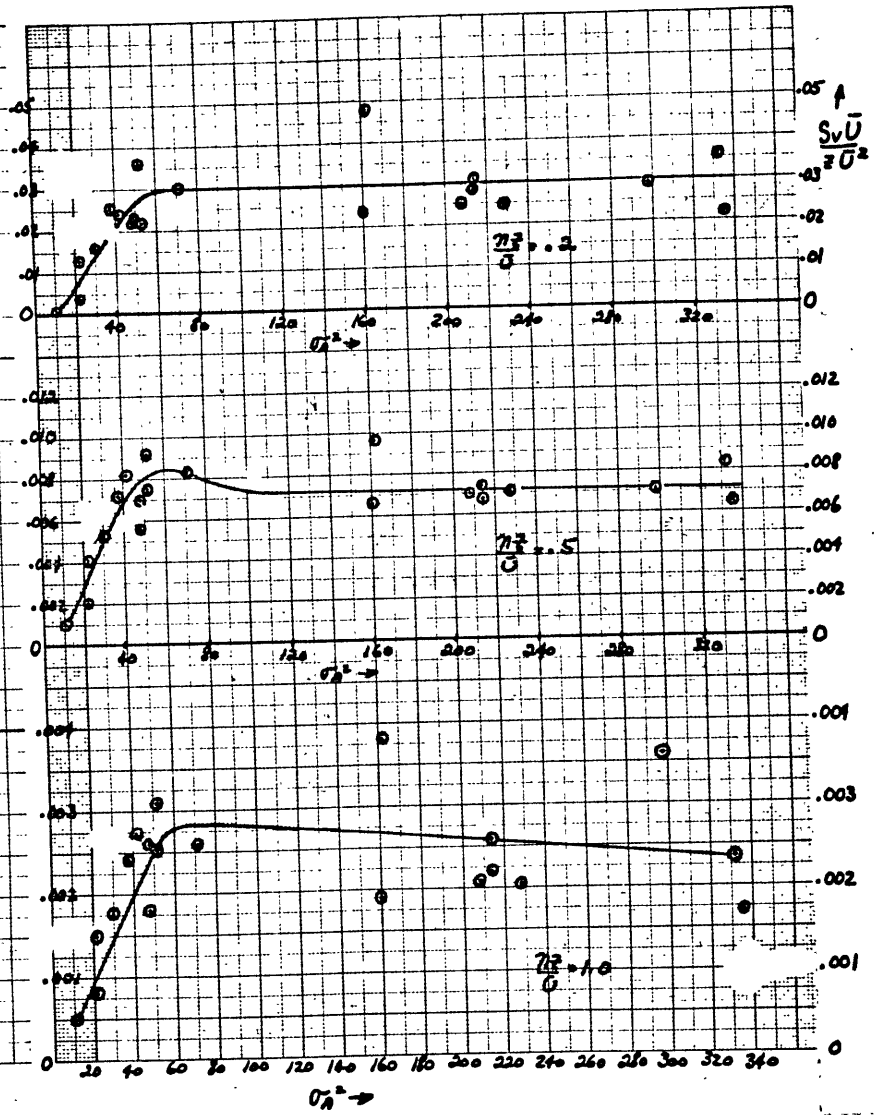
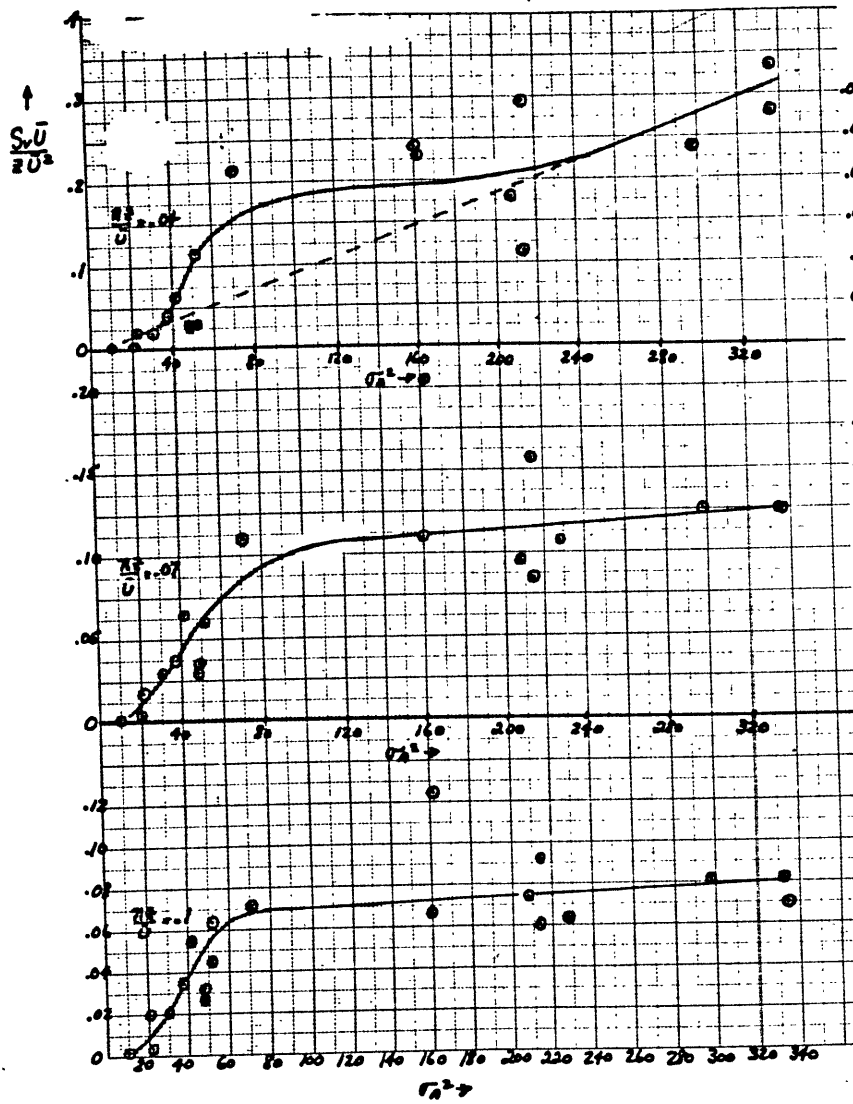


FIG. 24: ENERGY SPECTRAL DENSITY AS A FUNCTION OF STABILITY, OBTAINED BY REGRESSION.

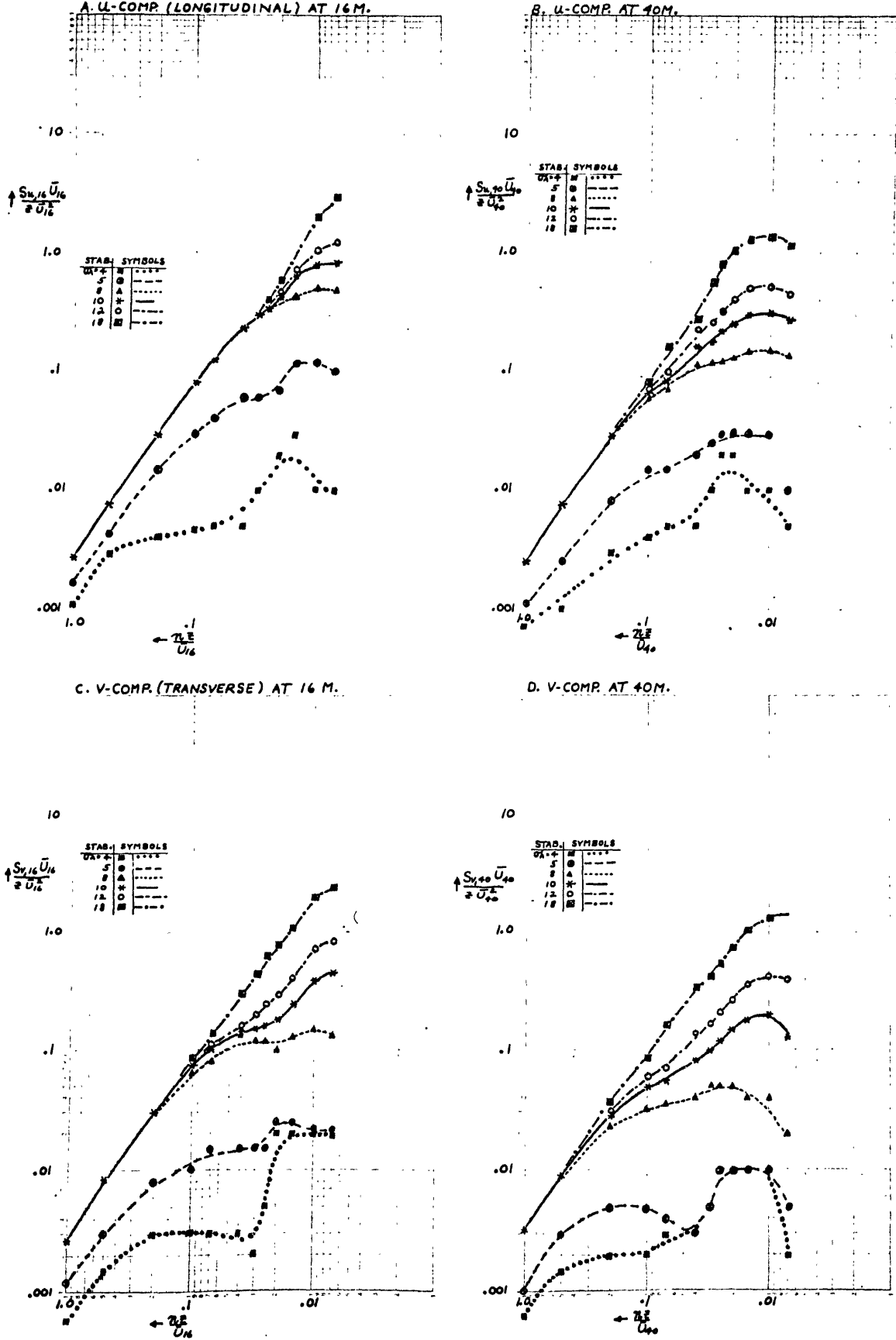


FIG. 25: ENERGY SPECTRAL DENSITY AS A FUNCTION OF STABILITY, OBTAINED BY REGRESSION.

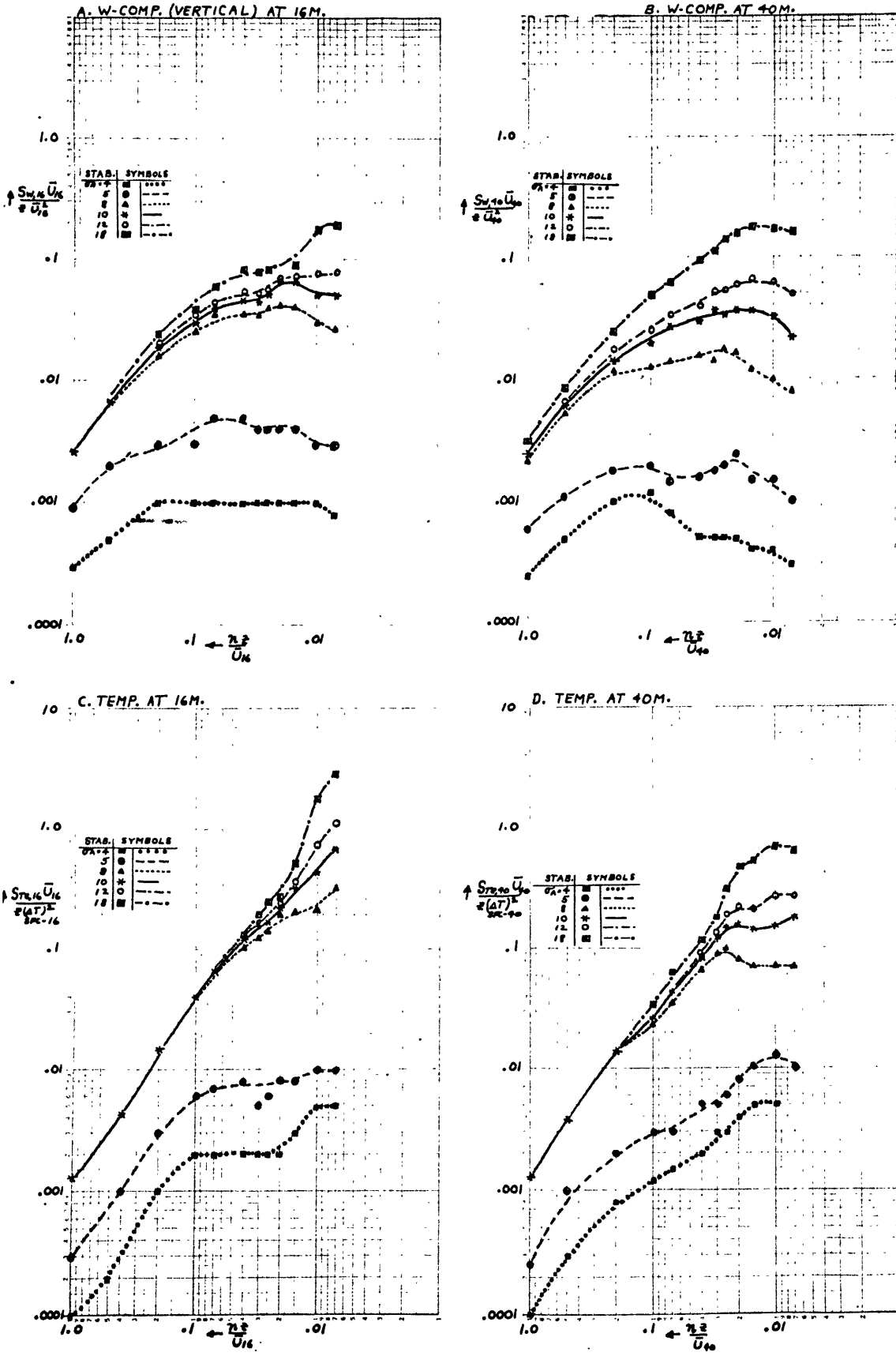


FIG. 26: SAME DATA AS SHOWN IN FIG. 24, IN SUITABLE SEMI-LOG. COORDINATES.  
 A.  $u$ -COMP. AT 16M. B.  $u$ -COMP. AT 40M.

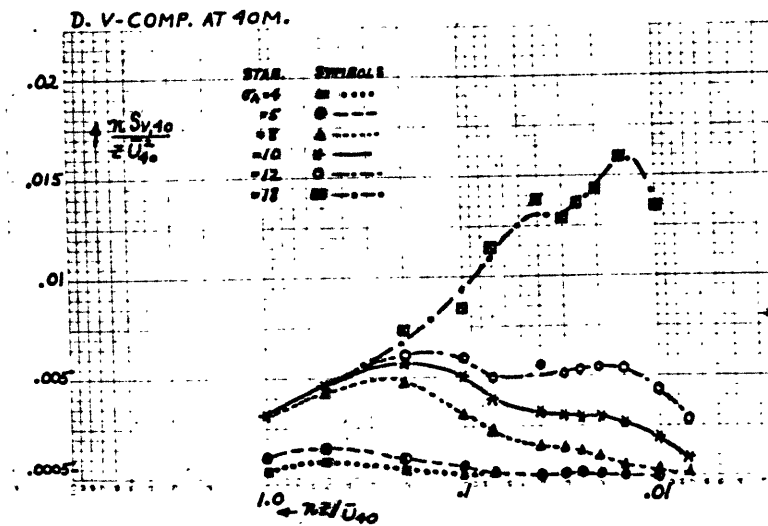
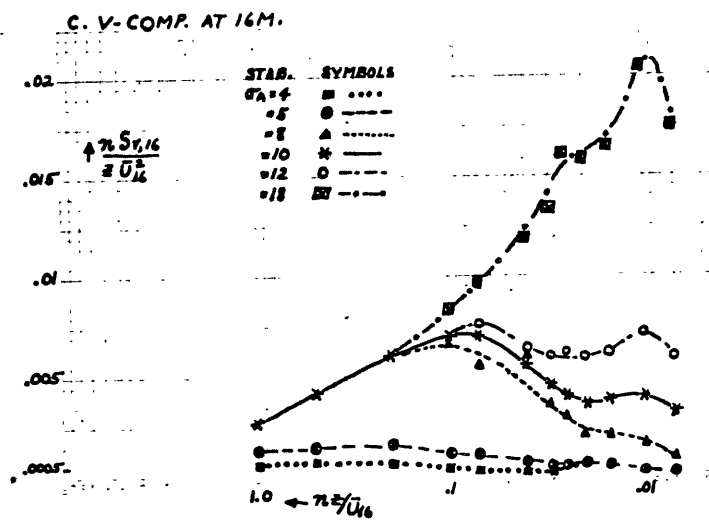
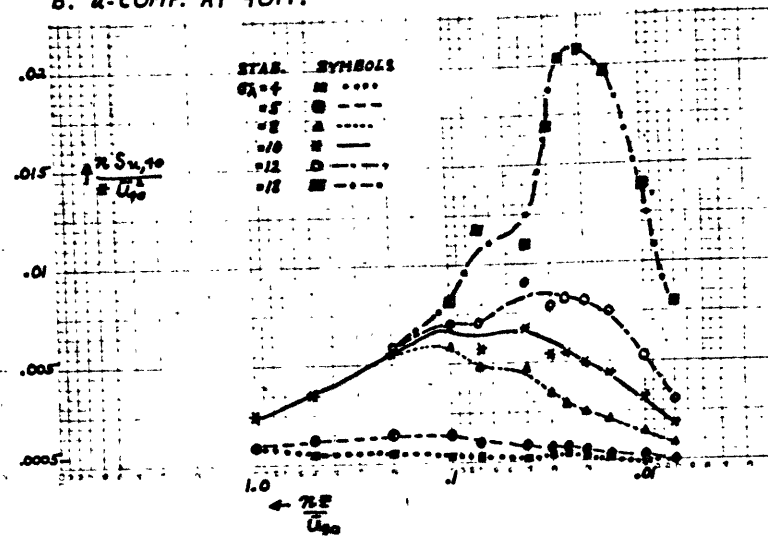
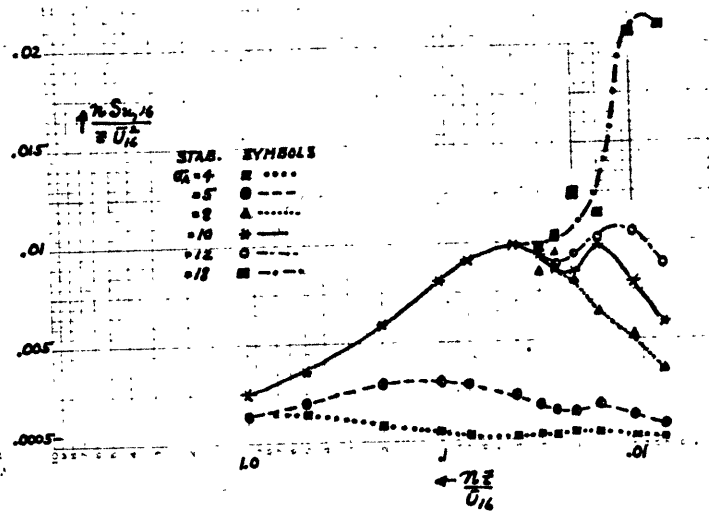
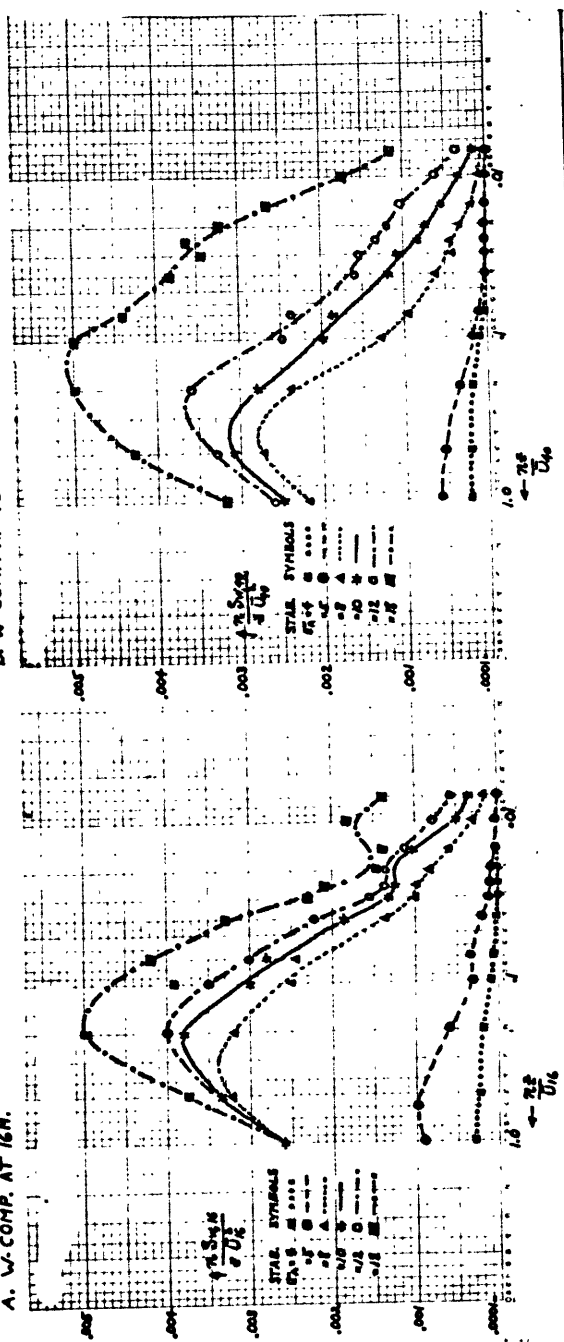
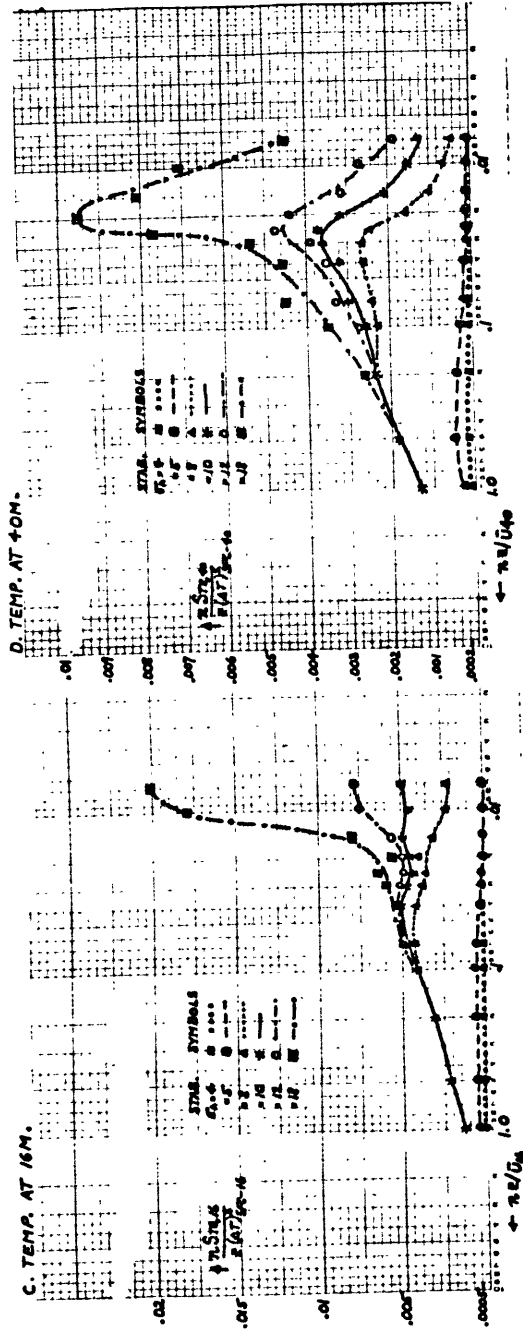


FIG. 27: SAME DATA AS SHOWN IN FIG. 25 IN SUITABLE SEMI-LOG COORDINATES.  
 A. W. COMP. AT 16M.



C. TEMP. AT 16M.



D. TEMP. AT 40M.

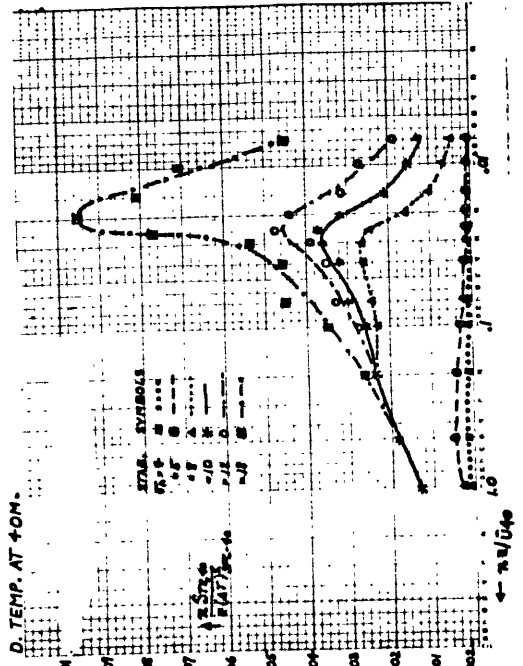


TABLE 8:  $\bar{U}^2$  NORMALIZED ENERGY SPECTRAL DENSITY VALUES FOR SELECTED FREQUENCIES ( $\pi z/\bar{U}$ ). (SAMPLE 1 OF 8)

V-COMP. :  $S_v \bar{U} / z \bar{U}^2$

RUN	$\sigma_A^2$ (16M) DEGREES	$\pi z/\bar{U}$	$X_1 = .007$	$X_2 = .01$	$X_3 = .015$	$X_4 = .02$	$X_5 = .025$	$X_6 = .03$	$X_7 = .04$	$X_8 = .07$	$X_9 = .1$	$X_{10} = .2$	$X_{11} = .5$	$X_{12} = 1.0$
66D	16M	47.7	.0262	.0330	.0291	.0238	.0238	.0277	.0335	.0301	.0282	.0218	.00703	.00257
+	40M			.0055	.0066	.0065	.0061	.0062	.0077	.0088	.0079	.0098	.00560	.00237
66E	16	29.8	.0228	.0220	.0226	.0221	.0186	.0214	.0209	.0271	.0209	.0163	.00542	.00176
⊗	40			.0129	.0106	.0082	.0063	.0055	.0049	.0054	.0075	.0058	.00450	.00202
66F	16	38.4	.0247	.0286	.0307	.0455	.0595	.0576	.0395	.0351	.0347	.0256	.00728	.00238
⊙	40			.0064	.0078	.0095	.0107	.0113	.0108	.0086	.0143	.0171	.0134	.00605
67A	16	42.0	.0272	.0361	.0506	.0620	.0608	.0526	.0664	.0646	.0550	.0241	.00824	.00272
∞	40			.0098	.0126	.0160	.0174	.0171	.0157	.0112	.0153	.0140	.0153	.00700
67B	16	52.8	.0518	.0564	.0613	.0724	.0845	.0853	.114	.0853	.0640	.0358	.00920	.00312
x	40			.0088	.0112	.0145	.0182	.0222	.0248	.0196	.0239	.0211	.0182	.00815
67C	16	70.6	.186	.220	.193	.199	.223	.203	.214	.109	.0710	.0300	.00835	.00257
*	40			.0450	.0555	.070	.0740	.0715	.0648	.0495	.0580	.0630	.0308	.00975
67D	16	160.0	1.71	1.52	.745	.487	.283	.197	.237	.110	.0672	.0234	.00658	.00191
A	40			.505	.530	.530	.462	.362	.294	.262	.0645	.0568	.0281	.00750
67E	16	208.	2.98	1.07	.705	.426	.284	.190	.180	.0950	.0740	.0251	.00705	.00210
v	40			1.26	1.45	.900	.388	.236	.187	.137	.0550	.0460	.0286	.00725
67G	16	216.	2.32	1.74	.650	.390	.239	.192	.113	.0836	.0610	.0272	.00683	.00225
◇	40			1.18	1.21	.846	.540	.390	.266	.152	.0870	.0533	.0212	.00728
31	16	162.5	.238	.322	.366	.321	.244	.252	.228	.208	.119	.0987	.00975	.00380
○	40			.033	.0477	.0621	.075	.077	.076	.0580	.119	.0760	.0128	.00522
32	16	214.	2.84	1.37	.590	.490	.220	.361	.294	.157	.0920	.0304	.00735	.00260
□	40			.595	.590	.400	.257	.213	.189	.116	.0663	.0429	.0105	.00429
33	16	298.	2.94	1.68	.750	.722	.700	.505	.238	.126	.0814	.0295	.00715	.00365
▽	40			.805	.770	.705	.476	.352	.254	.171	.102	.0427	.0115	.00312
34	16	333.	2.66	2.40	1.50	1.15	.805	.585	.334	.125	.0815	.0360	.00835	.00235
⊖	40			1.02	.875	.765	.645	.525	.515	.208	.0680	.0295	.00940	.00312
35	16	11.6	.0268	.0208	.0063	.0026	.0021	.0022	.0019	.0019	.0022	.0020	.00116	.00050
■	40			.0555	.0531	.0412	.0288	.0258	.0194	.0038	.0026	.0017	.00119	.00070
36	16	21.8	.0270	.0174	.0034	.0031	.0027	.0016	.0040	.0055	.0045	.0035	.00214	.00080
◆	40			.0193	.0126	.0038	.0021	.0018	.0017	.0006	.0005	.0002	.00024	.00012
38	16	335.	3.90	1.67	.654	.678	.550	.448	.282	.125	.0690	.0224	.00646	.00173
⊞	40			1.26	1.12	.782	.480	.391	.351	.125	.100	.0418	.00945	.00297
39	16	228.	1.62	1.03	.404	.385	.263	.244	.225	.108	.0620	.0253	.00713	.00206
⊠	40			.713	.595	.440	.333	.266	.184	.114	.0583	.0321	.00940	.00266
40	16	22.1	.0296	.0255	.0198	.0176	.0178	.0172	.0221	.0185	.0202	.0130	.00435	.00147
●	40			.0122	.0077	.0081	.0050	.0031	.0032	.0027	.0043	.0048	.00216	.00122
41	16	49.0	.0426	.0509	.0605	.0524	.0340	.0250	.0325	.0336	.0228	.00560	.00183	
▼	40			.0230	.0276	.0264	.0235	.0195	.0170	.0258	.0230	.0135	.00531	.00221
42	16	53.5	.0483	.0475	.0298	.0370	.0460	.0376	.0328	.0610	.0448	.0218	.00757	.00256
▲	40			.0049	.0071	.0095	.0133	.0167	.0201	.0190	.0125	.0122	.00750	.00284



TABLE 9: DERIVED DATA — a. FROM REGRESSION :  $S_v \bar{U} / z \bar{U}^2$  VS. SELECTED VALUES OF  $nz/\bar{U}$ , STABILITY EXPRESSED BY  $\sigma_n$ ; b. FROM ALGEBRAIC FUNCTIONS :  $S_v \bar{U} / z v^{*2}$  VS. SELECTED VALUES OF  $nz/\bar{U}$ , STABILITY EXPRESSED BY  $(\sigma_n / \sigma_n)^2$

a. V-COMP (16 M.)  $S_v \bar{U} / z \bar{U}^2$  — FROM REGRESSION

$\sigma_n$	$\frac{nz}{\bar{U}} =$	.007	.01	.015	.02	.025	.03	.04	.07	.1	.2	.5	1.0
4	$\frac{S_v \bar{U} / z \bar{U}^2}{n S_v \bar{U} / z \bar{U}^2}$	.02	.02	.02	.02	.005	.002	.003	.003	.003	.003	.0015	.0006
5		.00014	.0002	.0003	.0004	.000125	.00006	.00012	.00021	.0003	.0006	.00075	.0006
8		.02	.02	.025	.025	.015	.015	.015	.015	.01	.008	.003	.0012
10		.00014	.0002	.0005	.0005	.00038	.00045	.0006	.00105	.001	.0016	.0015	.0012
12		.13	.15	.13	.10	.12	.12	.15	.08	.067	.029	.009	.0028
18		.00091	.0015	.00195	.002	.003	.0036	.0060	.0056	.0067	.0058	.0045	.0028
4		.46	.40	.25	.18	.16	.15	.14	.10	.07	.03	.009	.0028
5		.00322	.0040	.0038	.0036	.004	.0045	.0056	.007	.007	.006	.0045	.0028
8		.85	.72	.41	.30	.25	.20	.16	.11	.07	.03	.008	.0027
10		.0060	.0072	.0062	.006	.0062	.006	.0064	.0077	.007	.006	.004	.0027
12		2.50	2.05	1.10	.80	.65	.45	.30	.14	.085	.03	.0075	.0025
18		.0175	.0205	.0165	.016	.0162	.0135	.012	.0098	.0085	.006	.0038	.0025

(40 M.)

4		.002	.01	.01	.01	.01	.005	.003	.003	.002	.002	.0015	.0003
5		.000014	.0001	.00015	.0002	.00025	.00015	.00012	.00021	.0002	.0004	.00075	.0003
8		.005	.01	.01	.01	.01	.005	.003	.004	.005	.006	.003	.001
10		.000035	.0001	.00015	.0002	.00025	.00015	.00012	.00028	.0005	.001	.0015	.001
12		.02	.04	.04	.05	.05	.05	.04	.035	.032	.024	.0085	.003
18		.00014	.0004	.0006	.001	.00125	.0015	.0016	.00245	.0032	.0048	.0042	.003
4		.13	.20	.18	.15	.12	.10	.08	.055	.05	.028	.009	.0033
5		.00091	.002	.0027	.003	.003	.003	.0032	.0038	.005	.0058	.0045	.0033
8		.40	.43	.36	.27	.21	.17	.14	.07	.06	.031	.009	.0032
10		.0028	.0043	.0054	.0054	.0053	.0051	.0056	.0049	.006	.0062	.0046	.0032
12		1.35	1.07	.77	.55	.43	.35	.165	.085	.037	.009	.0031	.0031
18		.0135	.0160	.0144	.0138	.0129	.0140	.0115	.0085	.0074	.0045	.0031	.0031

b. V-COMP (16 M.) FROM ALGEBRAIC FUNCTIONS

$(\frac{\sigma_n}{\sigma_n})^2$	$\frac{nz}{\bar{U}} =$	.005	.01	.04	.1	.2	.5	1.0
6.25	$\frac{S_v \bar{U} / z v^{*2}}{S_v \bar{U} / z v^{*2}}$	1.64	2.06	6.26	8.83	7.47	2.54	.873
4.0		3.2	4.03	9.95	11.45	7.60	2.14	.710
1.56		13.1	16.2	20.6	11.7	4.86	1.13	.360
1.0		25.4	30.8	26.0	11.8	4.22	.943	.299
.69		260.	146.	34.5	10.45	3.78	.891	.290
.31		502.	254.	46.5	12.1	4.12	.923	.296

(SAMPLE 1 OF 8)

(40 M.)

6.25		.97	1.38	2.14	4.13	5.40	2.58	1.13
4.0		1.71	2.16	3.30	5.30	5.87	2.32	.923
1.56		4.40	5.50	8.0	7.75	5.45	1.39	.472
1.0		7.0	8.6	11.8	9.8	6.5	1.22	.395
.69		50.5	58.5	39.0	13.8	5.6	1.02	.340
.31		106.	120.	46.5	13.2	3.16	.585	.186

coordinates,  $\eta \delta_i$  or  $\eta \delta_T$  versus  $\log \frac{\eta z}{\sigma}$  in Figures 26 and 27.

The data in Figures 22 - 29 show a number of important features. From Figures 29 and 30, despite considerable scatter in the graphs of  $\delta_i$  versus

$\sigma_A^2$  at a particular frequency, some general relationships are evident.

Two regions seem to appear: (a) for runs more stable than  $\sigma_A = 7$ , the graph of  $\delta_u$  is a rapidly increasing function of  $\sigma_A^2$ ; (b) for runs with  $\sigma_A > 7$ , the graph of  $\delta_u$  is less strongly dependent on  $\sigma_A^2$ . At low frequencies, the slope is less strongly dependent on  $\sigma_A^2$  and becomes independent of  $\sigma_A^2$  in going to higher frequencies. With very great stability ( $\sigma_A < 5$ ), the  $\delta_u$  values become insignificantly small. These graphs suggest two different regimes of turbulence with the transition region near  $\sigma_A = 7$  or  $(\frac{\partial \delta}{\partial z})^* \approx .01 \text{ } \alpha/m$ . Figures 6 and 18 also support some discontinuity in other functions as well, in that region. In the case of  $\delta_v$ , with  $\sigma_A < 7$ , there is no significant energy until  $\frac{\eta z}{\sigma} > .03$  at 16 m. or for  $\frac{\eta z}{\sigma} > .04$  at 40 m.. Otherwise, the behavior of  $\delta_v$  is such like that of  $\delta_u$ .  $\delta_{w,16}$  shows the same two regions with the zone of transition in the vicinity of  $\sigma_A = 7$  and its behavior is quite similar to  $\delta_u$ . The stable region ( $\sigma_A < 7$ ) shows a very strong dependence of  $\delta_{w,16}$  on  $\sigma_A^2$ , possibly  $\delta_{w,16} = a[\sigma_A^2]^2 + b$ . In the unstable region, the graph of  $\delta_{w,16}$  is less dependent on  $\sigma_A^2$  than is  $\delta_u$  but shows the same decreasing dependence on  $\sigma_A^2$  with increasing frequency, characteristic of the  $\delta_u$  and  $\delta_v$  functions.  $\delta_{w,40}$  is similar to  $\delta_{w,16}$  except that no significant energy is seen in the stable region until  $\frac{\eta z}{\sigma} > .04$ . The  $\delta_T$  behavior is most like that of  $\delta_u$ .

As shown in Figures 24, 25, 28 and 29, the  $\bar{U}^2$  and  $(\Delta T)^2$ -normali-

FIG. 28: COMPARISON OF ENERGY SPECTRAL DENSITY FUNCTIONS AT 16 AND 40 MHz.

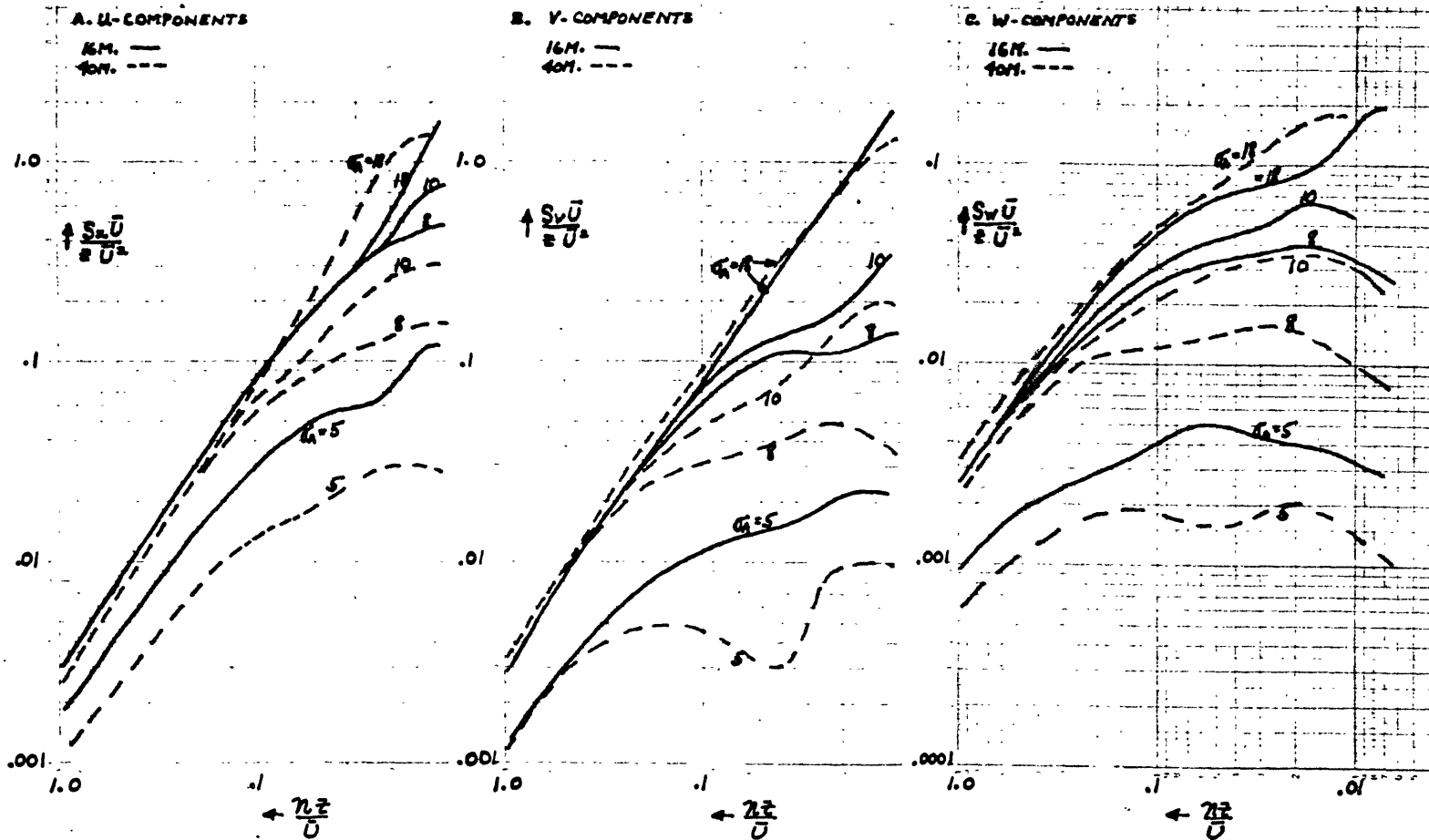
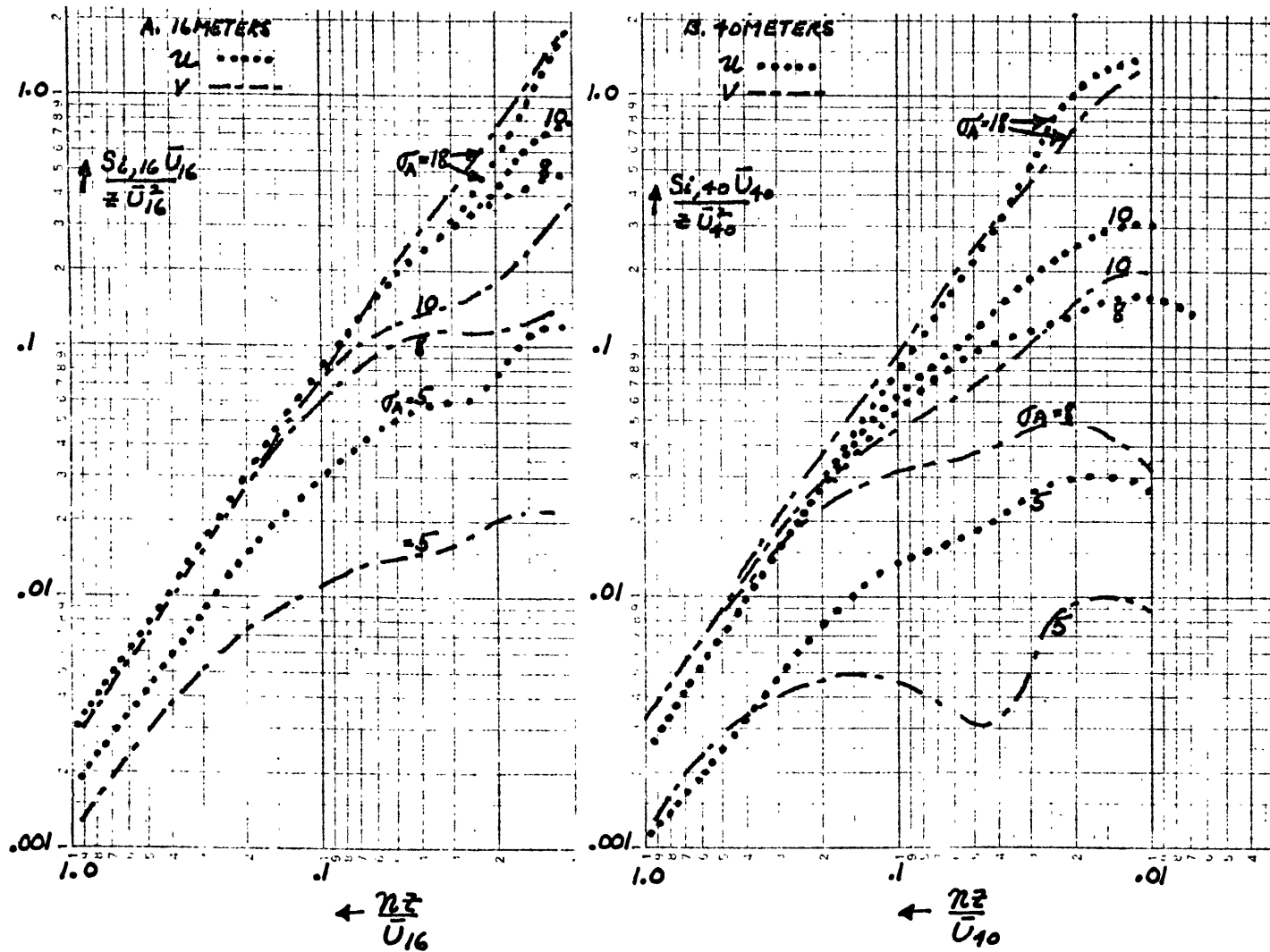


FIG. 29: COMPARISON OF ENERGY SPECTRAL DENSITY FUNCTIONS OF  $u$  AND  $v$  COMPONENTS



zations are successful at high frequencies for  $\sigma_A > 7$ , except for  $S_{w,40}$ . All functions show the increasing dependence on stability in going toward lower frequencies. At the highest frequencies, a  $-5/3$  slope will fit well but toward lower frequencies, the slope takes a less absolute value, which is nearly uniform over a considerable frequency range for the  $S_u$ ,  $S_v$ , and  $S_T$  functions. A comparison of Figures 28 and 29 shows that, at high frequencies, the normalized spectral density function is nearly the same for  $S_{u,16}$ ,  $S_{u,40}$ ,  $S_{v,16}$  and  $S_{v,40}$ . Also  $S_{w,16}$  and  $S_{w,40}$  are in close agreement, although the normalization is not as good at 40m.

Figures 24-27 show a huge peak of low-frequency "convective" energy, with unstable stratification, which appears to be separate from the higher-frequency maximum, which is less stability-dependent and apparently associated with mechanical energy input. Individual runs show this behavior more clearly and it is significant that this feature is retained, after the amount of smoothing of the data which is inherent to this analysis method. The semi-log plots, Figures 26 and 27, give the energy comparison more graphically. More is said about these two separate areas of suggested energy input later. The main purpose of these figures grouped under Section V E 3 is to exhibit the general effect of the combination of frequency and stability on normalized power spectral density functions.

#### 4. Discussion of normalizing techniques.

Seven runs, selected for their diversity in wind speed and stability, are replotted in the coordinates indicated below. These runs are:  
 Run 31,  $\sigma_A = 12.7^\circ$ ,  $\bar{U}_{16} = 3.6\text{m./sec}$ ; Run 34,  $\sigma_A = 18.2^\circ$ ,  $\bar{U}_{16} = 4.7\text{m./sec}$ ;  
 Run 35,  $\sigma_A = 3.4^\circ$ ,  $\bar{U}_{16} = 4.0\text{m./sec}$ ; Run 40,  $\sigma_A = 4.7^\circ$ ,  $\bar{U}_{16} = 3.7\text{m./sec}$ ;

Run 66E,  $\bar{\sigma}_A = 5.4^\circ$ ,  $\bar{U}_{16} = 4.3\text{m/sec}$ ; Run 67C,  $\bar{\sigma}_A = 8.4^\circ$ ,  $\bar{U}_{16} = 6.2\text{m/sec}$ ;  
 Run 67E,  $\bar{\sigma}_A = 14.4^\circ$ ,  $\bar{U}_{16} = 9.6\text{m/sec}$ . The coordinates are  $\log \frac{S_{ij} \bar{U}_j}{z_j \bar{U}_{(2)}^2}$   
 versus  $\log T$ , where  $S$  = kinetic energy spectral density and  $i = u, v$ ;  
 $j = 16\text{m}, 40\text{m}$ ;  $\bar{U}_{(2)}$  = mean wind at 2 meters;  $T$  = time in seconds (see  
 Figure 30).

These same runs are also presented in the form  $\log \frac{S_{ij} \bar{U}_j}{\bar{U}_{(2)} z_j}$  versus  
 $\log \frac{n z_j}{\bar{U}_j}$  where  $i = u, v$ , and  $j = 16\text{m}, 40\text{m}$ . (see Figure 31).

The last set to be presented here is  $n S_{ij}$  versus  $\log T$ ;  
 $T$  = period in seconds,  $i = u, v, w$ , Temp.;  $j = 16, 40\text{m}$ ., giving eight figures;  
 (see Figures 32 - 39).

Two systems used by Cramer (1960) are of particular interest because  
 of their success in "normalizing" a variety of runs. These are (a) use  
 of  $\bar{U}^{2/3}$  for normalization of spectral density values and (b)  $\log \frac{S_i \bar{U}}{\bar{U}^2}$   
 versus  $\log \frac{n z}{\bar{U}}$ .

The purpose of examining various coordinate systems here is to see  
 which is best suited to describe the functional behavior of the spectral  
 density functions in terms of physically relevant quantities. A summary  
 of the six systems to be compared is:

(a) Similarity coordinates,  $\log \frac{S_i \bar{U}}{z \bar{U}^2}$  or  $\log \frac{S_T \bar{U}}{z \bar{U}^2}$  versus  $\log \frac{n z}{\bar{U}}$   
 (Figures 8 - 15).

(b) Normalization by  $\bar{U}^2$  or  $(\Delta T)^2$ ,  $\log \frac{S_i \bar{U}}{z \bar{U}^2}$  or  $\log \frac{S_T \bar{U}}{z (\Delta T)^2}$  versus  
 $\log n z / \bar{U}$ , (Figures 24 and 25).

(c) Semi-log plot of (b),  $\frac{n S_i}{z \bar{U}^2}$  or  $\frac{n S_T}{z (\Delta T)^2}$  versus  $\log n z / \bar{U}$ , (Figures  
 26 and 27).

(d)  $\log \frac{S_i}{z \bar{U}_{(2)}^2}$  versus  $\log T$ , (Figure 30.)

FIG. 30: ENERGY SPECTRAL DENSITY FOR A SELECTION OF DIVERSIFIED RUNS AS A FUNCTION OF PERIOD; NORMALIZATION IS WITH RESPECT TO  $U^2$  AT 2M LEVEL.  
 A. W-COMP. AT 16M.  
 B. V-COMP. AT 16M.

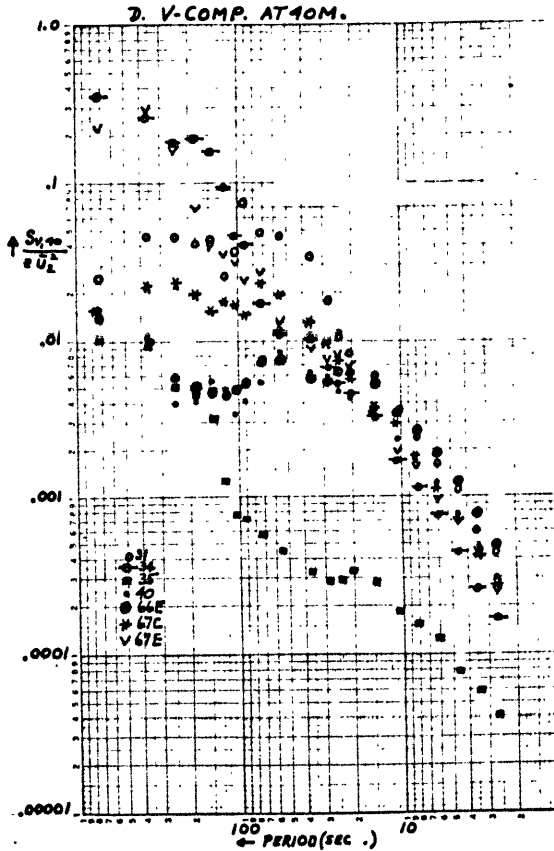
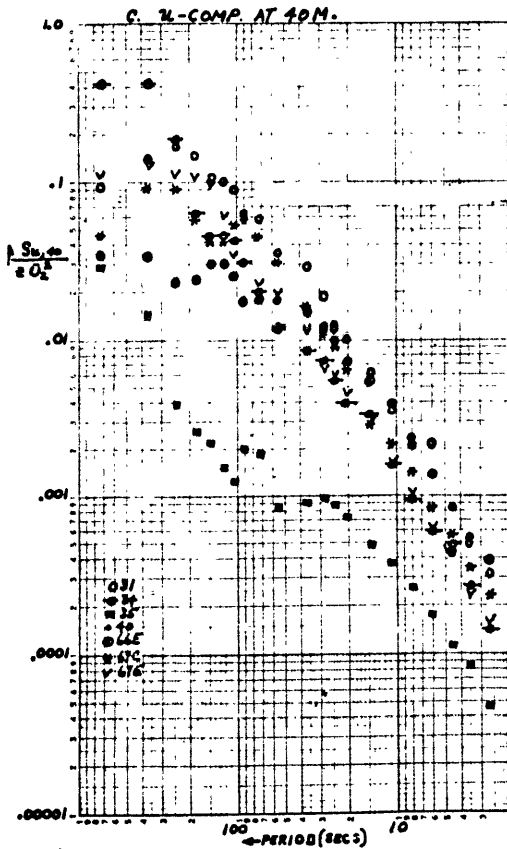
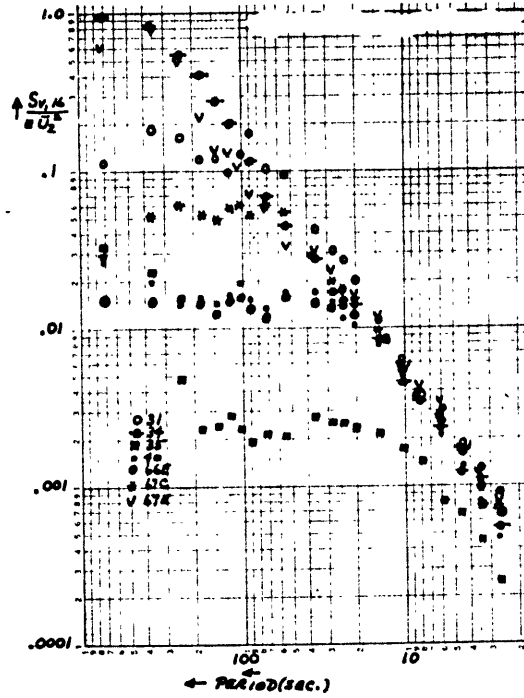
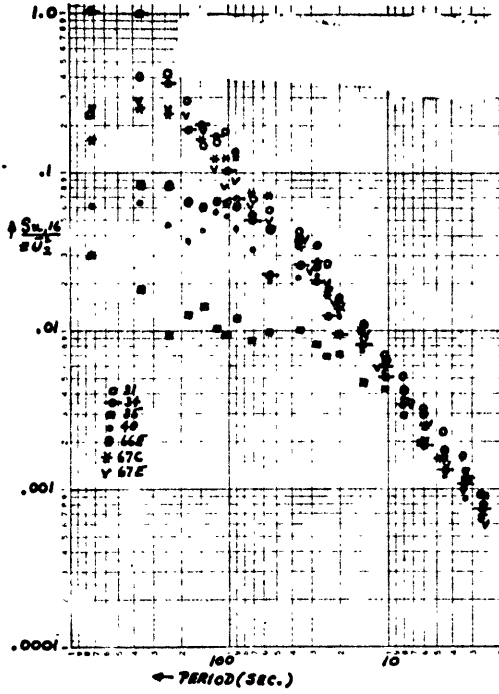


FIG. 31: SAME DATA AS FIG. 30, BUT USING COORDINATES  $\frac{S_{u,z}}{U_0}$  VS.  $\frac{z}{U_0}$ , WHERE  $z = u$  OR  $v$   
 A. u-COMP. AT 16M. B. v-COMP. AT 16M.  
 z = 16 OR 40M.

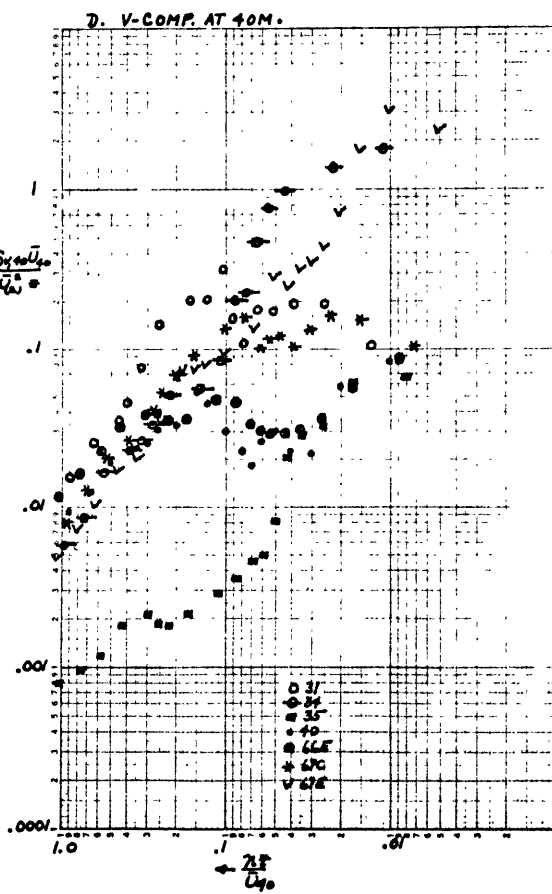
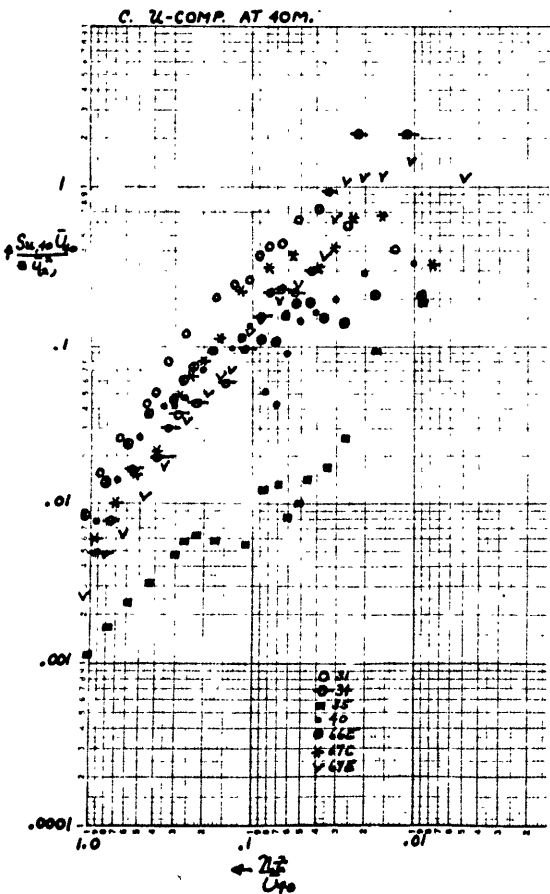
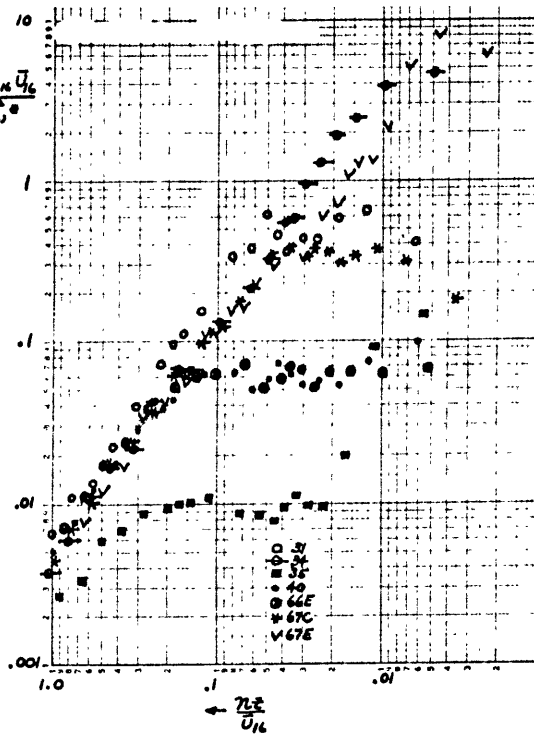
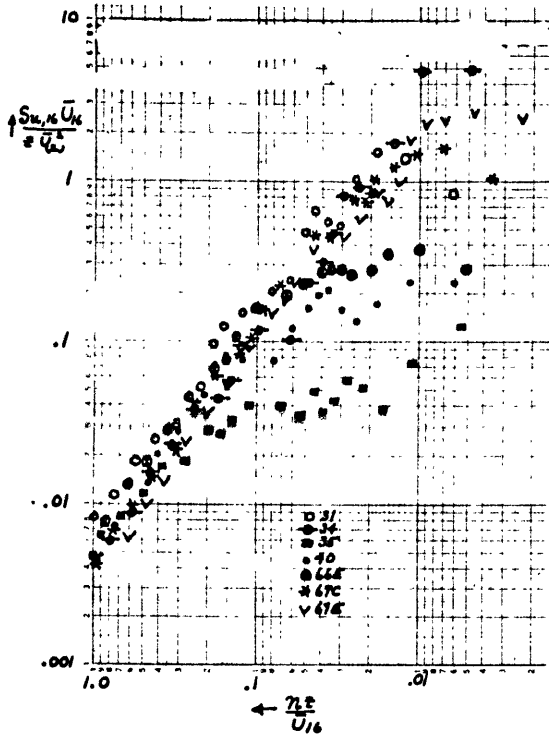




FIG. 32: POWER SPECTRA FOR 9 RUNS IN COORDINATES  $nS_{u,16}$  VS. LOG T,  
T - PERIOD (SEC)

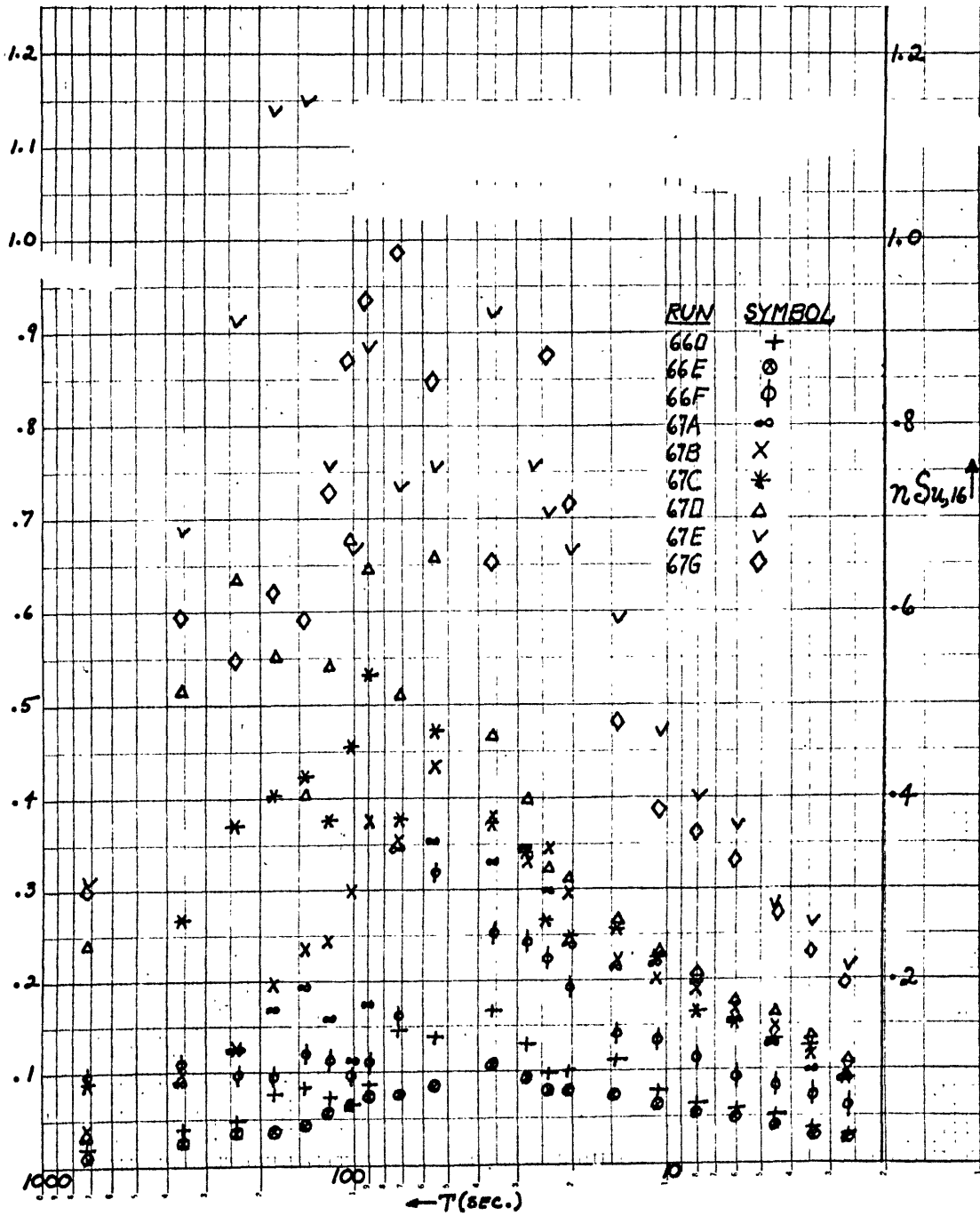


FIG. 33: POWER SPECTRA FOR 9 RUNS IN COORDINATES  $\pi S_{y,16}$  VS. LOG T.

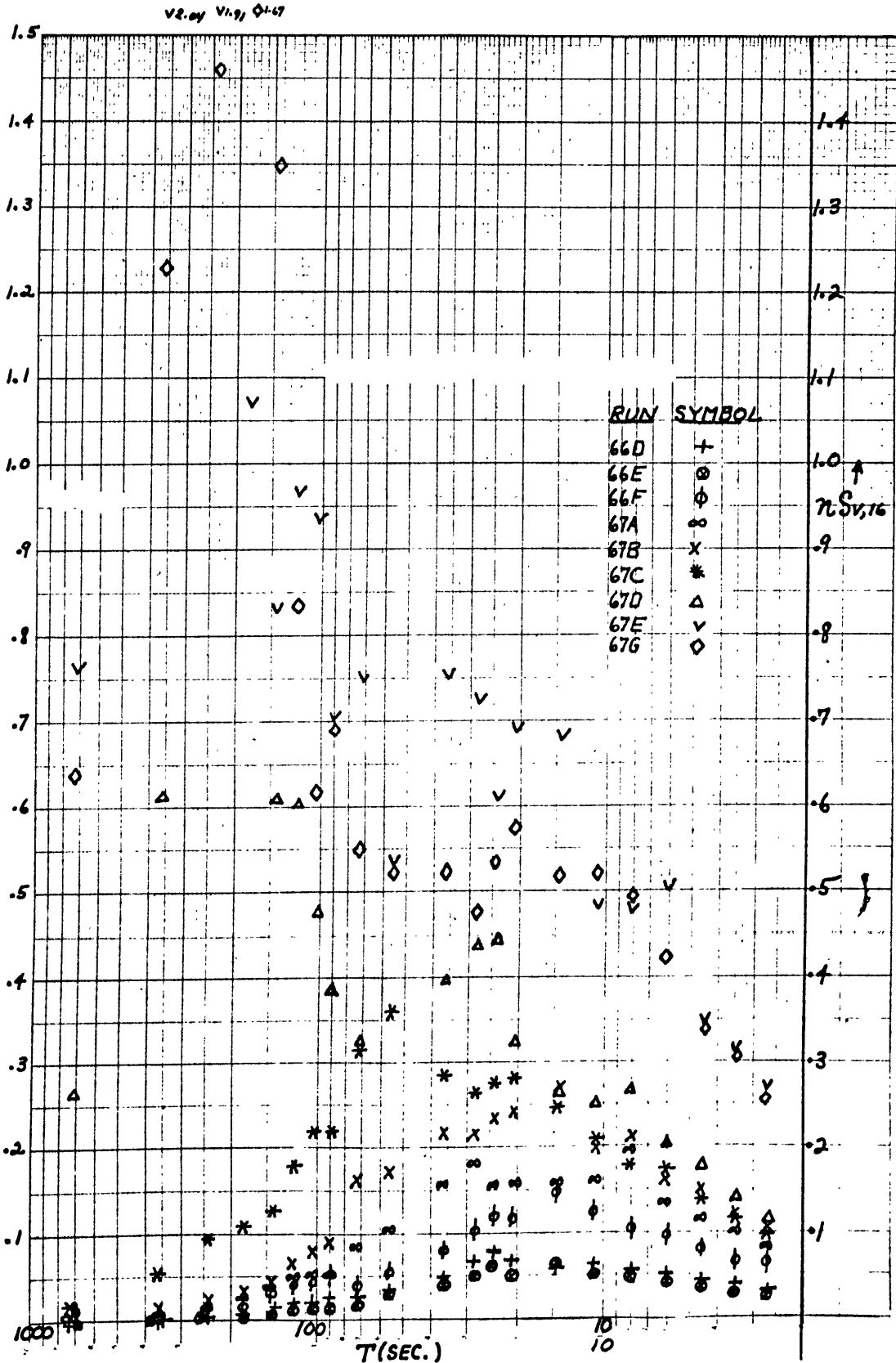


FIG. 34: POWER SPECTRA FOR 9 RUNS IN COORDINATES  $\pi_{Sw,16}$  VS LOG T.

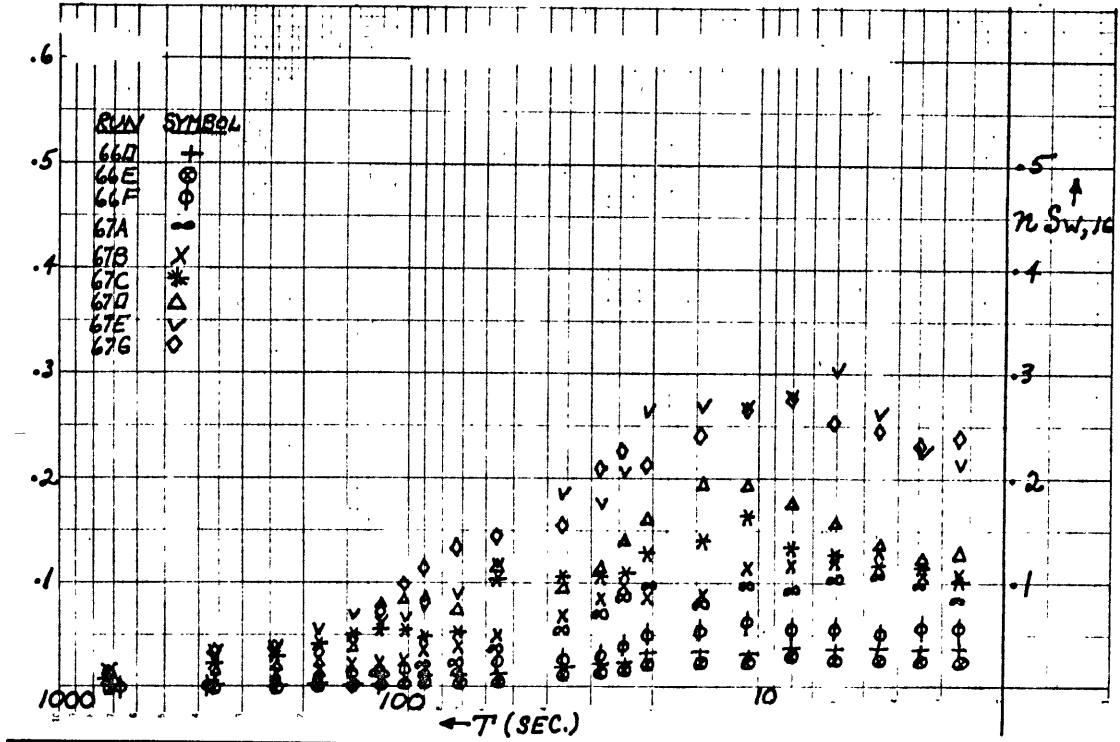


FIG. 35: POWER SPECTRA FOR 9 RUNS IN COORDINATES  $\pi_{TEMP,16}$  VS. LOG T.

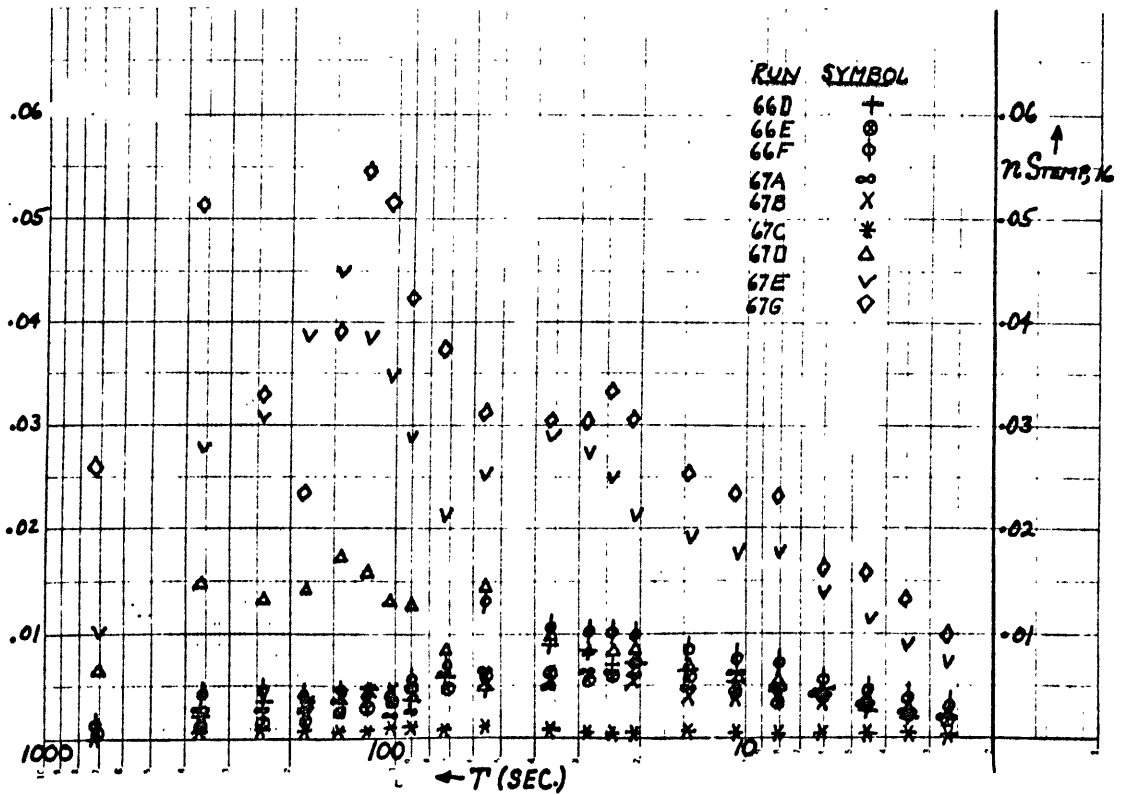


FIG. 36: POWER SPECTRA FOR 9 RUNS IN COORDINATES  $\eta_{S_{u,40}}$  VS. LOG T.

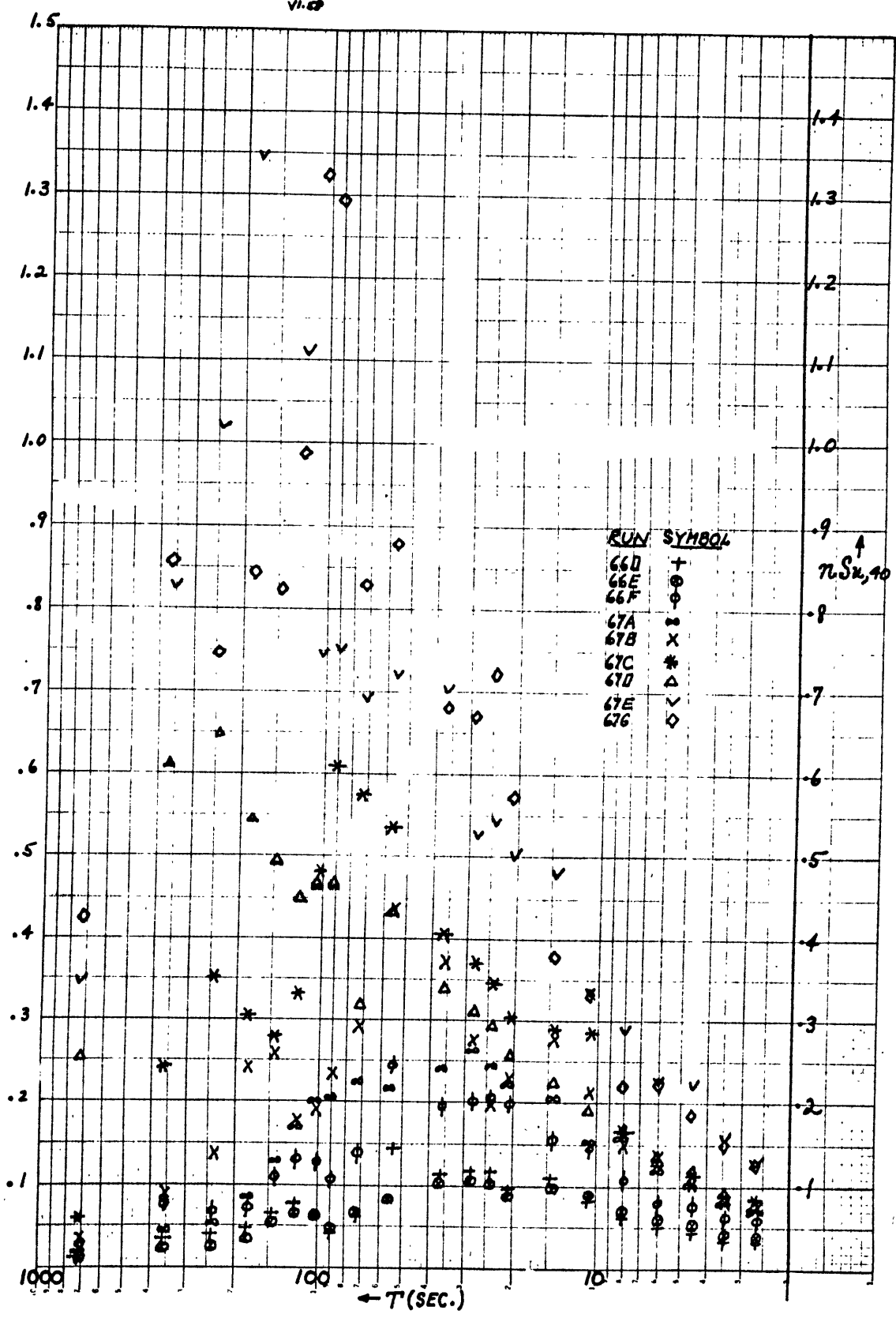


FIG.37: POWER SPECTRA FOR 9 RUNS IN COORDINATES  $\eta_{SV,10}$  VS. LOG T.

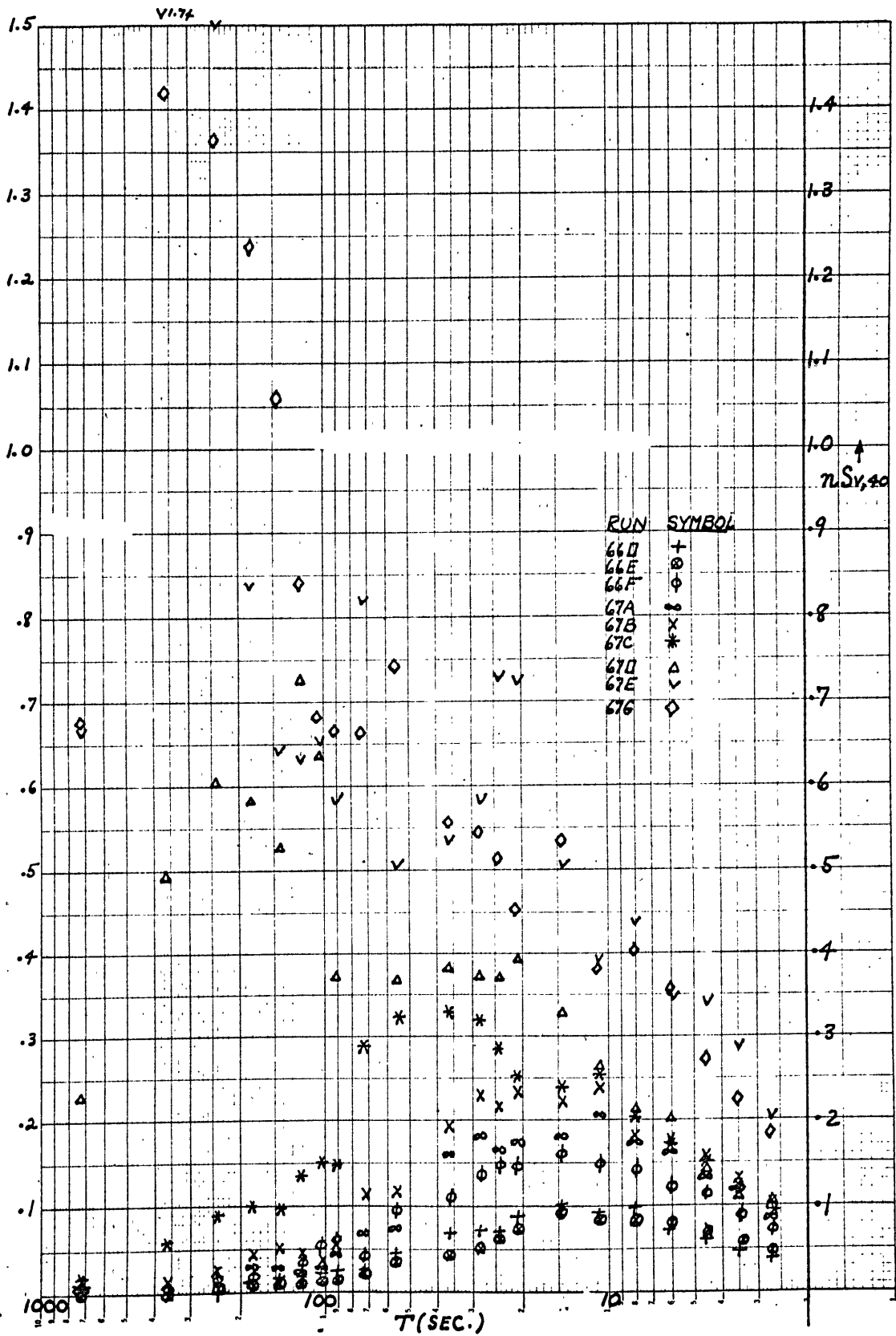


FIG.38: POWER SPECTRA FOR 9 RUNS IN COORDINATES  $\eta_{SW,40}$  VS. LOG T.

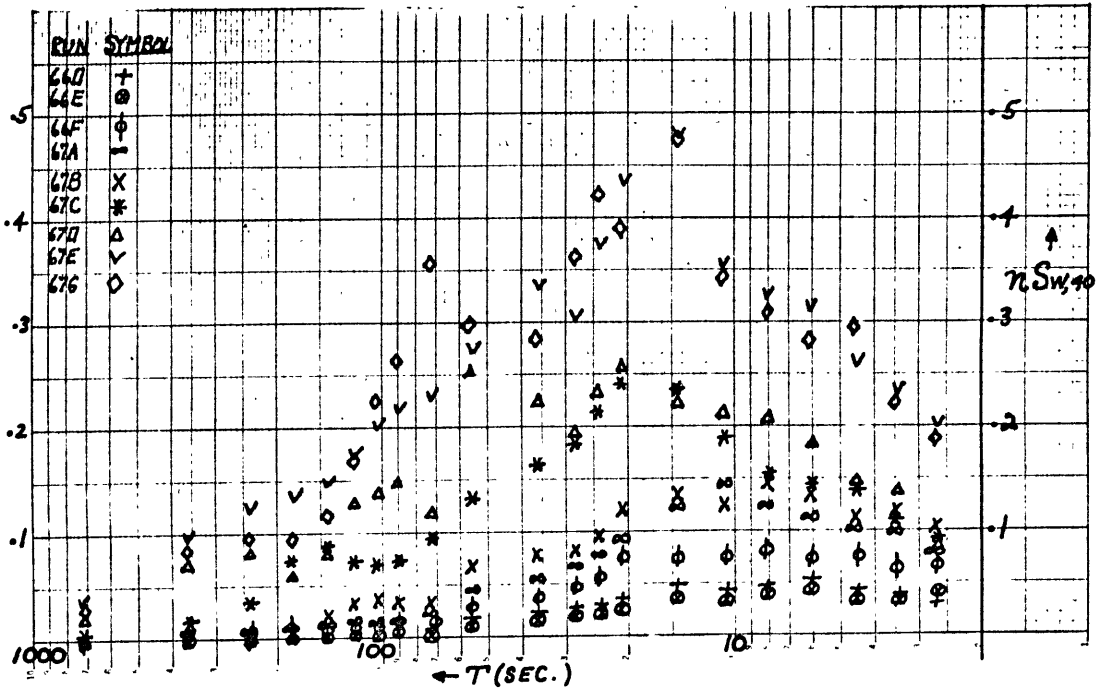
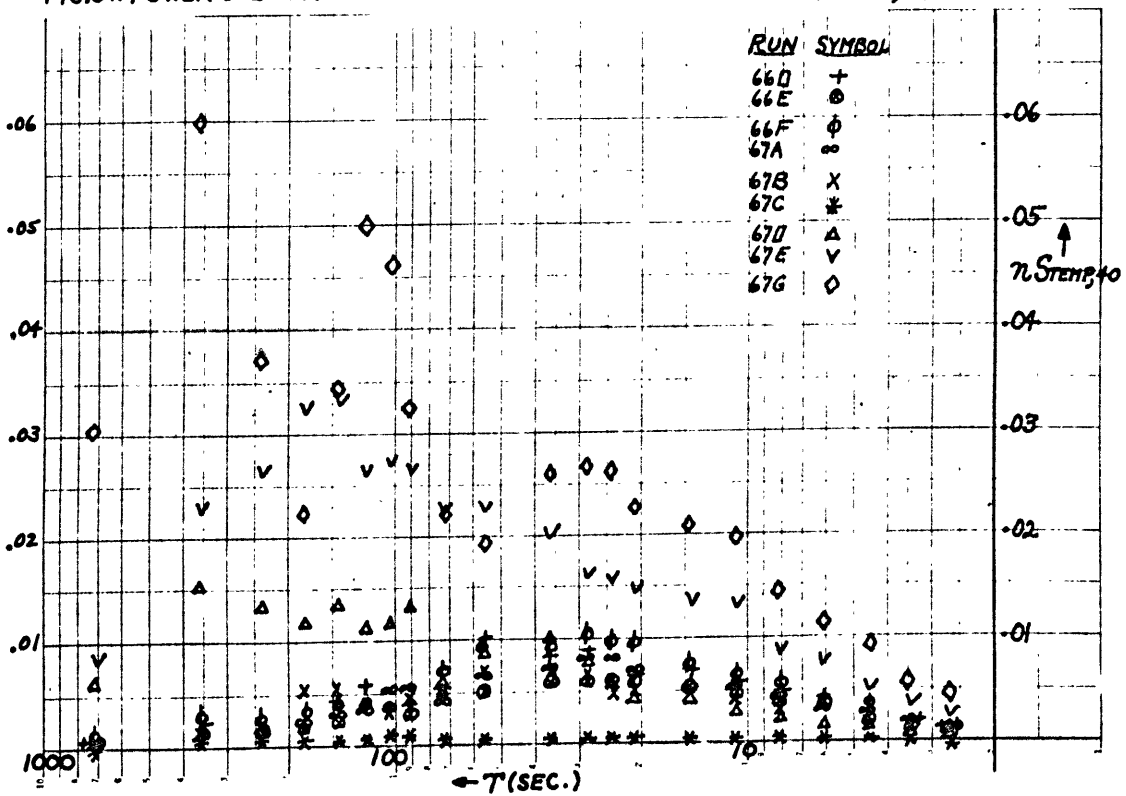


FIG.39: POWER SPECTRA FOR 9 RUNS IN COORDINATES  $\eta_{TEMP,40}$  VS. LOG T.



(c)  $\log \frac{S_i \bar{U}}{\bar{U}_{(2)}^2}$  versus  $\log n\bar{z}/\bar{U}$ , (Figure 31).

(f)  $n S_i$  versus  $\log \bar{T}$ , (Figures 32 - 39)

Similarity coordinates, (a) although not the most successful for "high frequency normalization", are probably the best behaved for a wide variety of runs, including the very stable ones, as indicated by the capability of deriving algebraic and graphic expressions for the spectral density functions in these coordinates. In the high frequency range, the  $\bar{U}^2$  and  $(\Delta T)^2$ -normalizations are the most successful in reducing all the runs to a single function; for high frequencies,  $S_i = f(\bar{U}^2)$  only, except for runs more stable than  $\sigma_A = 7^\circ$ . This system is very successful at separating the frequency range where  $S_i = f(\bar{U}^2)$  only or the "mechanical range" from the frequency range where  $S_i = g(\sigma_A)$  primarily or the "convective range". Another consideration of practical importance is that, in the case of  $\bar{U}^2$  or  $(\Delta T)^2$  normalization, one needs to know only the  $\bar{U}$  or  $(\Delta T)$  to return to dimensional quantities. Whereas in the similarity coordinates, the originally more reliable estimate of the non-dimensional quantity must be multiplied by  $v^{*2}$  or  $T^{*2}$  (which depend on  $\bar{u}^0 \bar{w}^0$  and  $\bar{w}^0 \bar{T}^0$ ); these quantities must either be estimated from figures and graphs or by means of formulas (see Sections V E 2 and VIII C). In summary, it is difficult to say which of these methods provides better estimates the dimensional densities. The semi-log system, (c) has the advantage of showing the total normalized energy as the area under the curve. In (d) and (e) the  $\bar{U}_{(2)}^2$  normalization was used in an effort to find a level for the mean wind that would permit the very stable runs to have the same normalized value at high frequencies as the more unstable

runs. In use,  $\overline{u'v'}$  was seen to be too small a quantity and the high frequency normalization was overdone for the stable cases. However, use of the mean wind at observation height led to a quantity in the denominator for the stable case that was too large. Since the vertical wind profile has more shear in stable than in unstable cases, an intermediate level not far from the surface is suggested. Even this technique is not very successful for very stable cases, especially at 40 meters. In these cases, the turbulence may be very localized and not fully developed and therefore not definable in this framework. An associated problem may arise in using  $\overline{U_{(z)}^2}$  or similar normalization when one tries to generalize the conclusions to apply to other sites, because the level of best normalization may be site dependent. The  $z$  of best normalization may be the effective level of the most important roughness elements, such as bushes, trees, buildings, etc. Hence, the energy of the mean flow at that level would be physically most pertinent in evaluating the mechanically introduced turbulent energy. In general, the coordinates of (d) were more successful than (e) in reducing high frequency range variance among the runs. In coordinates (d) the system was quite successful (the best of the list) for  $\delta_u$  and  $\delta_v$  at 16 meters but were less successful at 40 meters. The coordinate system (e) was fair at 16 meters but rather poor at 40 meters. Coordinate system (f) gives the total energy as the area under the curve. By using  $T =$  period in seconds, rather than a "reduced" or non/dimensional frequency, one may study the low frequency peaks of convective energy. Taylor's hypothesis is less reliable for these large scales of motion and the period in dimensional time units should be





$$F(n)_{\text{TRANS}} = -4 \int_0^{\infty} \frac{1}{2} f(\omega) \cos 2\pi n r dr + 4 \int_0^{\infty} \frac{1}{2} f(\omega) r \sin 2\pi n r dr \cdot 2\pi n$$

$$= \frac{1}{2} F(n)_{\text{LONG}} + \frac{n}{2} \left[ 4 \int_0^{\infty} f(\omega) \sin 2\pi n r dr \cdot 2\pi r \right]$$

$$F(n)_{\text{TRANS}} = \frac{1}{2} F(n)_{\text{LONG}} - \frac{n}{2} \frac{dF(n)_{\text{LONG}}}{dn}$$

In the isotropic region, the Kolmogoroff hypothesis gives  $F(n)_{\text{LONG}} = C n^{-5/3}$  and the Kraichnan hypothesis gives  $F(n)_{\text{LONG}} = D n^{-3/2}$

Then for the Kolmogoroff hypothesis:

$$F(n)_{\text{TRANS}} = \frac{1}{2} C n^{-5/3} - \frac{n}{2} \left(-\frac{5}{3}\right) C n^{-8/3} = \frac{8}{6} C n^{-5/3} = \frac{4}{3} F(n)_{\text{LONG}}$$

And for the Kraichnan model:

$$F(n)_{\text{TRANS}} = \frac{1}{2} D n^{-3/2} - \frac{n}{2} D \left(-\frac{3}{2}\right) n^{-5/2} = \frac{5}{4} D n^{-3/2} = \frac{5}{4} F(n)_{\text{LONG}}$$

So as a consequence of the isotropic condition,  $\overline{u^2} = \overline{v^2} = \overline{w^2}$ , the spectral energy density of the longitudinal component is 3/4 or 4/5 of the spectral energy density of the transverse component. In order to examine this property, fourteen of the twenty runs were selected. Six runs were eliminated from consideration because of suspected high frequency aliasing at the highest frequency data points. The ratio of the energy density of the v and w components relative to that of the u component is computed and plotted as a function of  $nz/\bar{U}$ . They are  $R_v = \frac{S_v(n)}{S_u(n)}$  and  $R_w = \frac{S_w(n)}{S_u(n)}$ . Both levels for six of the fourteen runs are shown in Figure 40. Values of  $R_v$  and  $R_w$  of 1.33 or 1.20 would be considered a verification of the theoretical results. At the very highest frequencies,  $R_v$  and  $R_w$  consistently average above 1.0 and certainly quite close to the desired values of 1.2 to 1.33. The w-component energy is so strongly

controlled by the height above ground that  $R_v$  drops very quickly with increasing eddy size. At the highest frequencies, these data seem to be in agreement with the theoretical results. Close inspection of Figure 40 shows that, once the turbulence starts to become anisotropic, it does so very quickly. Table 10 (1 of 3 sheets) gives these isotropic ratios to be used in locating the lowest  $nz/\bar{U}$  value where the atmospheric turbulence is nearly isotropic. The following rather arbitrary criterion is used: the  $nz/\bar{U}$  value where either transverse component energy value falls to less than 80 per cent of the longitudinal value, in going from high to low frequencies. These values of  $nz/\bar{U}$  for each run at each level were calculated and are listed in Table 11 under the column:  $\overline{u'^2} \approx \overline{v'^2} \approx \overline{w'^2}$ , (column 2).

(b) Location of the point where the slope of the spectral density function vs. frequency (in log-log coordinates) ceases to be  $-5/3$  as predicted by the Kolmogoroff hypothesis. This point was located for each run and the results are entered in Table 11, column 3 for the u-component energy function and in column 4 for the v-component. This point is not easy to locate because, in most runs, there is a gradual transition from a slope of  $-5/3$  at high frequency to a lesser slope at intermediate frequencies.

(c) Use of the cospectrum and quadrature estimates of the various pairs of fluctuation quantities ( $uw$ ,  $uv$ ,  $vw$ ,  $vT$  and  $wT$ ).

In the presence of gradients of the mean wind and potential temperature, these fluxes would have finite values even for isotropic turbulence. However, it is reasonable to expect, in examining the coherence (flux or

FIG.40: ISOTROPY RATIOS AS A FUNCTION OF FREQUENCY

$R_v = S_v/S_u$  ;  $R_w = S_w/S_u$  ;  $R_{u1} \equiv 1.0$   $R_{v,16}$  — ,  $R_{v,40}$  ···· ,  $R_{w,16}$  - - - ,  $R_{w,40}$  - - - - -

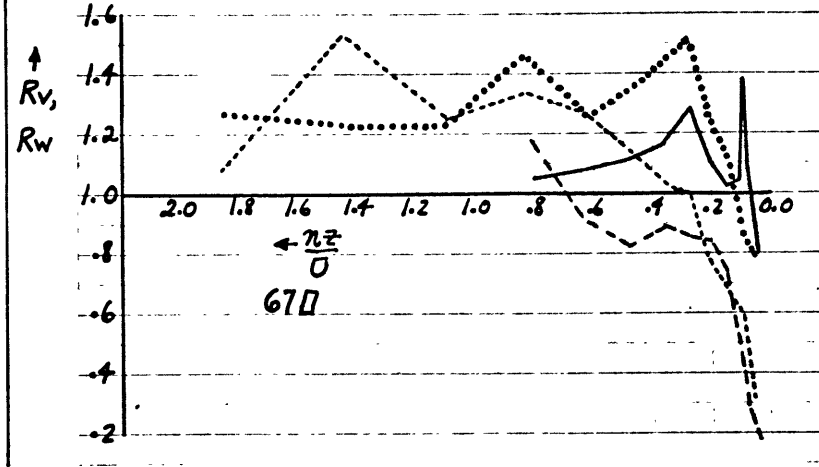
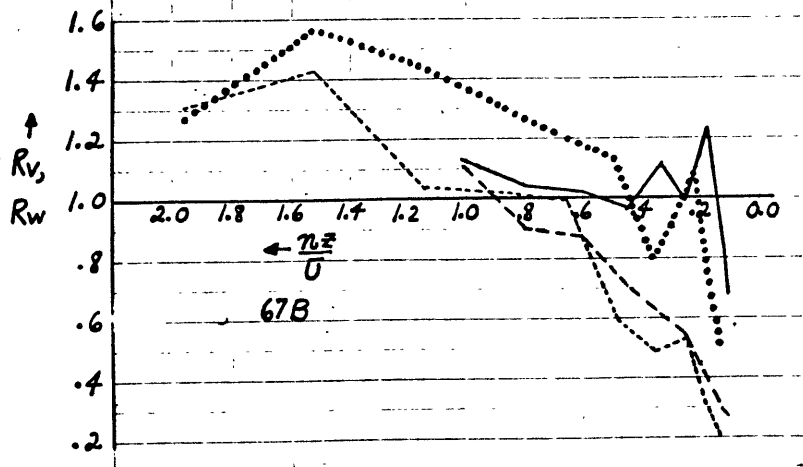
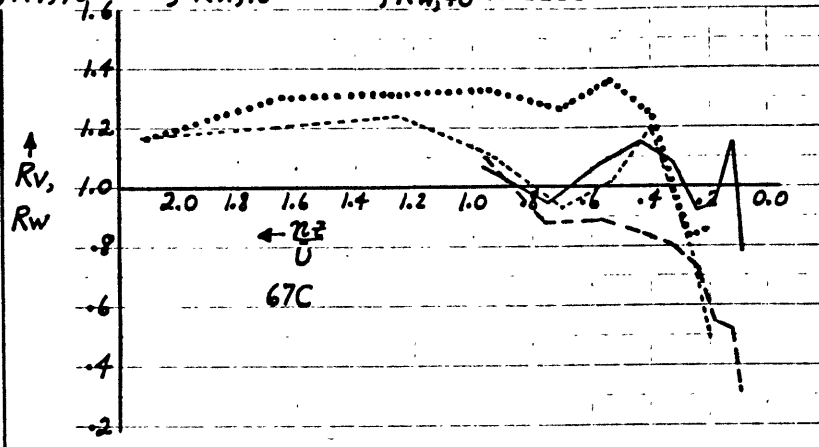
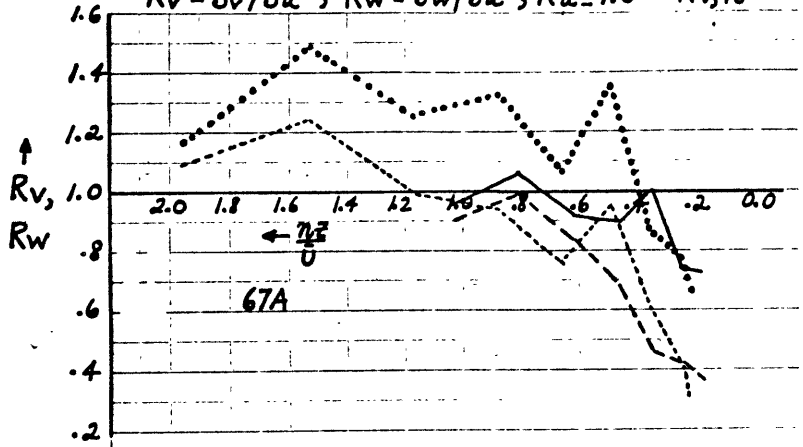


TABLE 10: (SAMPLE 1 OF 3) GIVING ISOTROPIC RATIOS AS A FUNCTION OF  $\eta/\mu$

67B-16M.			67C-16M.			67D-16M.			67E-16M.			67G-16M.		
$\eta/\mu$	$R_v$	$R_w$	$\eta/\mu$	$R_v$	$R_w$	$\eta/\mu$	$R_v$	$R_w$	$\eta/\mu$	$R_v$	$R_w$	$\eta/\mu$	$R_v$	$R_w$
0			0			0			0			0		
1.02	1.13	1.11	.96	1.07	1.11	.81	1.05	1.18	.63	1.27	1.01	.63	1.28	1.21
.77	1.04	.90	.75	.75	.88	.63	1.08	.91	.69	1.20	.87	.69	1.01	1.36
.60	1.02	.87	.57	1.08	.89	.48	1.11	.83	.37	1.24	.82	.37	1.23	.88
.45	.97	.70	.43	1.15	.84	.36	1.17	.87	.21	1.37	.82	.21	1.28	.77
.34	1.12	.62	.32	1.07	.80	.27	1.27	.85	.16	1.20	.70	.16	1.35	.77
.26	.99	.55	.24	.92	.72	.20	1.10	.84	.12	1.03	.57	.12	1.34	.70
.17	1.23	.39	.18	.98	.54	.15	1.02	.74	.08	1.15	.45	.12	.93	.47
.13	.83	.29	.12	1.15	.52	.11	1.04	.52	.07	1.04	.39	.08	.84	.50
.11	.68	.27	.11	1.04	.41	.09	1.38	.43	.06	.86	.29	.07	.60	.26
			.07	.78	.32	.06	1.10	.27	.05	.76	.23			
			.07	.77	.29	.06	.86	.21	.04	.82	.20			
						.04	.80	.18	.03	.70	.16			

67B-40M.			67C-40M.			67D-40M.			67E-40M.			67G-40M.		
$\eta/\mu$	$R_v$	$R_w$	$\eta/\mu$	$R_v$	$R_w$	$\eta/\mu$	$R_v$	$R_w$	$\eta/\mu$	$R_v$	$R_w$	$\eta/\mu$	$R_v$	$R_w$
0			0			0			0			0		
1.96	1.27	1.31	2.11	1.17	1.17	1.86	1.27	1.08	1.41	1.57	1.59	1.43	1.45	1.48
1.53	1.57	1.43	1.64	1.31	1.21	1.45	1.23	1.53	1.10	1.83	1.98	1.11	1.49	1.49
1.16	1.44	1.04	1.25	1.31	1.24	1.10	1.23	1.24	.84	1.55	1.19	.83	1.46	1.59
.87	1.30	1.02	.94	1.33	1.11	.83	1.46	1.34	.63	1.56	1.40	.64	1.60	1.29
.65	1.20	.99	.70	1.27	.93	.62	1.26	1.26	.47	1.53	1.14	.48	1.85	1.42
.49	1.13	.60	.53	1.36	1.02	.46	1.38	1.13	.35	1.18	1.07	.36	1.16	1.04
.36	.80	.49	.39	1.23	1.21	.35	1.46	1.02	.26	1.05	1.01	.26	1.41	1.26
.25	1.02	.53	.27	.84	.80	.24	1.52	1.00	.18	1.44	.87	.19	.83	.72
.22	1.09	.49	.23	.83	.62	.21	1.26	.79	.16	1.34	.67	.16	.71	.57
.19	.83	.29	.20	.86	.50	.18	1.20	.63	.13	1.10	.59	.14	.82	.55
.15	.57	.21				.14	1.12	.66	.10	.76	.48	.11	.81	.42
						.09	.85	.59	.07	.70	.38			
						.07	.91	.38						
						.056	.80	.22						

TABLE II: VALUES FOR AVERAGE SLOPE AND VALUES FOR  $w=70$  DEFINING THE EXTENT OF THE VARIOUS REGIONS - ISOTROPIC DATA AND UNIFORM SLOPE DATA SUMMARY.

RUN	$w=70$	LOWER LIMIT OF ISOTROPY						UNIFORM SLOPE REGION		"CONVECTIVE" SUB-RANGE							
		$w_1/w_2$	$S_u$	$S_v$	$w_1/w_2$	$w_1/w_2$	$w_1/w_2$	$OA$	WEIGHTED CONSENSUS	EXTENT	AVERAGE SLOPE	EXTENT	AVERAGE SLOPE	EXTENT	SLOPE	EXTENT	SLOPE
66D	16	.9	.4	.6	.35	.7	.9	6.9	.9	.4-.11	1.57	.6-.17	1.34				
66E	16	1.0	.5	.8	.7	1.3	.9	5.5	.7	.5-.12	1.26	.8-.33	1.00				
66F	16	1.0	.5	.8	.7	1.5	.75	5.4	1.0	.5-.10	1.43	.5-.15	1.15				
66G	16	.9	.4	.5	.75	.95	.95	6.2	.6	.4-.06	1.50	.5-.22	1.60				
67A	16	.8	.4	.7	.9	1.2	.8	5.4	.8	.4-.10	1.21	.7-.4	1.28				
67B	16	.6	.3	.4	.3	.5	.3	6.5	.4	.3-.04	1.26	.4-.10	1.21				
67C	16	.65	.5	.5	.5	1.3	.7	5.5	.7	.5-.09	1.21	*					
67D	16	.6	.4	.35	.35	.75	.35	7.3	.5	.4-.05	1.49	.35-.13	1.05				
67E	16	.6	.35	.6	.5	1.3	.5	5.6	.6	.35-.05	1.45	.6-.25	1.20				
67F	16	.4	.25	.4	.2	.04	.2	8.4	.3	.25-.027	1.41	.4-.046	1.32				
67G	16	.3	.2	.5	.35	<.04	<.04	7.7	-.35	.2-.063	1.43	.5-.10	1.15				
67H	16	.2	.35	.25	.15	.4	.2	12.6	.25	.35-.021	1.49	.25-.04	1.47	.15-.01	1.92	.03-.012	1.96
67I	16	.2	.35	.25	.15	.65	.35	10.8	.3	.35-.021	1.38	.25-.07	1.00	.04-.02	1.57	.07-.02	1.57
67J	16	.25	.25	.2	.15	.4	.25	14.4	.25	.25-.047	1.55	.2-.06	1.24	.16-.04	2.02	.03-.007	1.88
67K	16	.18	.2	.2	.2	.65	.4	12.8	.3	.2-.02	1.44	*		.04-.025	2.68	.025-.01	2.07
67L	16	.3	.3	.2	.25	.4	.25	14.7	.3	.3-.024	1.44	.2-.08	1.18			.003-.009	2.21
67M	16	.2	.15	.25	.35	.8	.3	13.7	.3	.15-.037	1.54	.25-.06	1.24			.04-.016	1.72
67N	16	.2	.2	.2	.2	<.03	<.03	12.7	~.25	.6-.047	1.42	.2-.062	1.24	.03-.02	2.11		
67O	16	.4	.5	.6	.35	<.06	<.06	11.8	~.4	.5-.08	1.38	.6-.2	1.69				
67P	16	.15	.3	.15	.2	.25	.15	14.6	.2	.3-.064	1.48	.15-.06	1.41	.025-.01	3.02	.014-.007	2.13
67Q	16	.22	.2	.4	.25	.9	.5	12.3	.3	*		.4-.15	1.54	.05-.016	2.06	.057-.017	1.66
67R	16	.1	*.3	.25	.25	.4	.07	17.2	~.2	.35-.03	1.37	.25-.025	1.52	.016-.007	3.31	.016-.008	2.16
67S	16	.6	.3	.2	.2	.75	.2	14.5	.4	.3-.04	1.37	.2-.06	1.14	.027-.017	2.18	.027-.017	1.45
67T	16	.14	.25	.2	.5	.4	.4	18.2	.25	.35-.04	1.37	.2-.015	1.61	.02-.007	2.25	.034-.02	2.10
67U	16	.14	.3	.4	.5	.65	.4	18.5	.3	.2-.07	1.37	.4-.22	1.43	.056-.022	2.34	.14-.04	2.11
67V	16	>.15	**	.5	.5	.7	.9	3.4	~1.1	1.0-.11	.84	*					
67W	16	.69	.6	1.0	1.2	1.9	1.2	2.3	~1.5	1.0-.22	1.13	*					
67X	16	>.13	**	.5	.5	>.3	1.2	4.7	~1.1	.8-.24	1.18	*					
67Y	16	>.2	**	.6	.6	<.04	1.58	4.4	~1.4	.7-.4	.73	*					
67Z	16	.2	.4	.2	.15	.35	.2	18.3	.25	.4-.03	1.34	.2-.022	1.55	.022-.007	2.20	.045-.007	2.27
68A	16	.25	.25	.12	.25	.65	.35	17.9	.25	.25-.026	1.53	*		.063-.017	1.95	.016-.002	1.91
68B	16	.25	.2	.25	.2	.2	.25	15.1	.25	.2-.023	1.54	.3-.16	1.51	.019-.009	1.67	.05-.008	2.03
68C	16	.2	.3	.3	.25	.25	.8	14.7	.3	.3-.043	1.44	.3-.16	1.29				
68D	16	.7	.4	.3	.35	.45	.6	4.7	.5	.1-.15	1.45	.3-.15	1.29				
68E	16	.42	.4	.7	.7	.63	.75	3.5	.7	.2-.10	1.03	.7-.26	.915				
68F	16	.4	.4	.7	.35	.45	.35	2.0	.35	.4-.057	1.44	*					
68G	16	.4	.4	.7	.35	.45	.35	2.5	.35	.3-.17	1.22	.7-.25	1.27				
68H	16	.4	.4	.7	.35	.45	.35	2.3	~.6	.2-.042	1.13	.35-.11	1.04				
68I	16	.35	.35	.35	.35	.4	.4	2.0	.35	.35-.10	1.34	.8-.48	1.44				
68J	16	.6	.35	.8	.5	1.3	.75	2.0	.7	*							

\*\* NO SLOPE

\* NO UNIFORM SLOPE

11

covariance plus the quadrature term) as a function of frequency, that the values of the fluxes under isotropic conditions are minimal and that non-isotropic fluxes would be larger. The quadrature term actually becomes zero (Lumley [1964]). So a test for isotropic conditions, which requires the coherence to be not significantly different from zero, may be unnecessarily strict, but it is easier to apply. In this case it gives good agreement with the other criteria, though it has the capability of introducing a bias toward high frequency of the lower limit of isotropy. Then the procedure is to locate the lower limit of isotropy as the  $\frac{\pi^2}{\sigma}$  where the coherence (see Panofsky and Brier [1958]) for an explanation of this term) does not differ significantly from zero in going from low toward higher frequencies.

Panofsky and Brier (1958) also give the formula,  $\beta = \sqrt{1 - p \frac{df-1}{df}}$  where  $p$  is the probability of obtaining a coherence as high as  $\beta$  when the true coherence is zero, and where  $df$  is degrees of freedom (see Table 12 below). Then for 60 lag analysis,  $\beta = .15$  was arbitrarily selected because that value could occur 10 per cent of the time when the true coherence is zero. Then the criterion becomes: the lower limit of isotropy is located at the point, in going from low to higher frequencies, where the coherence falls to a value less than .15 and stays below that value for higher frequencies. All six of these coherences have been calculated and three of them are shown in Tables 13, 14 and 15, below. Tables for  $vT$ ,  $vw$  and  $uv$  coherence are not shown since these combinations did not yield values significantly different from zero. Then  $uw$ ,  $wT$ , and  $uT$  coherences were used to determine the  $\frac{\pi^2}{\sigma}$  values desired and are listed in columns 5, 6 and 7 of Table 11, below.

Finally the three methods of locating the lower limit of isotropy

A COMPOSITE OF FOUR SMALL TABLES.

df = 19.5		df = 99.5	
P, %	β	P, %	β
1%	.470	1%	.212
5%	.317	5%	.173
10%	.316	10%	.152
20%	.288	20%	.127

TABLE 12: PERCENT PROBABILITY OF OBSERVING A COHERENCE AS HIGH AS "β" WHEN THE TRUE VALUE IS ZERO.

STRATIFICATION	Su, 16M.	Su, 40M.	Sv, 16M.	Sv, 40M.
VERY STABLE	1.00	1.01	*	*
MODERATELY STABLE	1.42	1.22	1.34	1.19
NEAR NEUTRAL	1.41	1.43	1.32	1.15
UNSTABLE	1.45	1.43	1.40	1.36
AVERAGE	1.39	1.30	1.33	1.27

TABLE 17: AVERAGE VALUES FOR THE UNIFORM SLOPE, JUST BELOW THE LOWER LIMIT OF ISOTROPY.

STRATIFICATION	Su, 16M.	Su, 40M.	Sv, 16M.	Sv, 40M.	RUNS
VERY STABLE (2 cases)	.15	.30	*	*	35, 36
MOD. STABLE (8 cases)	.09	.11	.16	.34	66D, 66E, 66F, 67A, 67B, 40, 41, 42, 67C
NEAR NEUTRAL (1 case)	.03	.06	.05	.10	67D, 67E, 67G, 31, 32, 33, 39, 38, 37
UNSTABLE (9 cases)	.03	.045	.04	.13	

\* NO uniform slope  
TABLE 16: AVERAGE VALUES FOR  $wz/\sigma$  AT THE LOW FREQUENCY LIMIT OF THE UNIFORM SLOPE REGION.

RUN	T <sub>max</sub> (secs)	PERIOD OF MAX. FOR (N/F) <sub>0</sub>	HEAT FLUX		W.T. (UPWARD)
			OBSERVED 40M.	CALC. 40M.	CALC. (W.T. 16 & 24)
67D	16	250			
67E	16	150	.130	.153	.112
67G	16	300/120	.154	.232	.171
32	16	250	.246	.287	.211
33	16	300	.133	.191	.141
34	16	400	.159	.182	.134
37	16	400	.117	.152	.116
38	16	400	.216	.220	.214
39	16	400/100	.078	.077	.057

$$W.T. (CALC.) = \left[ \frac{20}{16} \right]^{2/3} W.T. 16$$
 ASSUMING W.T. 16 IS CORRECT.

TABLE 18: PERIOD ASSOCIATED WITH MAXIMUM OF THE NS(w) FUNCTION, COMPARISON OF CALCULATED AND OBSERVED VERTICAL DIVERGENCE OF HEAT FLUX (FREE CONVECTION CASES)

112



TABLE 13: COHERENCE VALUES FOR U,W FLUCTUATIONS AS A FUNCTION OF PERIOD.

		UW COHERENCE													
RUN	PERIOD (SECS)	144	72	48	36	28	24	20.6	14.4	10.7	8.0	6.0	4.5	3.4	2.7
66D	16M									.24	.12	.08			
	40M									.29	.15	.22	.16	.05	
66E	16									.24	.12	.17	.17	.09	
	40									.26	.19	.17	.114	.105	.04
66F	16									.20	.18	.21	.06		
	40									.25	.17	.20	.10	.04	
67A	16								.27	.16	.28	.10	.075		
	40								.26	.19	.27	.35	.16	.07	
67B	16										.17	.14	.12	.05	
	40									.32	.13	.12	.07		
67C	16					.25	.16	.14	.14	.15	.12	.03			
	40							.23	.10	.08					
67D	16						.18	.116	.14	.07					
	40				.19	.12	.10	.113	.10	.07					
67E	16							.38	.30	.10	.10	.11	.08		
	40							.27	.21	.10	.07				
67G	16							.32	.21	.18	.21	.116	.06		
	40							.25	.21	.10	.02				
31	16	.47		.12		.19		.09	.015	.034	.015				
	40	.33		.18		.15		.05	.019						
32	16			.21		.175		.145	.14	.145	.095				
	40			.38		.22	.13	.09	.10	.002	.032				
33	16			.16		.16		.155	.23	.03	.04				
	40			.20	.21	.10		.075	.10	.009					
34	16		.19	.10	.22	.156	.11	.08	.08	.155	.22	.02			
	40	.18	.12	.065		.055		.057	.009	.006					
35	16							.15	.26	.32	.23	.08	.09	.065	
	40							.10	.17	.20	.21	.28	.09	.144	.12
36	16								.20	.18	.17	.065	.12	.21	.045
	40									.20	.03	.09	.0085	.02	.03
38	16	.15		.105		.17		.165	.08	.08	.03	.06	.01	.05	.11
	40					.33	.12	.07	.02						
39	16					.26		.17	.15	.10					
	40				.24	.15	.115	.08							
40	16							.28	.29	.07	.12	.095	.005		
	40							.155	.155	.155	.04				
41	16							.20	.20	.20	.138	.084			
	40							.23	.10	.10	.064				
42	16							.35	.28	.14	.026				
	40							.21	.075	.125	.06	.055			

TABLE 14: COHERENCE VALUES FOR W,T FLUCTUATIONS AS A FUNCTION OF PERIOD.

RUN	PERIOD [SECS.]	WT COHERENCE													
		144	72	48	36	28	24	20.6	14.4	10.7	8.0	6.0	4.5	3.4	2.7
66D	16M. 40M.								.23	.14	.16	.20	.11	.10	.04
66E	16 40							.23	.21	.20	.15	.125	.11	.09	
66F	16 40									.24	.085	.19	.12	.06	
67A	16 40								.30	.16	.20	.11	.10	.085	
67B	16 40									.29	.18	.17	.12	.11	
67C	16 40	.23	.15	.04		.03		.002	.0125	.18	.195	.20	.13	.074	
67D	16 40	.055	.035	.03		.03		.005		.23	.20	.17	.076		
67E	16 40							.275	.16	.16	.163	.064			
67F	16 40								.22	.195	.15	.077	.185	.097	
67G	16 40									.17	.10	.11	.10	.067	
67H	16 40									.29	.23	.15	.13	.12	
31	16 40	.10		.055		.08		.025	.0001	.20	.16	.13	.145	.075	
32	16 40	.02	.06	.12	.095	.06		.05		.25	.06				
33	16 40	.19		.43		.24		.17	.095	.28	.09	.10			
34	16 40			.41		.23		.37	.27	.165	.25	.04			
35	16 40	.45		.11		.28		.16	.28	.11	.15	.06			
36	16 40	.43		.21		.27		.29	.32	.21	.11	.08			
37	16 40	.46		.22		.15		.23	.047	.23	.04	.09			
38	16 40							.28	.17	.11	.05	.08			
39	16 40								.175	.34	.29	.15	.09	.055	
40	16 40							.10	.135	.185	.09	.12	.17	.16	
41	16 40								.24	.14	.13	.26	.13	.12	
42	16 40	.07		.055		.05		.014	.045	.045	.016	.026	.001	.007	
43	16 40	.41		.13		.24		.26	.15	.105	.21	.10	.035	.003	
44	16 40					.21		.20	.21	.25	.03	.08	.07		
45	16 40							.175	.15	.04	.035	.18	.02		
46	16 40					.21	.125	.064	.09	.09	.05	.095	.025		
47	16 40							.27	.21	.185	.05	.155	.034		
48	16 40								.23	.19	.22	.125	.098	.073	
49	16 40								.36	.25	.175	.032	.036		
50	16 40									.24	.24	.08	.11	.055	
51	16 40								.29	.18	.12	.08	.11		
52	16 40									.23	.20	.175	.065		

111

TABLE 15: COHERENCE VALUES FOR U,T FLUCTUATIONS AS A FUNCTION OF PERIOD.

		UT COHERENCE													
RUN	PERIOD [SECS.]	144	72	48	36	28	24	20.6	14.4	10.7	8.0	6.0	4.5	3.4	2.7
66D	16M. 40M.								.22	.20	.04	.075	.003		
66E	16 40								.27	.14	.175	.086	.03		
66F	16 40									.26	.105	.074			
67A	16 40									.185	.26	.073	.03		
67B	16 40									.175	.20	.05	.04		
67C	16 40								.41	.17	.25	.195	.116	.075	
67D	16 40								.25	.13	.17	.115	.06	.035	
67E	16 40								.35	.26	.135	.07	.045		
67G	16 40								.17	.155	.055				
31	16 40	.105	.095	.34	.21	.09	.035	.17	.155	.025	.026				
32	16 40			.077	.155	.065	.18	.16	.175	.14	.075				
33	16 40			.23		.14		.215	.137	.057					
34	16 40							.24	.26	.135	.155	.06	.053		
35	16 40							.25	.195	.19	.07	.01			
36	16 40							.24	.21	.125	.155	.037	.088		
37	16 40							.23	.15	.13	.055				
38	16 40	.05		.01		.07		.03	.0003	.06	.03	.01	.04		
39	16 40	.02		.007		.03		.015							
40	16 40	.50		.18		.195		.30	.075	.08					
41	16 40	.78		.33		.22		.23	.23	.055	.09				
42	16 40	.45		.17	.13	.08		.075							
43	16 40	.67		.27	.24	.09		.02							
44	16 40	.46		.12		.47		.145	.10	.17	.075				
45	16 40	.42		.22		.155		.155	.12	.03					
46	16 40							.52	.27	.44	.20	.095	.15	.11	.09
47	16 40							.46	.42	.46	.28	.29	.26	.16	.043
48	16 40								.47	.39	.29	.16	.06	.175	.045
49	16 40								.11	.045	.10	.004	.0018	.004	.0012
50	16 40	.29		.25	.20	.09		.20	.15	.05	.033				
51	16 40			.14		.10		.225	.08	.084					
52	16 40			.31		.185		.175	.185	.14	.006				
53	16 40					.30		.20	.16	.27	.165	.125	.10		
54	16 40								.35	.25	.197	.053	.105	.045	
55	16 40								.35	.27	.08	.135	.11		
56	16 40								.29	.28	.07	.07	.04		
57	16 40								.26	.21	.08	.10	.115	.165	.14
58	16 40								.48	.165	.20	.05	.06		
59	16 40								.44	.24	.23	.029	.024		

were combined to give a "weighted consensus" value. This consensus value is one third dependent on each of the three methods or: 1/3 dependent on column 2; 1/6 dependent on columns 3 and 4 each; and 1/9 dependent on columns 5, 6 and 7 each. The results are listed in column 9. Considering the stability as listed in Table 3, these results show that the lower limit of isotropy is strongly dependent on the stratification. At 16 meters,  $nz/\bar{U} = 1.0$  for the very stable cases, .5 or .6 for the moderately stable cases, and .2 to .3 for neutral and unstable cases. At 40 meters, the  $nz/\bar{U}$  stability dependence is similar to that at 16 meters and somewhat greater in magnitude, varying between 1.5 and .3. This is discussed by Cramer (1959), Priestley (1959), Panofsky and DeLand (1959) and others.

#### 6. Form of the spectra at intermediate frequencies.

As mentioned earlier, most runs have an extensive region at intermediate frequencies, immediately adjacent to the lower limit of isotropy, where the slope is uniform (or very slowly decreasing toward lower frequencies) and less steep than the  $-5/3$  value of Kolmogoroff theory, which seems to be valid at higher frequencies.

For each run, at each level, starting at the lower limit of isotropy as indicated in Section V E 5, the extent and value of this uniform slope was measured and is recorded in Table 11, columns 12, 13, 14 and 15. The lower limit of this uniform slope is also stability dependent in about the same manner as the lower limit of isotropy. This is shown in Table 16, which gives average values for this lower limit for  $S_u$  and  $S_v$  at the two levels for several classes of stratification. In general, this lower limit decreases with decreasing stability and is larger, for all stabilities, at

40 meters than at 16 meters. The neutral case is not significantly different from the unstable case. For the most stable runs, a  $-5/3$  slope may not appear and there is some doubt that an inertial sub-range occurs. This is especially true for the  $v$ -component at 40 meters. Coherence calculations for  $wT$ , and  $uw$  for Runs 35 and 36 also suggest this, because even at the highest frequencies, the coherence values are still in the vicinity of .15 rather than following the usual pattern of dropping to very low values.

The value of this slope is also very important, theoretically, (see Kraichnan 1958; 1959). Table 17 gives average values of this slope for  $S_u$  and  $S_v$  at both levels and for the same stratification groupings used in Table 16.

The effect of stability on this slope is more pronounced for  $S_v$  than for  $S_u$ , and also more pronounced at 40 meters than at 16 meters. A slope of 1.4 is an acceptable value for the slope of  $S_{u,16}$  (except very stable cases),  $S_{u,40}$  in neutral and unstable cases and  $S_{v,16}$  in unstable cases.

#### 7. Form of spectra at low frequencies.

For unstable runs, there is usually a large peak of energy at low frequency for  $S_u$  and  $S_v$ . On the high frequency side of this peak, there usually occurs a region of fairly uniform slope (very steep). The data for the extent and slope of this region is listed in Table 11 under the columns headed: "convective sub-range". The average values of these slopes are: 2.31 for  $S_{u,16}$ , 2.13 for  $S_{u,40}$ , 2.09 for  $S_{v,16}$ , 1.79 for  $S_{v,40}$  and an overall average is 2.09. The occurrence of these large slopes may be due to the fact that the energy density at the largest scales is being augmented

more rapidly by convective energy introduction than it is being decreased by energy transfer to higher frequencies. Because the time scale of eddies increases with increased linear scale, it may be that the system does not establish an energy balance between input and inertial transfer of energy for these largest scales before the meteorological parameters  $\bar{U}_z$  and  $\frac{\partial \theta}{\partial z}$  have changed.

8. A comparison of results with those of other investigators.

(a) The results of the regression analysis of Section V E 3, using  $\bar{U}^2$ -normalization and expressed in log-log and semi-log coordinates, are now compared with the results obtained by Cramer (1960), Panofsky and Deland (1959) and Cramer, Record, Tillman and Vaughan (1962). There is agreement among these analyses on the general shape of the energy spectral densities for the various velocity components as a function of frequency and, also, on the successful normalization in the high frequency range.

(b) These same data, expressed in similarity coordinates, are compared to the results shown by Takeuchi (1961) in his figures 18b, 19a, b and by Monin (1962) in his Figures 4, 5 and 7 and by Takeuchi (1963) in his Figures 4a, b. Takeuchi (1961) uses the non-dimensional,  $z/L$ , (where  $L$  is the stability length) to express stratification and his spectral densities are calculated from data taken at the 2-meter level. Monin (1962) used the Richardson number and his measurements are at the 1-meter level. Takeuchi (1963) used  $\sigma_{\theta}^2$  and the 16-meter level, which is the same as the analysis here. Again there is good agreement on the general shape of the spectral density functions and also an approximation to a  $-5/3$  slope at high frequencies even though there are considerable differences in roughness

and observation height. However, as might be expected, the curve shapes at the lowest frequencies differ from the present result. Takeuchi (1961) did not show a maximum for the non-dimensional energy spectral densities (in log-log coordinates) at the lowest frequencies, which does show up here. The more serious disagreement, however, is in the high frequency range. In this region, Monin (1962) and Takeuchi (1961) show that the non-dimensional energy density,  $\frac{S_i \bar{U}}{u'^2 \bar{z}}$ , decreases with increasing stability, which is the opposite result that is shown in this research. Takeuchi (1963) used non-dimensional coordinates,  $\log \frac{\bar{U}^3 F_A}{\bar{U}_2^2}$  versus  $\log nz/\bar{U}$ , where  $F_A = \frac{S_V}{\bar{U}^2}$  in his Figures 4a, b.  $\bar{U}(2)$  is the mean wind at the 2 meter level. He also obtained, in the high frequency range, a decrease of this non-dimensional spectral density with increased stability, in agreement with the other two papers and again at variance with these results. An explanation of this disagreement is the following: in the first two papers, Takeuchi (1961) and Monin (1962), the spectral densities are normalized, using values of the gross statistics  $\overline{u'^2 w'^2}$  and  $T'^2$  (derived from  $\overline{w'^2 T'^2}$ ) measured at the 1 and 2 meter levels. At these levels, very little contribution to the covariance comes from the large eddies compared to what is observed at 16m. and 40m. These large eddies are very stability sensitive - sufficiently so to reverse the spectral density functional dependence on stability, when the gross statistics are measured at the 16 and 40 meter level, as is done with these data. Takeuchi (1963) uses  $\log \frac{\bar{U}^3 F_A}{\bar{U}_2^2}$  versus  $\log nz/\bar{U}$ . Since  $S_V \approx \bar{U}^2 F_A$ , this is about the same as  $\log \frac{\bar{U} S_V}{\bar{U}_2^2}$ , which is just normalization by  $\bar{U}^2$  at the 2 meter level. When these results are compared with Figure 31, they are found to be more in agreement.

(c) In comparing the total fluctuation energy of each component as a function of height (comparing 16 and 40 meter levels) with the findings of Panofsky and Deland (1959), there were situations where the agreement was dubious (see the data of Table 7 and pages 50-58, *Advances in Geophysics*, vol.6).

-1. w-component (vertical)

The data used in this investigation show: a) in unstable conditions: turbulent energy increases with height, b) in moderately stable conditions: little energy change with height, c) in very stable conditions, runs 35 and 36 : energy decrease with height. Panofsky and Deland (1959) obtained a slow increase with height of energy for the unstable case but obtained a decrease with height in "stable" cases. Apparently their "stable" or night time cases correspond to the "very stable" classification used here.

-2. v-component (transverse)

This investigation shows the lateral turbulent energy is relatively constant with height in convective cases, in agreement with Panofsky and Deland (1959) however, there is an actual increase in the energy with height for stable and very stable conditions, which is apparently in disagreement with their findings. Agreement can be achieved only if it is first assumed that their "stable" classification corresponds to the very stable Runs 35 and 36. Also, since the energy level is very low, it may be more affected by long-wave non-turbulent fluctuations (fractional contribution to the total variance) than would be the case in the higher energy levels associated with lesser stabilities. If the energy is filtered by a 601-point running mean (approximately 720 secs.), then the remaining



high frequency energy really does decrease with height.

-3. u-component (longitudinal)

This investigation shows little variation of the longitudinal total fluctuation energy with height for either stratification, but agrees with Panofsky and Deland (1959) in the stable case (decrease with height), if the same filtering is used as for the v-component. This filtering should be acceptable in the very stable cases, since spectral analyses suggest very little turbulent energy at the longer time scales.

(d) Reconciliation of a diversity of results for the lower limit of isotropy in terms of  $nz/\bar{U}$ .

A partial list of previous findings is: Gurvich (1960) shows (1)  $nz/\bar{U} = .4$  for unstable conditions, (2)  $nz/\bar{U} = .7$  for neutral conditions, (3)  $nz/\bar{U} = 1.9$  for stable conditions. Shiotani (1963) observed  $nz/\bar{U} = .46$  at 26m. (u and w-component comparison). Priestley (1959A), p.97, gives  $nz/\bar{U} \approx .6$  measured at 1.5 meters. Also see p. 98, Adv. in Geophysics, vol. 6, for several results at contrasting levels and stabilities varying between  $nz/\bar{U} = .4$  for unstable conditions at 29 m. to  $nz/\bar{U} \geq 1.1$  for low levels and light winds (presumably stable conditions). As shown in Table 11, the weighted consensus value for  $nz/\bar{U}$  increases slightly from 16 to 40 meters; the increase is more marked, the greater the stability. If one takes into consideration (1) roughness variability in these observational results, (2) variability in observation height, though this effect is not large, (3) the defining criteria used, and (4) the variability of stratification, then no serious disagreement seems to be present. The results of this investigation are quite similar to those of Gurvich (1960), but the values

for the neutral and unstable cases are about  $nz/\bar{U} = .3$ .

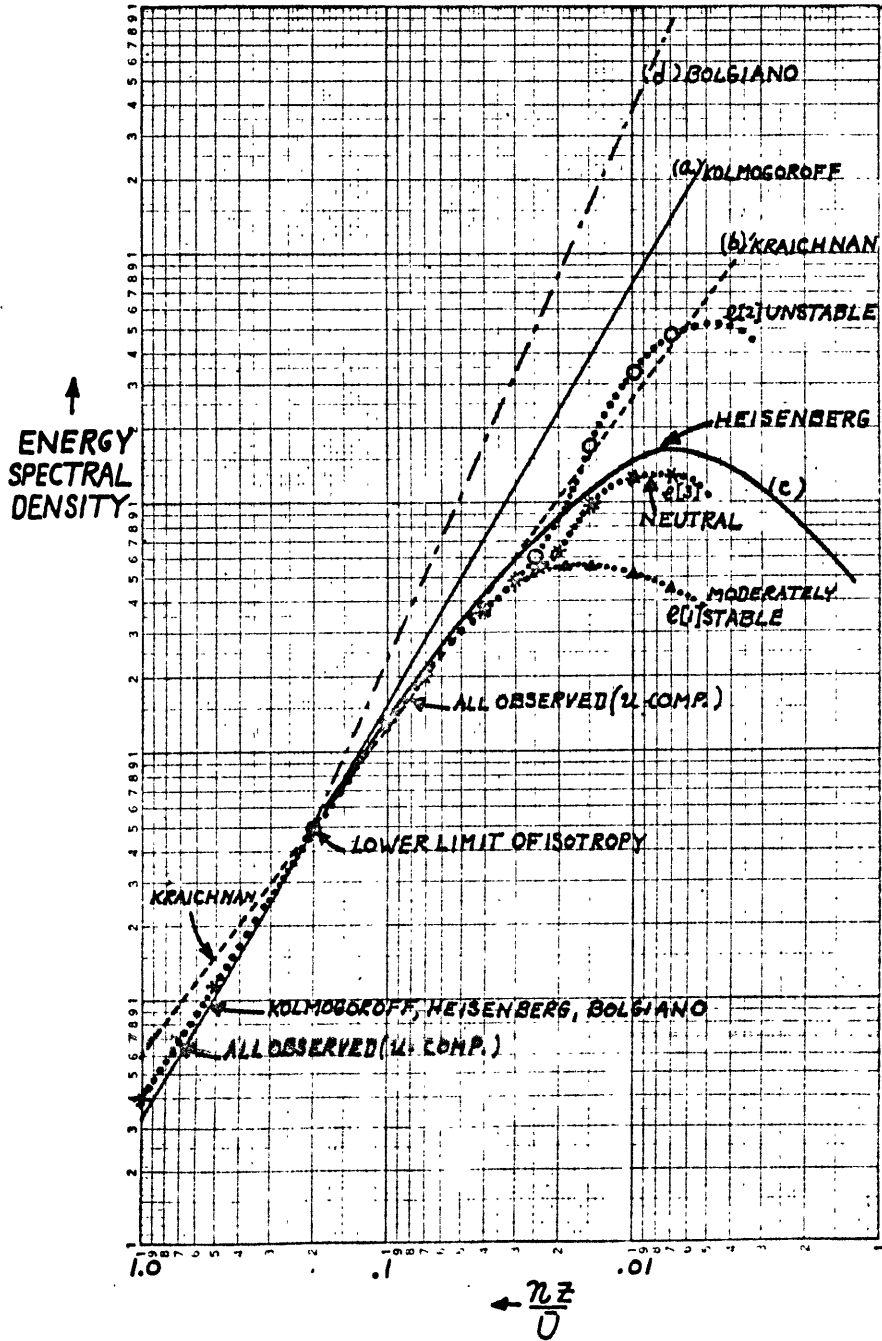
(e) Gramer (1960) concluded that for the higher frequencies, which includes the uniform slope and isotropic regions, for the u-component: (1) for levels near the roughness length, say 1 meter, the slope in log-log coordinates is - 1.0; (2) at intermediate levels, say 10-90 meters, the slope is near -4/3 and (3) above 90 meters the slope is nearer -5/3. Also Gramer, Record and Tillman (1962), using Round Hill data, computed an average value of this higher frequency uniform slope, including the  $S_u$ ,  $S_v$ ,  $S_w$  at 16 and 40 meters and obtained a value of -1.5 for this average slope. Table 17, if averaged with the slopes above the isotropy point, are in agreement with these values listed above. Table 17 breaks the slope values down into groupings to show the effect of stability and height on the slope for both the u and v-components.

#### F. Comparison of results with theoretical predictions.

1. Balow, is a review of theoretical predictions about the behavior of  $E(k)$  for the high frequency range to include the inertial sub-range and the uniform slope region below the lower limit of isotropy.

Figure 41 gives the  $E(k)$  function in log-log coordinates expected if: (a) Kolmogoroff's theory is valid, (b) Kraichman's theory is valid, (c) Heisenberg's transfer theory is valid, (d) Bolgiano's buoyancy sub-range exists, and (e) [1] [2] [3] are three observed spectra, representing stable, unstable and neutral runs. Lin and Reid (1969) show that, in the inertial sub-range, the Heisenberg's transfer theory gives the same result as Kolmogoroff's theory. Curve c in Figure 41 [taken from Lin and Reid (1969), Figure 13]

FIG. 41: COMPARISON OF VARIOUS THEORETICAL SPECTRAL FUNCTIONS WITH OBSERVED DATA ( $u$ -COMP. ENERGY AT 16 M.). ALL FUNCTIONS ARBITRARILY SUPERIMPOSED AT THE LOWER LIMIT OF ISOTROPY.



would result from the Heisenberg's theory assuming initial period similarity in addition to some other assumptions. No pretense is made that these various curves are exactly placed relative to each other; the lower limit of isotropy is used as a guide in positioning them, but because of the many unevaluated constants involved in the functions, their scaling relative to the abscissa may be bad. Even with these undesirable features, it is believed that considerable physical insight is revealed by this comparison. The curves are arbitrarily placed coincident at the lower limit of isotropy merely as an aid in evaluating the relative functional behavior of  $E(k)$ . Kraichnan's theory, curve b, seems to behave better below the lower limit of isotropy than Kolmogoroff's theory. Below this point, the assumption of independence of the widely separated (in  $k$ -space) Fourier components, may become sufficiently in error to cause a significant deviation from the  $k^{-5/3}$  forecast. However the "direct interaction approximation" of Kraichnan's may approximate the actual physics at much lower frequencies, although it also is based on the isotropic assumption. On the high wave number side of the lower limit of isotropy, these Fourier components may well act rather independently so that the Kolmogoroff hypothesis gives the correct spectrum. In this research, no frequencies are measured which are high enough to show the validity of Heisenberg's theory in the dissipation range where  $E(k) = ck^{-7}$ . Stewart, Grant and Moilliet (1962) have made measurements of turbulence in water which permit an evaluation of the theoretical functions in this range. Curve d is for Bolgiano's spectra (see Bolgiano (1962) Section IX A). This gives:

$$\begin{array}{llll}
 E(k) & k^{-11/5} & \text{for } k < & \text{lower limit of isotropy} \\
 E(k) & k^{-5/3} & \text{for } k > & \text{lower limit of isotropy}
 \end{array}$$

Curves c [1] [2] and [3] are self explanatory. One notes the closeness of the various functions to one another over a large range of the spectra that can be evaluated from the data in this research. There is considerable suspicion that the small differences in slopes may not be statistically significant and even for a data sample of this size, one may not have high confidence in ones ability to distinguish which function most closely fits the data. However, down to the lower limit of the uniform slope region, there seems to be a best choice, which is very close to the observed spectra and is acceptably consistent theoretically. This choice is: use Kolmogoroff's or Heisenberg's theory in the isotropic region and Kraichnan's theory in the uniform slope region so long as one remains above the regions of "mechanical input of energy". Away from energy source regions and in not too stable stratification, the spectrum in the uniform slope region is very close to Kraichnan's forecast of  $k^{-3/2}$  (see Table 17).

Bolgiano (1962) and Deissler (1962) have both considered the first order effects of buoyancy on turbulence (neglecting the triple correlation terms). The w-component energy is most directly affected by buoyancy and also by the distance to the lower boundary. Batchelor (1953) pointed out that the effect of "pressure forces" is to tend to distribute energy equally among the components, hence provide a source or sink for the total energy of the components,  $E(k)$ , through the w-component, see Deissler (1962) Figure 26 (using Prandtl number = .7). Although the buoyancy effect is somewhat stronger at low frequencies, a very wide range of frequencies are affected by this energy drain (or addition). In the case of energy addition, this is not to be confused with the input associated with convective cell

development.

Then, for the isotropic and uniform slope frequency regions, the previously discussed Kolmogoroff-Kraichman combination spectrum seems to be very close to the observed functional dependence of  $E(n)$  on frequency, using  $S_u$  and  $S_v$  as approximations to the total energy in the intermediate frequency range.

2. Low frequency region below the uniform slope region (see Table 17).

In this region, the energy spectral density functions are increasingly dependent on stratification as the frequency decreases. The presence of the lower boundary also becomes increasingly important, particularly through its influence on the  $S_w$  spectra. This is also the region where Taylor's hypothesis,  $x = \bar{U}t$ , is questionable. There is yet another complication: since the time scale of an eddy increases as its linear scale increases, there is the possibility that the energy level of these largest convective eddies is not in equilibrium with the meteorological parameters ( $\bar{U}$ ,  $\frac{\partial \bar{U}}{\partial z}$ ); this would infer varying values of energy even for the same meteorological parameters. Even with these difficulties, it seems profitable to examine a list of theoretical predictions about convection and see if these data support these predictions.

(a) the primary effect of instability on cell size of maximum energy would be through the expansion of the depth of the "boundary layer" (comparable to cell size) in which convection is occurring (see Rayleigh [1916]). This is not the same boundary layer used by Priestley (1959) or Monin and Obukhov (1954). Their definition refers to that layer (usually less than 50 meters deep) in which there are no heat flux or momentum flux divergence.

This is not so for the layer referred to by Rayleigh. The "boundary layer" has also been thought of as the layer of uniform mixing; this may be very shallow for stable cases or as deep as the distance to the bases of cumulus clouds in unstable cases. Thompson (1963) and Herring (1963) are referring to the shallow layer, in convective cases, which contains most of the temperature gradient. One can only infer that, with greater instability, the "boundary layer" would be deeper and hence the maximum energy would shift to longer waves, whose characteristic life times would be longer. Then, neglecting wind shear (assuming free convection), one would look for a direct relation between  $\partial\theta/\partial z$  and the period of maximum energy spectral density (see Figure 43) giving  $\log T_{\text{max energy}}$  versus  $\sigma_A$  and  $\log T_{\text{max}}$  versus  $\partial\theta/\partial z$ , where  $T_{\text{max}}$  is the period associated with the maximum point of the  $nF(n)$  function). The data sample is small (restricted to free convective cases) and Figure 43 does not seem to define a relation. See p. 41-42, Cramer, Record and Tillman (1962), where a relation in the expected sense is indicated. More research is needed on this point. Also the assumption that a depth of the convection can be inferred from  $\partial\theta/\partial z$  may be a bad one. Certainly  $\sigma_A$  would be a safer parameter. Since it is related to the scale of turbulence but  $\partial\theta/\partial z$  could change much more rapidly than adjustments in the boundary layer depth could be made.

(b) Priestley (1959) dealt with convective models and made predictions about the heat flux (see also Section III C for a brief summary of Priestley's predictions and see Table 3 for the  $H^*$  calculations). These are plotted in Figure 42 giving  $H^*$  vs.  $|Ri|$  but the range of  $|Ri|$  is insufficient to establish any good functional relation and the results are inconclusive

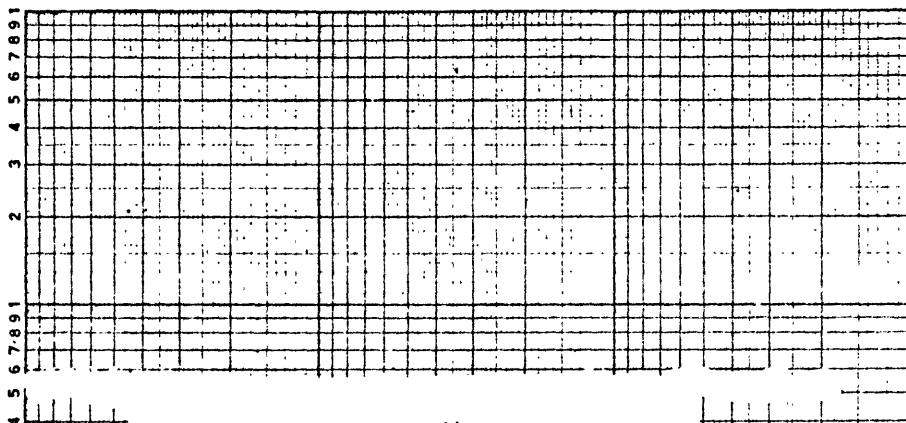


FIG. 42: NON-DIMENSIONAL HEAT FLUX,  $H^*$ , AT 16 AND 40M. AS A FUNCTION OF RICHARDSON NUMBER.

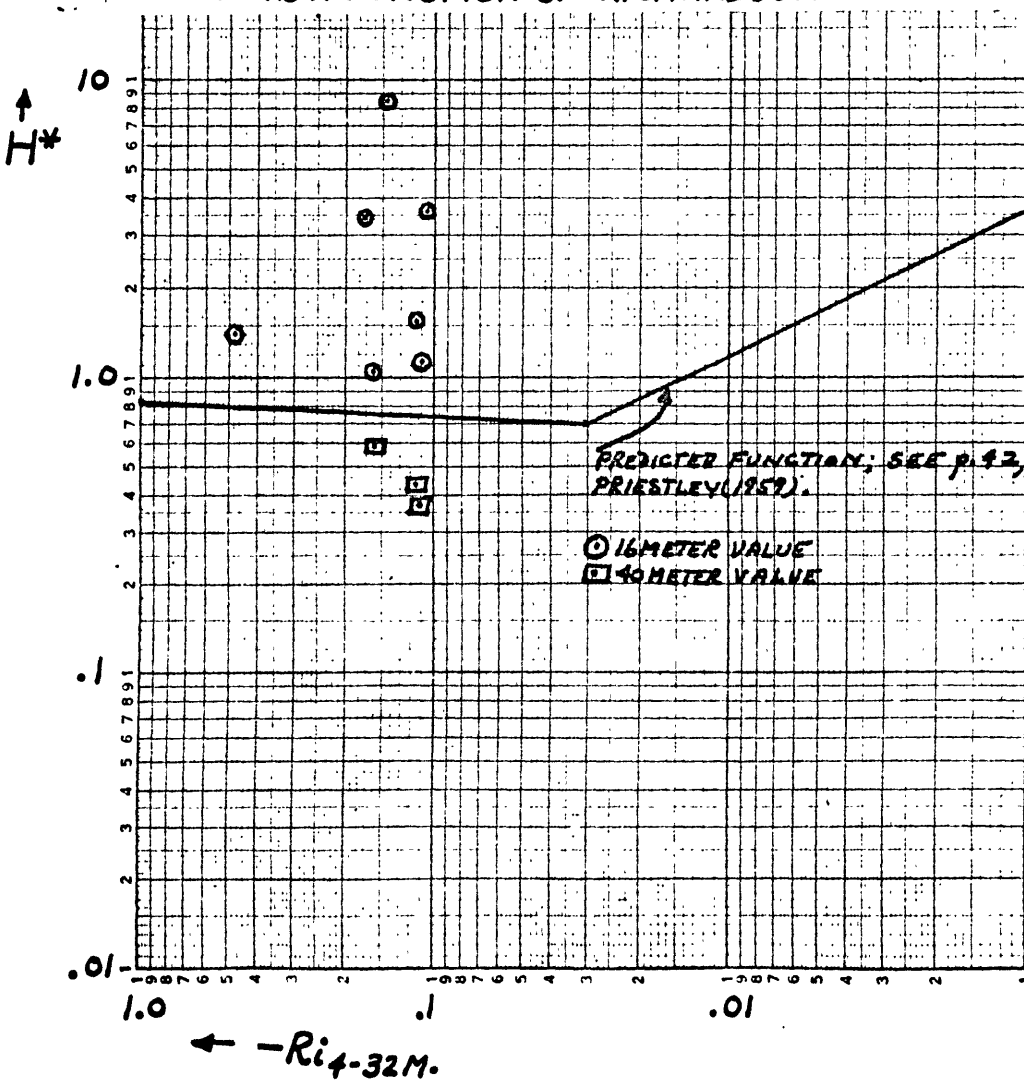
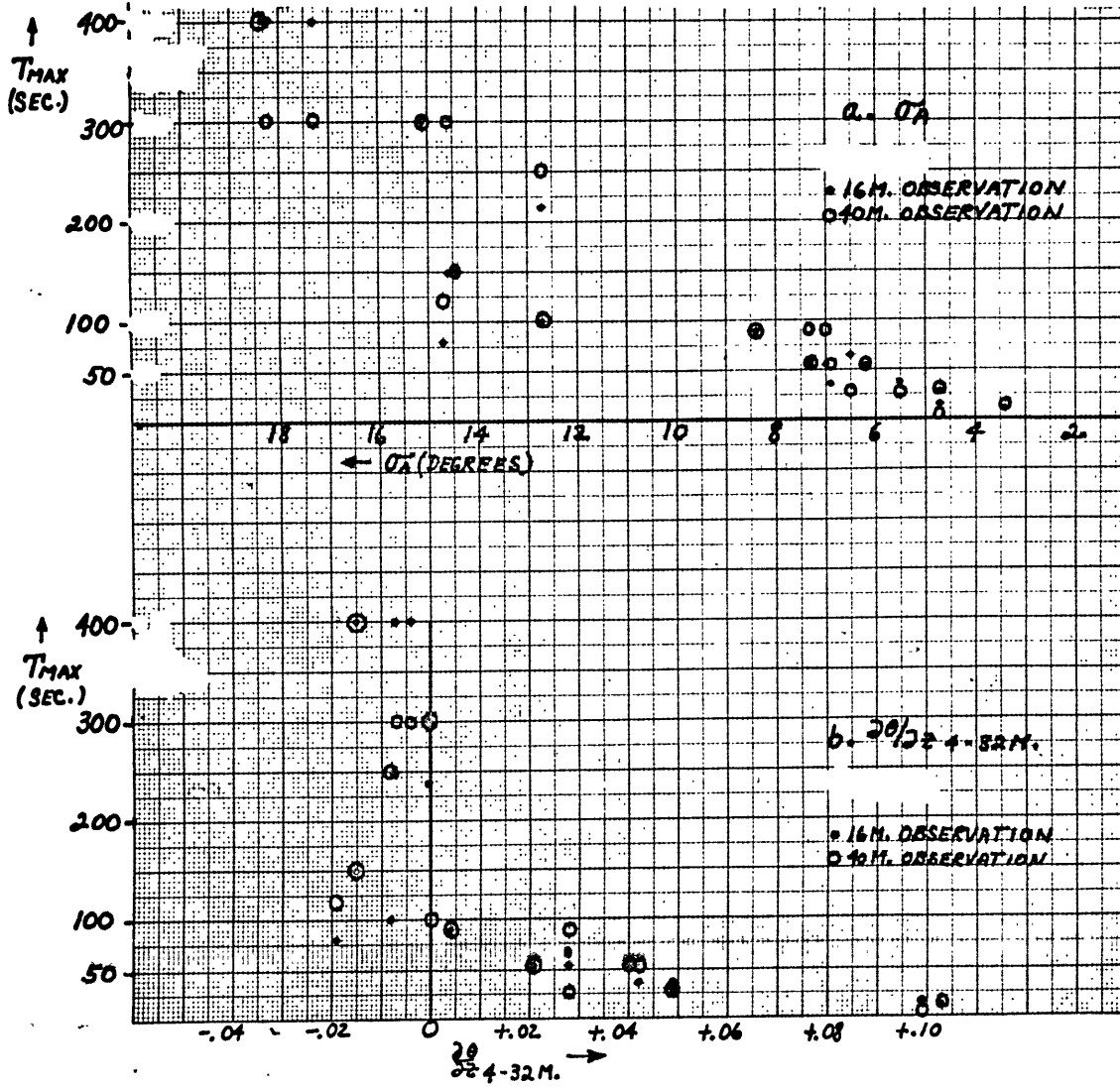




FIG. 43: PERIOD,  $T_{MAX}$ , AT 16M. AND 40M. ASSOCIATED WITH THE MAXIMUM VALUE OF  $\gamma_S(T)$  AS A FUNCTION OF: a.  $\sigma_A$   
 b.  $\frac{\partial \theta}{\partial z}$  4-32M.



(there is always the difficulty of evaluating  $Ri$  when it is small). Priestley also suggested that for  $Ri < -.03$ , the heat flux should be proportional to  $z^{2/3}$ . Table 18 gives results for 40 meters in fair agreement with this (assuming the  $\overline{w'T'}_{16}$  values are correct). Also calculations were made assuming a  $z^{1/3}$  law for the heat flux with results that are at least as good. From his model of axisymmetric plumes, Priestley also made the prediction that the heat flux becomes positive (upward) before the stratification reaches decreases to neutral conditions. The data in Figure 20 appears to support this prediction. However Prof. James Austin suggested that the one hour length of record, used for obtaining an average gross statistic for  $\overline{w'T'}$ , can introduce a bias in the following manner. If the average stratification for a one hour run appears to be neutral but really contained a combination of stable and unstable conditions, then the total heat flux would be positive, since the absolute value of the heat flux under unstable conditions is larger than for the same amount of stable stratification (as shown in Figure 20). All the near neutral runs were checked with the following results: the two runs (67 C and 31), which were near neutral for the entire period, did give  $\overline{w'T'} \approx 0$ . One run, (15), which was unstable at the beginning and slightly stable at the end, gave a positive heat flux. Several runs having  $\overline{w'T'} \approx 0$ , had a positive heat flux, but all of these had unstable stratification nearer the lower boundary. From an inventory of all the runs, no run could be found that was really slightly stable or neutral throughout, that had a positive heat flux, so Prof. Austin's less complicated explanation is preferable. Despite a lack of good evidence to support it here, there is still reason to believe that Priestley's axi-

symmetric plume model may be a useful one. The non-dimensional heat flux,  $H^*$ , from his similarity assumptions, may not have worked out in these calculations because of the troublesome Ri calculations.

(c) See Sections III C for a brief discussion of Thompson (1963) and also a discussion of Herring (1963) in Section IX A.

These two papers have in common similar geometry, the use of non-divergence, the steady state and the Boussinesq approximation; their other assumptions are quite different but the results are in good agreement. Only the results to which the data is pertinent, are listed below:

-1.  $\frac{\partial \theta}{\partial z} \approx 0$ , except negative near the boundary. A boundary layer was shown by Herring and was assumed by Thompson.

-2. The temperature variance reaches a maximum at the top of this layer (Thompson).

-3. The vertical velocity (and supposedly the vertical velocity variance,  $w'^2$ ) reaches a maximum deep in the interior of the fluid region where  $\frac{\partial \theta}{\partial z}$  (Thompson). See Figure 44 for the best that this data sample can do in evaluating the above theoretical results. With values only at  $z = 0, 16$  and  $40$  meters for the  $w$ - and  $T$ -variance, considerable latitude is available in drawing the vertical profile. Even so, the simplest analysis for the  $w$ -variance would indicate the maximum is far removed from the lower boundary. Drawing the profile of temperature variance is not so straightforward. The temperature profiles indicate the top of the boundary layer to be near 8 meters and several of the runs can be drawn to "force" a maximum of  $T$ -variance at this level, but it looks like better analysis if a maximum is indicated near the 30 meter level. In general, this is considerable support for the theoretical predictions of Thompson and Herring,

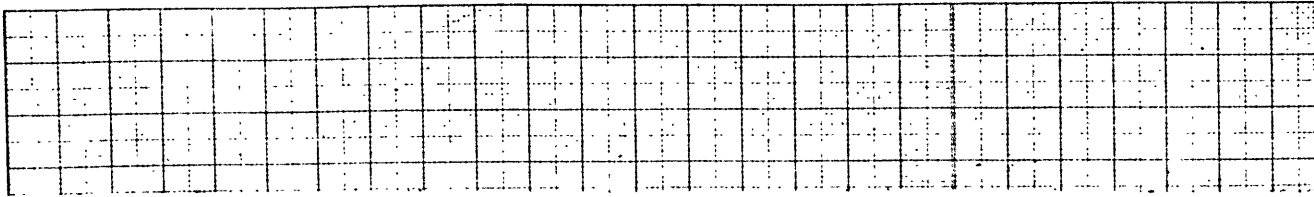
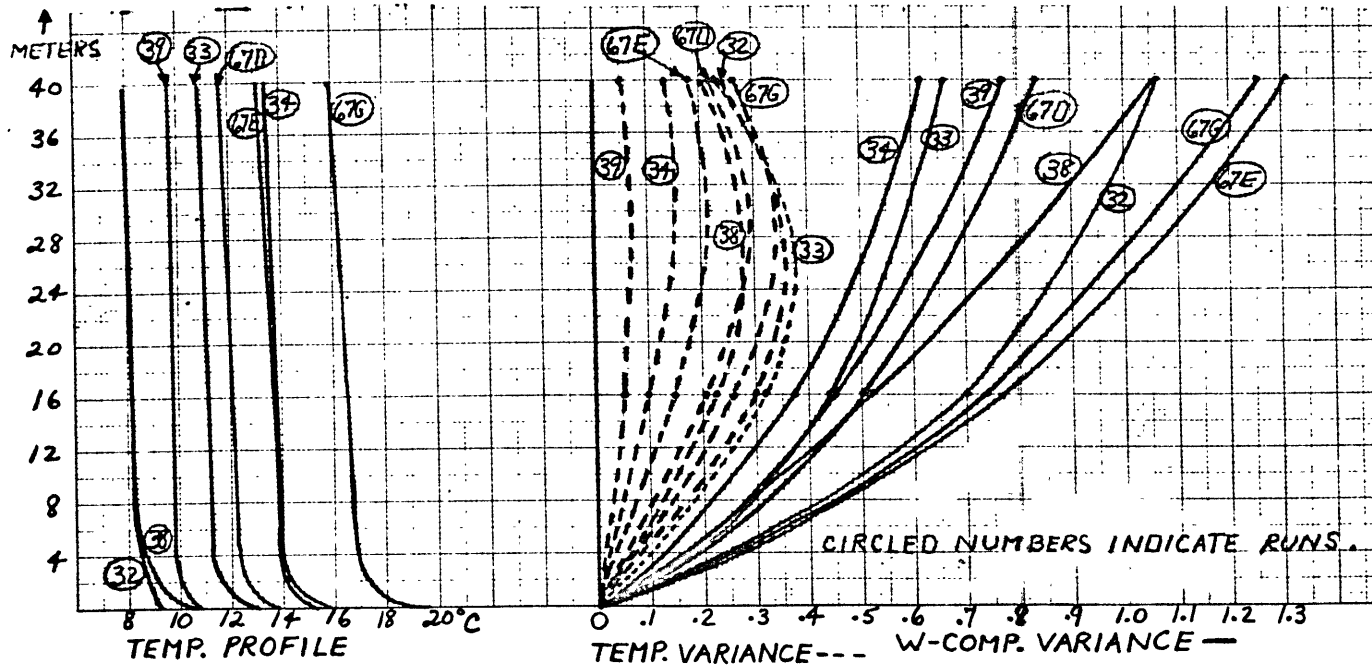


FIG. 44: VERTICAL PROFILES OF TEMPERATURE, VARIANCE OF TEMP. AND VERTICAL VELOCITY FOR 8 RUNS BELIEVED TO BE "FREE CONVECTIVE".



indicating that useful information can be obtained from judicious modelling and also that near the lower boundary, the transfers of various properties may be statistically "stationary".

(d) Lettau (1949) made predictions about the heat flux as a function of  $\frac{\partial \theta}{\partial z}$  (see Figure 3 and also the discussion in Section III C). If the adjustment to Figure 20, suggested in Section V F 2b above, was made (putting  $\overline{w'T'} = 0$  at  $\frac{\partial \theta}{\partial z} = 0$ ), then there is good agreement between theory and data. Lettau's introduction of the third parameter,  $w^*$ , seems to give a model quite adaptable to the data.

(e) A summary of the theory-data comparison for the low frequency range suggests the following conclusions:

-1. There is some evidence to indicate that the period for the maximum of  $nF(n)$  can be roughly estimated from the stability (if  $\sigma_A$  is used) - the greater the instability, the longer the period of the energy maximum).

-2. The use of the model of convection between parallel plates, with the assumptions indicated in Section (c) above, give good agreement with the statistics, though this data sample is not well suited for testing in the low frequency range.

-3. It is believed that Priestley's model of axisymmetric plume type convection is a good one near the lower boundary, despite the lack of statistical support here.

-4. Lettau's derived heat flux function is in good agreement with data and his use of three parameters,  $l = f(z, z_0)$ ;  $u^*$ , and  $w^*$ , may be adequate to describe much of the physics of turbulence in a stratified atmosphere

near the surface.

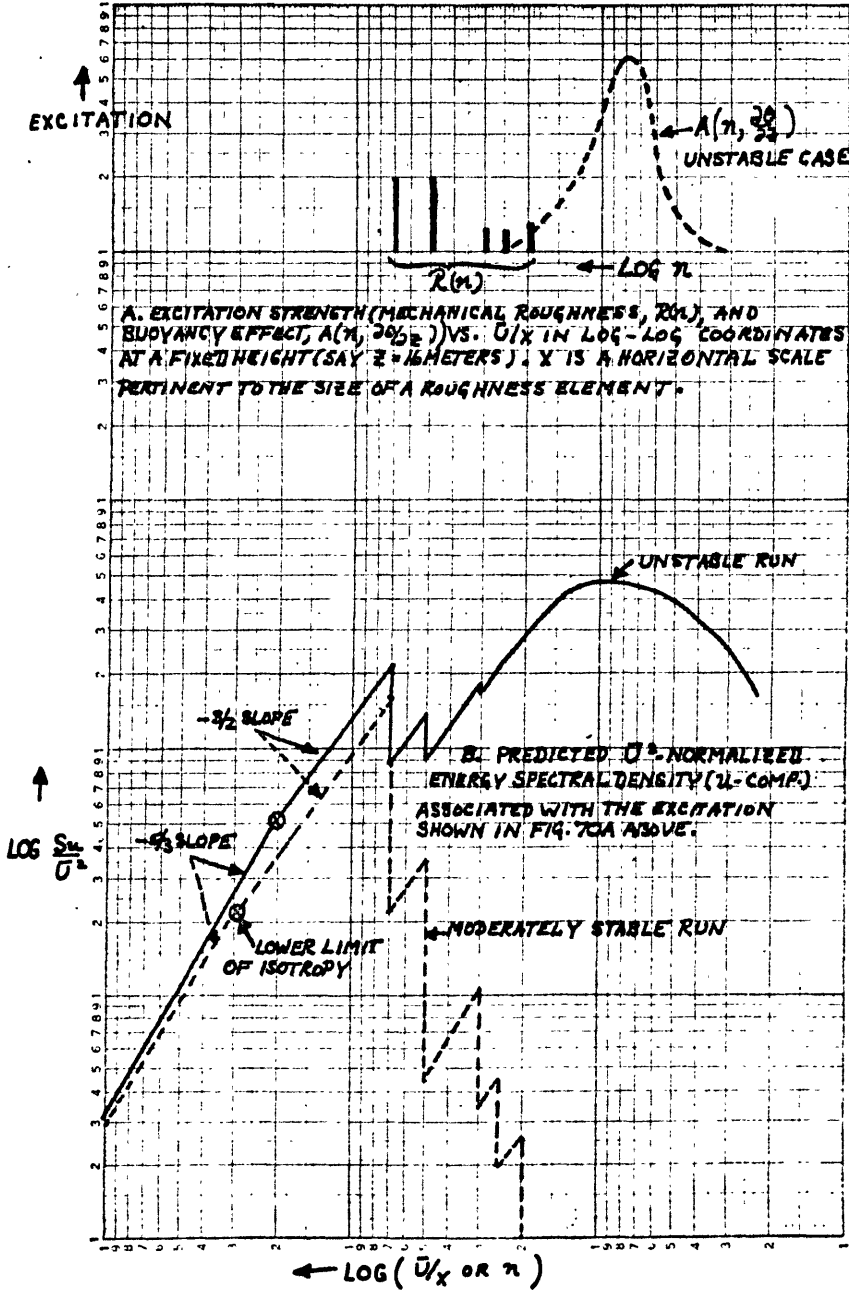
G. A composite model of energy spectral density functions in the surface layer.

The next step is to combine the preceding conclusions in a model which gives good forecasts for the energy spectral density functions and which is physically reasonable. This was begun in Section Vc, with the definitions of the roughness parameter,  $R(n)$ , and the convective excitation  $A(n, \frac{\partial \theta}{\partial z})$  as expressed in Equation 5-6. Then  $R(n)$  plus  $A(n, \frac{\partial \theta}{\partial z})$  integrated over all  $n$  would give the ratio of turbulent to mean flow kinetic energy, assuming the introduced energy is proportional to  $\bar{U}^2$  at some level  $z$ , which is the effective height of the most important roughness elements. In energy "production" (crudely approximated by  $\overline{u'w'} \frac{\partial \bar{u}}{\partial z}$ ), it can be seen that the  $w$ -fluctuations play a dominant role. Then the problem can be looked at from the viewpoint of the results of the "mechanical and convective excitation of the  $w$ -component. So the energy introduction at frequency,  $n$ , is

$$E(n) = \bar{U}_z^2 \left\{ R(n) + A\left(n, \frac{\partial \theta}{\partial z}\right) \right\}$$

where  $R(n)$  becomes a function of  $\frac{\partial \theta}{\partial z}$  only for very stable conditions, and  $A\left(n, \frac{\partial \theta}{\partial z}\right)$  is very small under stable conditions. In the evaluation of equations 5.4 and 5.5,  $c$  equals  $+ 5/3$  in the isotropic range and equals  $+ 3/2$  below the lower limit of isotropy. Then Figure 45b. shows the resulting energy spectral density function "produced" by a simplified excitation pattern Figure 45a. Comparison with individual runs, indicates that the general slope shown in Figure 45b is a reasonable one.

FIG. 45: DIAGRAMMATICAL EXPLANATION OF THE "MODIFIED BUSINGER" MODEL.



## VI. SUMMARY AND CONCLUSIONS.

A. The non-dimensional energy spectral density functions for  $u$ ,  $v$ ,  $w$  and  $T$  have been presented in several coordinate systems with stratification as a parameter. The standard deviation of the azimuth angle,  $\sigma_A$ , was chosen as the parameter for stability which had the most desirable characteristics. Associated with this parameter choice, then, is the choice of  $\sigma_N$  (standard deviation of azimuth angle for neutral conditions) as the desired way of describing lower boundary roughness. An expression,  $(\partial\theta/\partial z)^*$ , for stratification (or its equivalent  $\sigma_A$  value) is suggested as a way to incorporate the better features of the functional behavior of  $\sigma_A$  at neutral and unstable conditions and of  $\partial\theta/\partial z$  under stable conditions.

B. The lower limit of isotropy is determined, as a function of stability and height above ground (see Table 11). This limit was taken as a consensus average of the limits given by : 1. the lower limit of the  $k^{-5/3}$  functions for  $S_u$  and  $S_v$ , 2. the value of  $nz/\bar{U}$  where the energy of the components is no longer within 80 per cent of each other and 3. the value of  $nz/\bar{U}$  where the  $uw$ ,  $wT$  and  $uT$  coherence falls below .15 (values lower than this could occur 10 per cent of the time when the true coherence is zero).

C. From the plots of non-dimensionalized energy spectral density, three adjacent regions of the spectrum appear:

1. Isotropic or high frequency region where  $E(n) \propto n^{-5/3}$  and where the  $\bar{U}^2$ - and  $(T)^2$ -normalization is effective except in very stable cases ( $\sigma_A < 7$ ). The low frequency,  $\frac{n_z^2}{U}$ , limit of this region at the



16-meter level varies between 1.0 for very stable runs to .2 for neutral and unstable runs. At 40 meters the lower limits vary between 1.5 and .3 (see Table 11).

2. An intermediate frequency region of uniform slope where  $\bar{U}^2$  - and  $(T)^2$  - normalizations are still fairly good except in very stable cases. In this region, spectral density dependence on stability appears but is not serious.  $E(n) \propto n^{-c}$  where  $c$  is between 1.0 and 1.5 and is somewhat stability and height above ground dependent (see Tables 16 and 17). Toward lower frequencies, the effect of stability is increasing and the slope value is decreasing slowly, unless the run is very unstable. See Table 16, showing the range of the lower limit of the uniform slope region, varying between  $\frac{n_z}{\sigma} = .3$  for very stable 40-meter cases to .03 for neutral and unstable cases at 16 meters.

3. The low frequency convective range, where the effect of stability on the energy spectral density functions is dominant and increasingly strong in going toward lower frequencies. No normalizations work in this region. A large peak of very low frequency energy, somewhat separated from the higher frequencies, appears in the convective cases, the lateral (v) component is most graphically sensitive to stability in this range, because the longitudinal (u) component contains more mechanically introduced energy and the w-component energy is greatly modified by the height above ground. This region includes the region to the low frequency side of the lower limit of the uniform slope region.

D. Using both  $\bar{U}^2$  - or  $(T)^2$  - normalization and Monin-Obukhov similarity coordinates, the energy spectral density functions are presented

(both graphs and algebraic functions) as a function of  $\sigma_A$ , a modified stability parameter, and are shown in Figures 3 - 15, 24 and 25 and in Section IX B. Due to the behavior of the diabatic wind profile,  $\bar{U}_z^2$  - normalization was tried with  $z = 2$  meters with the idea that this level would be near the "effective height" of the most important roughness elements. If the wind speed at this level is a physically significant quantity, then  $\bar{U}_z^2$  normalization might help in the very stable cases. Actually it was only partially successful (see figure 31) and either the two meter level is still too high or this is much too crude a way to handle the effects of stratification.

E. Comparisons of these empirical results with those of other investigators, do not show any unreconcilable differences. This data sample, however, due to its size and diversity of stability conditions, permits more to be said about the stability dependence of: 1. the energy spectral density functions, 2. their functional dependence on  $z$ , 3. the location of the lower limit of isotropy and, 4. the uniform slope region.

F. A comparison of the empirical results with those predicted by theory, gives some very useful information:

-1. Above the lower limit of isotropy, the Kolmogoroff or Heisenberg predictions of  $E(n) \propto n^{-5/3}$  is in excellent agreement with the data.

2. In the uniform slope region just below the lower limit of isotropy, the Kraichnan theory of  $E(n) \propto n^{-3/2}$  was closer to the observed slope average of between -1.3 and -1.4, but then the isotropic assumption is no longer valid and this region is much closer to the energy sources and energy containing eddies.

3. See Figure 41 for a comparison of various theoretical and

observed energy spectral density functions. Over much of the observable frequency range here, these functions are so close together, that it is hard to say that the difference between them is statistically significant.

The combination of the Kraichnan and Kolmogoroff theories gives the best agreement.

4. In the low frequency convective region, very many difficulties arise, and despite observational care and statistical significance of the data, few inferences can be safely made. Some of these troubles are:

(a) these measurements are Eulerian and Taylor's hypothesis ( $x = \bar{u}t$ ) may be only partially valid in this region. Therefore conclusions involving spatial distributions and length scales are not safe.

(b) horizontal homogeneity cannot be assumed in convective situations.

(c) the characteristic time scale of a turbulence cell increases with its linear scale, therefore, these large eddies may not reach equilibrium for a particular environment before synoptic and diurnal changes (shown by  $\bar{u}$  and  $\frac{\partial \theta}{\partial t}$ ) of the parameters have occurred. Despite these difficulties an attempt was made to compare these low frequency results to theoretical predictions applicable to the convective case. Without convection there is little low frequency energy. In most cases, this comparison yielded nothing statistically dependable. However, there are three results which seem worth stating.

-1. there was some evidence to suggest that the maximum of energy was associated with lower frequencies, the greater the instability.

-2. the use of vertical profiles, although they contain only 3 points, of temperature variance and w-variance and temperature give

agreement with the expectations of Herring and Thompson. They infer a  $w$ -maximum far removed from the lower boundary and a temperature variance maximum near the top of the "boundary layer".

-3. use of Lottau's three parameters for turbulence in the stratified atmosphere, gives good results for heat flux predictions.

G. A model is suggested using the conclusions above and the model introduced by Businger (1961). This model contains a description of the roughness  $R(n)$  such that the effect of site variability can be accounted for (see Sections VC. and VG.). This model relates roughness,  $R(n)$  and  $A(n, \frac{\partial \theta}{\partial z})$ , energy introduction  $\mathcal{E}(n)$ ; total energy at a frequency,  $E(n)$ ; total energy,  $E$ ;  $\sigma_A$  and  $\sigma_N$  in what is believed to be a consistent manner. Sections VC. and VG. give more details.

## VII. SUGGESTED FURTHER RESEARCH

A. The model of Section VG. suggests the necessity of investigating the effect of site variability by comparing energy spectral density data from sites of contrasting roughness. This would show if the generalized Businger model is really a good one or not.

B. Collect and evaluate data especially designed to measure the energy and the vertical fluxes of heat and momentum in the very low frequency convective range. This would have to be done by determining the velocity correlation functions from a spatial net of measuring points and simultaneous measurements. This experiment would also have to be designed to evaluate the seriousness of the lack of horizontal homogeneity during convection. From this type of data, one might also hope to answer the question of how

low frequency it is possible to measure, before having to worry about the "balance" of the turbulent system with its environment.

G. If this very low frequency convective range behavior were well understood near the lower boundary, then the next steps would be to investigate how this regime "matches" into the atmospheric circulations at the gradient wind level and their relation, if any, to convective cloud scales. Equally important is the connection, if any, of these large convective eddies with the still larger terrain induced local circulations.

**ACKNOWLEDGMENTS**

The author wishes to express thanks to the following Faculty members: Prof. E.N. Lorenz, Prof. C.C. Lin, and Prof. J.M. Austin, and to Dr. H.E. Cramer, Dr. F.A. Record and their Round Hill Field Station Staff for assistance during this research. The author is especially grateful to Prof. E.N. Lorenz and Dr. H.E. Cramer for advice and guidance of his efforts. This area of research was chosen and commenced at the suggestion of Prof. J.M. Austin.

## APPENDIX

## A. RESUMES OF PAPERS (continuation of Section IIIe).

Deissler (1961), treated the problem of the effect of vertical shear of the horizontal mean wind in the absence of buoyancy. The approach was the treating of a single effect, the writing of two-point correlation functions and the closing of the set by neglecting the triple correlation terms. In this case the wind shear was assumed uniform and horizontal homogeneity was imposed. One of his results was: with increasing shear, the maximum of energy density shifts toward lower frequencies and is larger in magnitude.

Boigliano (1959).(1962) also dealt with the problem of anisotropic turbulence, using a model of steady state turbulence in a stably stratified atmosphere, composed of axisymmetric cells. In the perturbation equations of motion, only first order terms are retained and the following energy equation is obtained:

$$\frac{\partial}{\partial t} \left( \frac{1}{2} \overline{u_i u_i} \right) = \overline{u' w'} \frac{\partial \bar{u}}{\partial z} - u_j \frac{\partial}{\partial x_j} \left\{ \frac{1}{2} \overline{u_i u_i + \rho'} \right\} - \frac{\rho'}{\rho_0} \overline{w' \rho'} - \varepsilon$$

$p$  = pressure / static density;  $\rho$  = potential density. Operations on this equation finally yields his Figure 2 (see Figure 41) as the important result. This steepening of the slope in  $\log E(k)$  vs  $\log k$  plot for the stable atmosphere, just on the low frequency side of the inertial sub-range was not observed in this research but then the test certainly is not ideal because of the effect of the lower boundary, particularly on the w-component.

Bolgiano (1963) did show supporting evidence for his theoretical spectrum using high elevation data.

Lumley (1964) obtained a theoretical result similar to this, but with less constraint on the "inertial transfer" of energy.

Friestley (1959) dealt with convective regimes extensively. In Chapter 4, he differentiated between free and forced convective regimes and points out that although  $|\frac{\partial T}{\partial z} + \Gamma|$  or  $|\frac{\partial \theta}{\partial z}|$  decreases with height, its effect on the turbulence increases. With observational evidence to support it, he proposed a model of convection in the surface layer of axisymmetric plumes of penetrative convection. He used this model to explain the occurrence of an upward heat flux in the neutral and slightly stable atmospheres. By using similarity, an assumed Gaussian distribution of velocity profiles across these cells and dimensional arguments, he obtained a number of interesting predictions, some of which are compared to observations. A partial list of these conclusions are:

1. for forced convection ( $Ri > .03$ )

(a) lapse rate,  $\partial \theta / \partial z \propto z^{-1}$

(b)  $H^* = k^2 Ri^{-1/2}$

$$H^*(\text{definition}) = \frac{H}{\rho c_p (g/\theta)^{1/2} (\partial \theta / \partial z)^{3/2} z^2}$$

$H$  = heat flux,  $k$  = Von Karman constant

$$Ri = \frac{g}{\theta} \frac{\partial \theta / \partial z}{(\partial u / \partial z)^2}, \text{ or in the flux form, } = \frac{-g H}{c_p \theta \sigma \partial u / \partial z}$$

2. for free convection ( $Ri < .03$ )

(a)  $|\partial \theta / \partial z| \propto z^{-4/3}$

(b)  $H^* = \text{constant}$

(c)  $\sigma_w \propto z^{1/3}$  ;  $\sigma_T \propto z^{-1/3}$



He offered as an explanation of the  $H^* = f(Ri)$ : "at considerable wind speeds, mechanically generated turbulence is sufficient to perform the heat transfer, but at higher levels it is less. At some point, free convection must take over". The form of this convection is the axisymmetric plumes. Also see Businger (1955), who dealt with a means of determining when free or forced convection will occur.

See 18.5 and 18.6 of Hess (1959), for a presentation of the Prandtl mixing length theory, which leads to the logarithmic wind profile by letting the mixing length,  $l = kz$  and defining the friction velocity,  $u^* = \sqrt{c/\rho}$

Taylor (1960) examined the Monin-Obukhov similarity experimentally and suggested a value for " $\alpha$ " in the evaluation of the universal function:  $\phi(\frac{z}{L}) = 1 + \alpha \frac{z}{L} + \beta (\frac{z}{L})^2$ . . In the free convective case, he concluded that the functions given by similarity and by Priestley (1959) are acceptably accurate and he then evaluated the constants.

Macready (1953) used data taken from five runs, varying in length from 10 min. to 1 hour and under diversified meteorological conditions, and showed that at sufficiently high frequencies, the Kolmogoroff hypothesis gave the correct function:  $E(k) \propto \epsilon^{2/3} k^{-5/3}$  or  $f(r) = 1 - C \epsilon^{2/3} r^{2/3}$  for the spatial longitudinal correlation ( $r = \bar{U}t$  is assumed).

In Lettau and Davidson (1957), Lettau gave an extensive boundary layer theory, stressing non-dimensional characteristics to describe the relations between wind shear, stratification, and momentum and heat exchanges.

## B. LIST OF ALGEBRAIC EXPRESSIONS FOR THE ORTHOGONAL COMPONENTS AND TEMPERATURE POWER SPECTRA IN SIMILARITY COORDINATES.

See Section VE 1. for a general description of these functions. These are Figures 16 and 17 in algebraic form. In each case there will be a note such as : "F is introduced between  $n = .01$  and  $.02$ ". This means that at  $n = .01$ , F equals 1.0 and at  $n = .02$  it has the full value shown for F and between  $n = .01$  and  $n = .02$ , F increases or decreases linearly along the log scale from 1.0 to the high frequency value shown for F. The expressions are:

$$n < .01 \qquad \qquad \qquad n > .01$$

$$S_{u,16} = \frac{.3 n^{-5/3} F}{1 + \frac{5 \times 10^{-4}}{n^2} \left(\frac{\sigma_N}{\sigma_A}\right)^2} \quad ; \quad S_{u,16} = \frac{.3 n^{-5/3} F}{1 + \frac{5 \times 10^{-3}}{n^{3/2}} \left(\frac{\sigma_N}{\sigma_A}\right)^2}$$

$$F = 1 + 25 \frac{\partial \theta}{\partial z}, \quad \frac{\partial \theta}{\partial z} \geq .010 \left. \vphantom{F} \right\} \text{introduced between } n = .01 \text{ and } n = .2 .$$

$$= 1.0, \quad \frac{\partial \theta}{\partial z} < .010 \left. \vphantom{F} \right\}$$

$\left(\frac{\partial \theta}{\partial z}\right)^*$  should be used everywhere for  $\frac{\partial \theta}{\partial z}$ .

$$n < .01 \qquad \qquad \qquad n > .01$$

$$S_{u,40} = \frac{.3 n^{-5/3} F}{1 + \frac{12 \times 10^{-4}}{n^2} \left(\frac{\sigma_N}{\sigma_A}\right)^2} \quad ; \quad S_{u,40} = \frac{.3 n^{-5/3} F}{1 + \frac{12 \times 10^{-3}}{n^{3/2}} \left(\frac{\sigma_N}{\sigma_A}\right)^2}$$

$$F = 1 + 30 \frac{\partial \theta}{\partial z}, \quad \frac{\partial \theta}{\partial z} \geq .010 \left. \vphantom{F} \right\} \text{introduced between } n = .01 \text{ and } n = .2 .$$

$$= 1 + 20 \frac{\partial \theta}{\partial z}, \quad \frac{\partial \theta}{\partial z} < .010 \left. \vphantom{F} \right\}$$

For stable and near neutral conditions:

$$S_{V,16} = \frac{.3n^{-5/3}F}{1 + \frac{2 \times 10^{-3}(\sigma_N)^3}{n^2 \sigma_A}} ; F = 1 + 20 \frac{\partial \theta}{\partial z}, \frac{\partial \theta}{\partial z} \geq .010$$

= 1.0, otherwise,

introduced between  $n=.04$  and  $n=1.0$

For unstable conditions:

$$S_{V,16} = \frac{.3n^{-5/3}}{1 + \frac{5 \times 10^{-2}(\sigma_N)^2}{n \sigma_A}} ; S_{V,16} = \frac{.3n^{-5/3}}{1 + \frac{5 \times 10^{-3}(\sigma_N)^2}{n^{3/2} \sigma_A}}$$

$n > .01$   $n < .01$

For stable and near neutral conditions:

$$S_{V,40} = \frac{.4n^{-5/3}F}{1 + \frac{10^{-2}(\sigma_N)^2}{n^2 \sigma_A}} ; F = 1 + 20 \frac{\partial \theta}{\partial z}$$

introduced between  $n=.04$  and  $n=1.0$

For unstable conditions:

$$S_{V,40} = \frac{.4n^{-5/3}F}{1 + \frac{2 \times 10^{-3}(\sigma_N)^2}{n^2 \sigma_A}} ; F = 1 + 10 \frac{\partial \theta}{\partial z}$$

introduced between  $n=.01$  and  $n=.04$ .

$$S_{W,16} = \frac{.3n^{-1.3}F}{1 + \frac{4.5 \times 10^{-2}(\sigma_N)^2}{n^{1.3} \sigma_A}} ; F = 1 + 15 \frac{\partial \theta}{\partial z}, \frac{\partial \theta}{\partial z} \geq .010$$

= 1.0, otherwise,

introduced between  $n=.05$  and  $n=1.0$

For stable and near neutral conditions:

$$S_{W,40} = \frac{.35n^{-3/2}F}{1 + \frac{4 \times 10^{-2}(\sigma_N)^2}{n^{1.7} \sigma_A}} ; S_{W,40} = \frac{.35n^{-3/2}F}{1 + \frac{10^{-2}(\sigma_N)^2}{n^2 \sigma_A}}$$

$n > .01$   $n < .01$

$$F = 1 + 15 \frac{\partial \theta}{\partial z}, \frac{\partial \theta}{\partial z} \geq .010 \left. \vphantom{F} \right\} \text{introduced between}$$

$$= 1 + 10 \frac{\partial \theta}{\partial z}, \text{otherwise} \left. \vphantom{F} \right\} n=.1 \text{ and } n=1.0$$

For unstable conditions:

Same as  $S_{w,40}$ , stable, except use  $(\sigma_N/\sigma_A)^{2.5}$ .

For stable conditions:

$$F = 1 + 60 \frac{\partial \theta}{\partial z}, \quad \frac{\partial \theta}{\partial z} \geq .010$$

$$S_{temp,16} = \frac{.03 \eta^{-5/3} F}{1 + \frac{2.8 \times 10^{-4}}{\eta^2} \left(\frac{\sigma_N}{\sigma_A}\right)^2} ; \quad = 1.0, \text{ otherwise,}$$

introduced between  $\eta = .02$   
and  $\eta = 1.0$

For unstable conditions:

$$S_{temp,16} = \frac{.03 \eta^{-5/3}}{1 + \frac{4 \times 10^{-2}}{\eta} \left(\frac{\sigma_N}{\sigma_A}\right)^2}$$

The neutral case has no meaning in Similarity framework.

For stable conditions:

$$F = 1 + 30 \frac{\partial \theta}{\partial z},$$

$$S_{temp,40} = \frac{.04 \eta^{-1.8} F}{1 + \frac{17 \times 10^{-4}}{\eta^2} \left(\frac{\sigma_N}{\sigma_A}\right)^2} ; \quad \text{introduced between } \eta = .07$$

and  $\eta = .5$ .

For unstable conditions:

$$S_{temp,40} = \frac{.03 \eta^{-1.8} F}{1 + \frac{12 \times 10^{-4}}{\eta^2}}, \quad F = .6 \text{ for all } \frac{\partial \theta}{\partial z},$$

introduced between  
 $\eta = .02$  and  $\eta = .2$ .

$S_{temp,40}$  is the same for  $\sigma_A > 10^\circ$ .

### C. VARIOUS METHODS OF ESTIMATING STRESS AND HEAT FLUX\*

It is necessary to determine  $\overline{u'w'}$  and  $\overline{w'T'}$  in order to get dependable dimensional energy spectral density values, from similarity coordinates. Here are some recent methods:

Pasquill (1963) gave three methods for evaluating the eddy diffusivity "K", through which one could compute the stress by using  $\tau = K \frac{d\bar{u}}{dz}$ . His methods are:

1. The "high frequency" method uses:

$$S(k) = c \varepsilon^{2/3} k^{-5/3} \text{ and } \varepsilon = \frac{\tau}{\rho} \frac{d\bar{u}}{dz}. \text{ Measure } S(k) \text{ and compute } \tau.$$

2. "Total energy" method.

$$w\text{-variance, } \sigma_w^2 = \int_0^\infty S_w(n) dn, \quad K = A \sigma_w z, \quad \tau = K \frac{d\bar{u}}{dz}$$

3. Low frequency method.

Mean square displacement of particles,  $\sigma_p^2 = 2KT$  (assumed Gaussian distribution)  $T =$  time, a large value.  $\frac{\sigma_p^2}{T^2} = \left[ \sigma_w^2 \right]_{\infty, T/3}$ , then solve for  $K$ , knowing  $\sigma_w$  as before.

Panofsky (1963). From Monin-Obukhov similarity, the following quantities are used:

$$\text{Non-dimensional shear, } \frac{kz}{u_*} \frac{\partial v}{\partial z} = \phi(z/L), \quad \text{where } k = \text{Von}$$

Karman constant. He has not used  $K_M$  (momentum) =  $K_H$  (heat) and thus defined  $L^0 = L K_H / K_M$  and modified the universal function to be:

$$\psi\left(\frac{z}{L^0}\right) = \int_0^{-z/L^0} \frac{1 - \phi(\varepsilon)}{\varepsilon} d\varepsilon$$

$$\text{giving } v = \frac{u_*}{k} \left[ \log\left(\frac{z}{z_0}\right) - \int_{-z_0/L^0}^{-z/L^0} \frac{1 - \phi(\varepsilon)}{\varepsilon} d\varepsilon \right]$$

A number of expressions for  $\phi$  can be used and then knowing  $z_0$ , one can solve for  $u^* = \sqrt{z/\rho}$ . Some of these functions are:

1. Monin-Obukhov "log plus linear" profile derived from:

$$\phi(z/L) = \alpha z/L + \beta (z/L)^2$$

2. Keyps function:

$$\phi^4 - 18(z/L) \phi^3 = 1 \quad , \quad (\text{this function was used and the stress calculations are shown in Table 3})$$

3. Webb function:  $\phi = 1 + 4.5(z/L)$ , for  $(-z/L) \leq .0317$   
 $= .316(-z/L)^{-1/3} - .00173(-z/L)^{-4/3}$ ,  
 for  $-z/L \geq .0317$

Solutions for  $\tau$ , when  $z_0$  is not known, are also discussed.

Takeuchi and Yokoyama (1963) presented a more generalized form of the same approach. In place of  $l = kz$  (valid at neutral stability), they used  $l = kz f(z/L)$ . The result is  $\phi^4 - \gamma^2 z/L \phi^3 - f^{-4} = 0$ , where  $\gamma = \text{constant}$ .

$$\text{Near neutral } f = 1 - \sigma(z/L) + \frac{\sigma^2}{2} (z/L)^2$$

$$\text{Stable, } f = \frac{1}{2\sigma} (z/L)^{-1} - \left(\frac{1}{2\sigma}\right)^3 (z/L)^{-3}$$

$$\text{Unstable, } f = -2\sigma(z/L) - \frac{1}{2\sigma} (z/L)^{-1}$$

At neutral  $f = 1$ ,  $l = kz$ , giving the Keyps function. The more generalized form should be better under stable conditions than the Keyps function, but it was not used because of the presence of two constants,  $\sigma$  and  $\gamma$ , which must be determined from the data.

Taylor (1961) suggested evaluating the "structure function" in the

$$\text{inertial sub-range: } D_u(r) = \overline{[u(x) - u(x+r)]^2} \propto r^{2/3} r^{2/3}$$

$$D_T = \overline{[T(x) - T(x+r)]^2} \propto \chi r^{-1/3} r^{2/3} \text{ where } \chi = \kappa \left(\frac{dT}{dx_i}\right)^2 .$$

He then assumed  $\frac{\partial \bar{u}_i}{\partial t} = 0$  and neglected the vertical divergence of kinetic energy to get:  $\ell = \frac{\tau}{\rho} \frac{d\bar{u}}{dz} + \frac{gH}{c_p \rho T}$ . Next he assumed horizontal homogeneity and wrote a conservation equation for internal energy to get:

$$H \frac{\partial \bar{\theta}}{\partial z} + \frac{1}{2} c_p \frac{\partial}{\partial x_j} \{ (\rho u_j)^2 \} = \rho \ell \bar{T} + \lambda \frac{\partial^2}{\partial x_j^2} \left( \frac{1}{2} \bar{T}^2 \right) - \lambda \left( \frac{\partial T}{\partial x_j} \right)^2$$

where  $H$  = heat flux. Next, he showed that the dominant term is  $H \frac{\partial \bar{\theta}}{\partial z}$ ,

and used these values to solve for  $\ell$ . Also he gave a second more

empirical method:  $a = D_u(r) r^{-2/3}$ ,  $b = D_T(r) r^{-2/3}$   
 $\ell = \frac{1}{2} a^{3/2}$ ,  $H = -\frac{.893 c_p \rho b \ell^{1/3}}{\partial \theta / \partial z}$ .

## BIBLIOGRAPHY

- Barad, M.L., 1958: Project Prairie Grass, a field program in diffusion. Geophysical Research Papers no. 59, Vols. 1 and 2, AFRC-TR-58-235, Geophysical Research Directorate, Air Force Cambridge Research Center, Bedford, Mass.
- Batchelor, G.K., 1953: The Theory of Homogeneous Turbulence. Cambridge University Press, London.
- \_\_\_\_\_, 1953a: The conditions for dynamic similarity of motions of a frictionless perfect gas atmosphere. Quart. J. Roy. Meteor. Soc., 19, 224-235.
- Blackman, R.B. and Tukey, J.W., 1958: The Measurement of Power Spectra. Dover Publications, Inc., New York.
- Blackadar, A.K. and Panofsky, H.A., 1964: Recent Soviet Research in Atmospheric Turbulence. Bull. Am. Meteor. Soc., 45, 2, 80.
- Bolgiano, R. Jr., 1959: Turbulent Spectra in a stably stratified Atmosphere. J. Geophys. Res., 64, 2226-2229.
- Bolgiano, R. Jr., 1962: Structure of turbulence in stratified media. J. Geophys. Res., 67, 8, 3015-3023.
- Businger, J.A., 1955: On the structure of the atmospheric surface layer. J. Meteor., 12, 6, 553-561.
- \_\_\_\_\_, 1961: On the relation between the spectrum of turbulence and the diabatic wind profile. J. Geophys. Res., 66, 8, 2405-2409.
- Chandrasekhar, S., 1955: A theory of turbulence. Proc. Roy. Soc. A, 229, 1-18.
- Cramer, H.E., 1957: A practical method for estimating the dispersal of atmospheric contaminants. Proc. 1st Natl. Conf. on Applied Meteor., Am. Meteor. Soc.
- Cramer, H.E., 1959: Measurements of turbulence structure near the ground within the frequency range from .5 to .01 cycles sec<sup>-1</sup>. Advances in Geophysics, 6, 75-96. Academic Press, New York.
- \_\_\_\_\_, 1960: Engineering estimates of the power spectra of horizontal components of wind velocity. Presented at 3rd Applied Meteor. Conf., Santa Barbara, Calif.
- \_\_\_\_\_, Record, F.A., Tillman, J.E. and Vaughan, H.C., 1961: Annual Report: Studies of the spectra of the vertical fluxes of momentum,



- heat and moisture in the atmospheric boundary layer, DA-36-039-SC-80209, Division of Sponsored Research, Dept. of Meteor., Mass. Inst. of Tech., Round Hill Field Station, So. Dartmouth, Mass.
- Cramer, H.E., Record, F.A., and Tillman, J.E., 1962: Final Report, Studies of the spectra of the vertical fluxes of momentum, heat, and moisture in the atmospheric boundary layer, DA TASK 3A99-27-005-08, Division of Sponsored Research, Dept. of Meteor., Mass. Inst. of Tech., Round Hill Field Station, So. Dartmouth, Mass.
- Deissler, R.G., 1961: Effects of inhomogeneity and of shear flow in weak turbulent fields. Physics of Fluids, 4(10), 1192.
- \_\_\_\_\_, 1962: Turbulence in the presence of a vertical body force and temperature gradient. J. Geophys. Res., 67, 8, 3049 - 3062.
- Frenkiel, F.M. and Sheppard, P.A., Editors, 1959: Advances in Geophysics, 6: Atmospheric Diffusion and Air Pollution, Proc. of a Symposium held at Oxford, Aug. 24-28, 1958. Academic Press, New York.
- \_\_\_\_\_, Editor, 1962: Turbulence in Geophysics: Proc. of a Symposium of IUGG-IUTAM, Sept. 4-9, 1961, Marseille, France. Published by the Am. Geophys. Union, Washington, D.C.
- Grant, H.L., Stewart, E.W. and Moilliet, A., 1962: Turbulence spectra from a tidal channel. J. Fluid Mech., 12, 241-268.
- Gurvich, A.S., 1960: Frequency spectra and functions of probability of vertical velocity components. Izvestia Acad. Sci., USSR, Geophys. Ser., 1042-1055.
- Haugen, D.A., 1959: Project Prairie Grass, a field program in diffusion, Vol. III, Geophysical Research Papers, no. 59, AFRC-TR-53-235 III, Geophys. Research Directorate, Air Force Cambridge Research Center, Bedford, Mass.
- Herring, J.R., 1963: Investigation of problems in thermal convection. J. Atmos. Sci., 20, 4, 325-338.
- Hess, S.L., 1959: Introduction to Theoretical Meteorology. Holt-Dryden, New York.
- Hinze, J.O., 1959: Turbulence. McGraw-Hill, New York.
- Inoue, E., 1959: The effects of thermal stratification on turbulent diffusion in the surface layer. Adv. in Geophysics, 6, 310-330.
- Kolmogoroff, A.N., 1941: The local structure of turbulence in incompressible viscous fluid for very high Reynolds numbers. Doklady Akad. Nau. S.S.S.R., 30, 301-305.

- Kraichnan, R.H., 1958: A theory of turbulence dynamics. Second Symposium on Naval Hydrodynamics, 25-29 Aug., 1958, Wash., D.C.
- \_\_\_\_\_, 1959: The structure of isotropic turbulence at very high Reynolds numbers. J.Fluid Mech., 5, 497.
- \_\_\_\_\_, and Spiegel, E.A., 1962: Model for energy transfer in isotropic turbulence. Physics of Fluids, 5, 5, 583-588.
- Lettau, H.H., 1949: Isotropic and non-isotropic turbulence in the atmospheric surface layer, Geophys. Res.Papers no. 1, Air Force, Cambridge Research Laboratories, Cambridge, Mass.
- Lettau, H.H. and Davidson, B., Editors, 1957: Exploring the Atmosphere's First Mile, Vols. 1 and 2, Proc. of the Great Plains Turbulence Field Program, 1 Aug. to 8 Sept. 1953, O'Neill, Nebr. Pergamon Press, New York.
- Lin, C.C. and Reid, W.H., 1963: Turbulent flow, theoretical aspects. Handbuch der Physik, Bd 8/2, 438-523.
- Lumley, J.L., 1964: The spectrum of nearly inertial turbulence in a stably stratified fluid. J. Atmos. Sci., 21, 1, 99-102.
- Macready, F.B., 1953: Structure of atmospheric turbulence. J. Meteor., 10, 434-449.
- Monin, A.S., and Obukhov, A.M., 1954: The basic law of turbulence mixing in the atmospheric surface layer. Trudy Geofiz. Inst.Akad.Nauk S.S.S.R., no. 24 (151), 163-187.
- \_\_\_\_\_, 1962: Empirical data on turbulence in the surface layer of the atmosphere. J.Geophys.Res., 67, 8, 3103-3110.
- Neumann, J., 1961: Richardson's number and the Monin-Obukhov wind profile. J.Meteor., 18, 6, 808.
- Obukhov, A.M., 1958: Laws governing the microstructure of temperature and wind in the surface layer. Symposium at Leningrad, 1958, M.I., Rudyko, Editor.
- Ogura, Y., 1962: Energy transfer in an isotropic turbulent flow. J.Geophys. Res., 67, 8, 3143-3149.
- Panofsky, H.A., and McCormick, R.A., 1954: Properties of spectra of atmospheric turbulence at 100 meters. Quart.J.Roy.Meteor.Soc., 80, 546-564.
- Panofsky, H.A., and Brier, G.W., 1958: Some applications of statistics to Meteorology. The Penn.State Univ., Univ. Park, Pa.

- Fanofsky, H.A., Cramer, H.E., and Rao, V.R.K., 1958: The relation between Eulerian time and space spectra. Quart.J.Roy.Meteor.Soc., 84, 270-273.
- \_\_\_\_\_, and Deland, R.J., 1959: One dimensional spectra of atmospheric turbulence in the lowest 100 meters. Adv. in Geophysics, 6, 41-64.
- \_\_\_\_\_, 1962: The budget of turbulent energy in the lowest 100 meters. J.Geophys.Res., 67, 8, 3161-3166.
- \_\_\_\_\_, 1963: Determination of stress from wind and temperature measurements. Quart.J.Roy.Meteor.Soc., 89, 85-94.
- \_\_\_\_\_, and Pasquill, F., 1963: The constant of the Kolmogoroff law. Quart.J.Roy.Meteor.Soc., 89, 550.
- Pasquill, F., 1961: Atmospheric Diffusion. Van Nostrand, Princeton, N.J.
- \_\_\_\_\_, 1963: The determination of eddy diffusivity from measurement of turbulent energy. Quart.J.Roy.Meteor.Soc., 89, 95.
- Fedlosky, J., 1962: Spectral considerations in two-dimensional incompressible flow. Tellus XIV, 2, 125-132.
- Fellow, A. and Southwell, R.V., 1940: On maintained convective motion in a fluid heated from below. Proc. Roy. Soc.A, 176, 312-343.
- Frischley, C.H.B., 1959: Turbulent Transfer in the lower Atmosphere. Univ. of Chicago Press.
- \_\_\_\_\_, 1959a: The isotropic limit and the microscale of turbulence. Adv. in Geophysics, 6, 97.
- Lord Rayleigh, 1916: On convection currents in a horizontal layer of fluid when the higher temperature is on the under side. Philosophical Magazine, Series 6, 32, 529-526.
- Saltzman, B. and Peixoto, J.P., 1957: Harmonic analysis of the mean northern hemisphere wind field for the year, 1950. Studies of the Atmospheric General Circulation II, General Circulation Project, AFRC-TR-58-204, AD 146847, Dept. of Meteor., Mass. Institute of Tech., Cambridge, Mass.
- Shiotani, H., 1963: Some notes on the structure of wind and temperature fields in the lowest layers. J.Meteor.Soc.Japan, Series II, 41, 5, 261, Oct. 63.
- Sutton, O.G., 1949: Atmospheric Turbulence. John Wiley and Sons, Inc., New York.

- Takasuchi, K., 1961: On the structure of the turbulent field in the surface boundary layer, Analysis of the data obtained at O'Neill, Nebr. J. Meteor. Soc. Japan, Series II, 39, 346-367.
- \_\_\_\_\_, 1963: Some studies on the fluctuation of wind direction near the ground. J. Meteor. Soc. Japan, Series II, 41, 1, 40-52.
- \_\_\_\_\_, and Yokoyama, O., 1963: The scale of turbulence and the wind profile in the surface boundary layer. J. Meteor. Soc. Japan, Series II, 41, 2, 108-117.
- Taylor, G.I., 1921: Diffusion by continuous movements. Proc. London Math. Soc., 20, 196.
- \_\_\_\_\_, 1935: Statistical theory of turbulence. Proc. Roy. Soc. A, 151, 421.
- \_\_\_\_\_, 1938: The spectrum of turbulence. Proc. Roy. Soc. A., 164, 476.
- Taylor, R.J., 1960: Similarity theory in the relation between fluxes and gradients in the lower atmosphere. Quart. J. Roy. Meteor. Soc., 86, 67-78.
- \_\_\_\_\_, 1961: A new approach to measurement of turbulent fluxes in the lower atmosphere. J. Fluid Mech., 10, 3, 449.
- Thompson, P.D., 1963: Statistical theory of highly turbulent convection. Paper given at Jan. 1963 meeting of Am. Meteor. Soc. at New York.
- Van der Hoven, I., 1957: Power spectrum of horizontal wind speed in the frequency range from .0007 to 900 cycles per hour. J. Meteor., 14, 160-164.

### Biography of author

Born October 10, 1923 at Chester, Pa. and was raised near Taylor's Bridge, Delaware, attending elementary school there. Graduated from John Bassett Moore High School, Smyrna, Delaware in 1941; was a member of the Army Air Forces from May 1943 until June 1945, serving as a weather observer and radiosonde technician. Graduated from West Point June 1949 and presently in the U.S. Air Force. Have served overseas tours in Spain, Alaska and also with the Fletcher Island (T - 3) project in the Arctic Ocean. Received a M.S. in Meteorology from New York University in 1954; the thesis was on Arctic Meteorology (unpublished).